Measurement of Real-World Stack Emissions in the Athabasca Oil Sands Region with a Dilution Sampling System during August, 2008

DRI Contract Number: 010109-123109

Submitted to:

Kevin E. Percy and Kenneth R. Foster

Wood Buffalo Environmental Association
#100 – 300 Thickwood Boulevard
Ft. McMurray, AB, Canada T9K 1Y1

Prepared for:
Wood Buffalo Environmental Association

By:

John G. Watson, Ph.D.
Judith C. Chow, Sc.D.
Xiaoliang Wang, Ph.D.
Steven D. Kohl, M.S.
David A. Sodeman, Ph.D.*

Desert Research Institute
Nevada System of Higher Education
2215 Raggio Parkway
Reno, NV 89512

* Currently with: County of San Diego
Air Pollution Control District
1600 Pacific Highway
San Diego, CA 92101

Finalized: March 31, 2013

Table of Contents

List of Abbreviations

ΔP: differential pressure
ρ_i : density for emittant i.
σ: uncertainty
AAS: atomic absorption spectroscopy
AC: automated colorimetry
$AgNO_3$: silver nitrate
AOSR: Athabasca Oil Sands Region
AP42: U.S. EPA Compilation of Air Pollution Emission Factors
ARB: California Air Resources Board
ARD: Arizona road dust
ASTM: the American Society for Testing and Materials
ATN: optical attenuation
b_{abs}: light absorption coefficient
BC: black carbon
Ca^{++}: calcium ion
CAC: criteria air contaminants
$CaCl_2$: calcium chloride
$CaCO_3$: calcium carbonate; limestone
$CaSO_4$: calcium sulfate
CFR: Federal Register
CH_4: methane
Cl^-: chloride
CMB: chemical mass balance
C_i: concentration of emittant i
CO: carbon monoxide
CO_2: carbon dioxide
CPC: condensation particle counter
C_s: pitot tube constant (0.84)
CSA: stack cross section area
CTM: Conditional Test Method
DELCD: dry electrolytic conductivity detector
DR: dilution ratio
DNPH: 2,4-dinitrophenylhydrazine
DRI: Desert Research Institute
EAF: DRI's Environmental Analysis Facility
EC: elemental carbon
EF: emission factors
ER: emission rate
ESP: electrostatic precipitators
FCCU: fluidized catalytic cracking unit
FGD: flue gas desulfurization
FID: flame ionization detector
FRM: Federal Reference Method
GC-FID/MS: gas chromatography-flame ionization detector/mass spectrometry
GHG: greenhouse gases
H_2O: water
H_2O_2: hydrogen peroxide
H_2S: hydrogen sulfide
H_2SO_4: sulfuric acid
HCl: hydrogen chloride
He: helium
HEPA: high efficiency particulate air
HPLC: high performance liquid chromatograph
HULIS: humic-like substances
ICP/MS: inductively coupled plasma/mass spectrometry
IC: Ion chromatography
ID: inner diameter
IMPROVE: Interagency Monitoring of Protected Visual Environments
IR: infrared
JBR: jet bubbling reactor
K^+: potassium ion
K_2CO_3: potassium carbonate
K_p: stack velocity constant (34.97),
LEL: lower explosive limit
Mg^{++}: magnesium ion
MDL: Minimum detection limit
$MeCl_2$: methylene chloride
M_i: atomic or molecular weight of species i
MMD: mass median diameter
MW: molecular weight
N_2: nitrogen
Na^+: sodium ion
NAAQS: U.S. National Ambient Air Quality Standards
NDIR: nondispersive infrared
NH_3: ammonia
NH_4^+: ammonium
$(NH_4)_2SO_4$: ammonium sulfate
NH_4Cl: ammonium chloride
NH_4HSO_4: ammonium bisulfate
NMHC: non-methane hydrocarbon
NO: nitrogen oxide
NO_2: nitrogen dioxide
NO_2^-: nitrite
NO_3^-: nitrate
NO_x: nitrogen oxides
O_2: oxygen
O_3: ozone
OAL: DRI's Organic Analytical Laboratory
OAQPS: U.S. EPA's Office of Air Quality Planning and Standards
OC: organic carbon
OC1, OC2, OC3, and OC4: organic carbon evolved at 140, 280, 480, and 580 °C, respectively, in a 100% He atmosphere
OES: optical emission spectrometry
OP: pyrolyzed carbon
OPC: optical particle counter
P: pressure
PAH: polycyclic aromatic hydrocarbon

PAMS: photochemical assessment monitoring stations
PDS: phenoldisulfonic acid
PID: photo ionization detector
PM: particulate matter
$PM_{2.5}$: particles with aerodynamic diameter < 2.5 µm
PM_{10}: particles with aerodynamic diameter < 10 µm
PM_{25}: particles with optical diameter < 25 µm
$PO_4^{\equiv}$: phosphate
PSL: polystyrene latex spheres
R: universal gas constant
RH: relative humidity
RMSE: root mean square error
SEM: scanning electron microscopy
SO_2: sulfur dioxide
SO_3: sulfur trioxide
$SO_4^{=}$: sulfate
SRM: standard reference method
SVOCs: semi-volatile organic compounds
T: temperature
TC: total carbon
TD-GC/MS: thermal desorption-gas chromatography/mass spectrometry
TOC: total organic carbon analyzer
TOR: thermal-optical reflectance
TOT: thermal/optical transmittance
TSP: total suspended particles
UFP: ultrafine particles
U.S. EPA: United States Environmental Protection Agency
UV: ultraviolet
V: volume of air sampled
VIS: visible
VOCs: volatile organic compounds
V_{St}: average stack velocity
WBEA: Wood Buffalo Environmental Association
WSOC: water-soluble organic carbon
XRF: X-ray fluorescence

List of Tables

List of Tables, continued

List of Figures

List of Figures, continued

List of Figures, continued

List of Figures, continued

Executive Summary

Real-world emission rates and compositions were measured for three large stationary sources in the Athabasca Oil Sands Region (AOSR) from 8/9/2008 thro0ugh 8/20/2008. Current stationary source certification and compliance tests measure each emission component individually and do not account for the evolution of small particles ($PM_{2.5}$ and PM_{10}, particles with aerodynamic diameters <2.5 μm and μm) as they cool and dilute in the atmosphere. A dilution stack sampler was applied to three stacks (A, B, and C) at two facilities (A and B) for gas and $PM_{2.5}$ particulate pollutant concentrations, emission rates (ER), and chemical source profiles to simulate aerosol evolution. Source profiles are used for speciated emission inventories and for receptor-oriented source apportionment, which infers source contributions to ecosystem effects.

Stack A at Facility A exhausts flue gas from two carbon monoxide (CO) boilers that oxidize overhead gas from two fluid cokers, sour water treating units, and sometimes the sulfur recovery units. Most of the solid PM is removed by two electrostatic precipitators (ESPs) before being routed through the stack and into the atmosphere. Stack B at Facility A releases CO boiler flue gas from a third fluid coker and sulfur recovery units after most primary PM is removed by an ESP and sulfur dioxide (SO_2) is scrubbed using an ammonia-based flue gas desulfurization (FGD) process. Stack C at Facility B vents emissions from a powerhouse that burns coke and uses limestone slurry as the FGD SO_2 scrubbing reagent.

Effluent velocities were measured by a type-S pitot tube. CO, carbon dioxide (CO_2), nitrogen oxide (NO), $PM_{2.5}$, PM_{10}, and mass distributions for particles in the size range of ~0.23-25 μm were measured in real time. SO_2, ammonia (NH_3), hydrogen sulfide (H_2S), $PM_{2.5}$ mass, light transmission (b_{abs}) through filters, elements, isotopes, ions, carbon fractions, total water-soluble organic carbon (WSOC), WSOC classes (neutral compounds, mono- and di-acids, and poly-acids including humic-like substances (HULIS)), carbohydrates, organic acids, and speciated organic compounds were measured on gas- and particle-absorbing filters.

Stack B at Facility A had the highest CO concentrations (843 ppm or 915 mg/m^3), while Stack C at Facility B had the highest CO_2 (1.31×10^5 ppm or 2.36×10^5 mg/m^3), NO (134 ppm or 164 mg/m^3), and PM concentrations (38 mg/m^3 for PM_{10}). In all three stacks, CO_2 had the highest emission rate (ER; 177–270 tonnes/hr) among the measured gases, followed by CO, SO_2, NO, and NH_3. The ER for H_2S was low (5–38 g/hr). Stack A had the highest ER for CO (1.6 tonnes/hr), NO (0.3 tonnes/hr), SO_2 (>1.0 tonnes/hr), H_2S (38 g/hr), and PM_{10} (68.6 kg/hr).

Stack B had the lowest particulate ER (11 kg/hr for PM_{10}), ~15-25% of the other two stacks. Stack C has 1-2 orders of magnitude lower NH_3 ER, only 1.1% and 0.2% of Stacks A and B, respectively. It also has significantly lower SO_2 ER, only <19% and 28% of Stacks A and B.

For Stack A, the NO_x, and total suspended particle (TSP) ERs from dilution sampling were 52% and 17%, respectively, of those from compliance tests in 2007. PM_{10} ER by the in-stack filter method (modified U.S. EPA Method 201A) and dilution sampling method differed by <15%. The $PM_{2.5}$ ER from this study was 2.7 times higher than the in-stack survey, while the TSP was only 66% of the in-stack survey. For Stack B, NO_x ER by dilution sampling was 45% higher than compliance tests, SO_2 ERs were similar by the two methods, and total suspended particulate (TSP) ER by dilution sampling was ~3% of the TSP or 21% of the filterable PM from compliance tests in 2007. For Stack C, the TSP ER from dilution sampling was 16% lower than one compliance test in 2010.

Soluble $SO_4^=$ in $PM_{2.5}$ had the highest concentrations and ERs for all stacks, accounting for ~>40% of the $PM_{2.5}$ emissions. Cerium had the highest rare-earth ERs for all three stacks. Non-polar organic compound ERs were low for all three stacks, with Stack A show the highest, and Stack C showing the lowest. n-alkanes had the highest ERs among all non-polar compounds. Most PAHs, all hopanes, and all steranes were below detection limits for Stack C. Most carbohydrates and organic acids were at or below the detection limits, as was WSOC.

Stack B had the highest abundances of NH_3 and SO_2 (1025±241% and 9205±1762% of $PM_{2.5}$, respectively), while Stack C had the lowest abundances of NH_3 and SO_2 (0.43±0.05% and 472±62% of $PM_{2.5}$, respectively). Soluble $SO_4^=$ was the most abundant species, contributing 39.2 ± 2.0%, 67.9 ± 0.9%, and 49.7 ± 1.5% to $PM_{2.5}$ mass for Stacks A, B, and C, respectively. NH_4^+ was the main cation for Stacks A and B, where it accounted for 15.1± 0.8% and 24.9 ± 0.4% of $PM_{2.5}$. NH_4^+ only accounted 0.9± 0.4% of $PM_{2.5}$ at Stack C, indicating that most of the $SO_4^=$ was present as sulfuric acid (H_2SO_4) rather than as neutralized ammonium sulfate ($(NH_4)_2SO_4$). 6.1% and 43.1% of $PM_{2.5}$ were unidentified for Stacks A and C, respectively. Stack C's $PM_{2.5}$ mass lost ~77% after exposing to the vacuum in X-ray fluorescence (XRF), indicating a substantial amount of water associated with volatile H_2SO_4.

Carbon accounted for a minor fraction of $PM_{2.5}$ but an important fraction of non-sulfate $PM_{2.5}$, with total carbon (TC=OC+EC) being 12.9 ± 0.9%, 6.9 ± 0.2%, and <1.4% of $PM_{2.5}$ for the three stacks, respectively. Trace element abundances were low (typically < 0.1%) with elevated abundances for S (9–20%), mostly in the form of $SO_4^=$. Stacks A and B had higher abundances of Fe (2.8 ± 0.2% and 1.6 ± 0.2%, respectively) than Stack C (0.3 ± 0.1%). Rare earth elements were all <0.01% of $PM_{2.5}$. Abundances in samples from Stack A were 2.5–5 times those measured in samples from Stack B, and 4.5–7.5 times those from Stack C for most rare earth elements. With respect to lead isotopes, emitted $PM_{2.5}$ contained 5.5% lower abundance for ^{204}Pb, 6.0% higher abundance for ^{206}Pb, 6.1% lower abundance for ^{207}Pb, and 0.05% lower abundance for ^{208}Pb compared to the naturally-occurring lead isotopic ratios. Stack C showed higher ^{208}Pb /^{207}Pb and lower ^{204}Pb /^{207}Pb ratios than Stacks A and B.

Organic compound abundances in $PM_{2.5}$ were low. n-alkanes were the most abundant category among quantified non-polar organic compounds, accounting for 0.019±0.012%, 0.028±0.007%, and 0.002±0.001% of $PM_{2.5}$, and 0.34±0.14%, 0.62±0.22%, and 0.73±0.98% of OC for Stacks A, B, and C, respectively. Other nonpolar compounds including PAHs had low abundances.

1 Introduction

1.1 Background

Clearstone Engineering (2003) reported that stack emissions in the Athabasca Oil Sands Region (AOSR) contribute important fractions of total anthropogenic emissions: 97.6% of sulfur dioxide (SO_2), 30.2% of nitrogen oxides (NO_x), 43.9% of carbon monoxide (CO), nearly 100% of ammonia (NH_3) and sulfuric acid (H_2SO_4), and 80% of $PM_{2.5}$ (particles with aerodynamic diameters < 2.5 μm).

Large stationary sources in Alberta are tested for compliance using hot filter-impinger methods (Alberta Environment, 1995), which are similar to U.S. EPA Methods 1-8 (http://epa.gov/ttn/emc/promgate.html). These compliance tests collect particulate matter (PM) from stack effluents onto filters at high temperatures. Condensable species that would contribute to PM at lower temperatures are intended to be collected by passing the filtered stack gases through ice-cooled glass impingers. The hot filter deposits underestimate real-world PM emissions because the filterable mass does not account for condensable species. The impinger catch overestimates PM because gases as well as particles are collected by the impinger solutions (Richards et al., 2005; Corio and Sherwell, 2000). Furthermore, some widely used compliance test methods, e.g., the U.S. EPA Method 5 (U.S.EPA, 2000a), only measure total suspended particles (TSP) and do not segregate mass into different fractions that are regulated by ambient air standards, such as $PM_{2.5}$ and PM_{10} (particles with aerodynamic diameters <2.5 and 10 μm, respectively). Modern industrial emitters with pollution controls typically have most of their PM in the $PM_{2.5}$ fraction.

PM in stack emissions derive from incomplete combustion as well as from mineral matter and other impurities in the process or fuel (Lighty et al., 2000). Carbonaceous particles form during combustion by condensation of inorganic and organic vapors, and by complex chemical reactions. As emissions exit the stack, hot exhaust rapidly mixes with ambient air and cools, resulting in vapor species nucleating homogeneously and heterogeneously or condensing on pre-existing particles. Condensational growth of particles in a diluted plume depends on temperature, relative humidity (RH), aging time, mixing rate, and partitioning of species between the gaseous and solid phases. Real-world stack emissions to the ambient environment differ greatly from those measured from hot-stack filter-impinger tests (Watson et al., 2012b).

An alternative method to the hot filter-impinger method is dilution sampling, where the hot moist stack emission is diluted with clean air in a mixing chamber that simulates dilution and cooling when the flue gas exits the stack. The dilution sampling method provides a more representative estimate of $PM_{2.5}$ stack emissions after the effluent is mixed and cooled with ambient air (U.S.EPA, 2004; Chang et al., 2004b; England et al., 2007a; 2007b).

Air quality models used to apportion contributions from local and regional sources to $PM_{2.5}$ measured at monitoring sites (i.e., receptor) require comprehensive chemically speciated profiles for all major sources (Watson and Chow, 2013; Watson et al., 2008). The quality and representativeness of existing source emission data are often questionable because of a lack of information for different process configurations to account for site-specific differences, and data based on measurements using older, less sensitive or selective techniques. Therefore, there is a need for real-world source emission data from specific sources and locations using state-of-the-art measurement technologies to provide more reliable emission estimates. Gases and particles

collected from dilution sampling can be submitted to comprehensive laboratory chemical source profile analysis (Chow and Watson, 2012).

1.2 Study Objectives

The goal of this study is to quantify emissions from major emitters in the AOSR under real-world conditions. Emissions and chemical characteristics from three selected stacks measured by a dilution sampling system are reported here.

Specific objectives are to:

- Develop, test, and apply a dilution sampling system to quantify stack emissions that more realistically represent actual operations of modern stacks than compliance tests.
- Quantify emission rates (ERs) from major stacks in the AOSR under real-world conditions. Quantified pollutants include CO, carbon dioxide (CO_2), NH_3, NO_x, hydrogen sulfide (H_2S), SO_2, PM_1 (particles with aerodynamic diameters < 1 μm), $PM_{2.5}$, PM_{10}, and PM_{25} (particles with aerodynamic diameters < 25 μm).
- Determine chemical source profiles for $PM_{2.5}$ for receptor modeling source apportionment and speciated emission inventories.

1.3 Report Overview

Section 1 summarizes the background and differences between hot filter-impinger and dilution sampling methods and states the study goal and objectives. Section 2 describes different stack testing methods with a focus on comparing the hot filter-impinger and dilution sampling methods. Section 3 documents the dilution sampling and measurement system developed as part of this project and its application to measure emissions from three stacks in the AOSR during the summer of 2008. Experimental conditions, data reduction procedures, and laboratory analysis methods are also described. Section 4 describes analytical specifications and data validation. Section 5 summarizes particle size distribution, stack concentration, and emission rates for different pollutants. Section 6 explains the characteristics and chemical abundances of emission source profiles for $PM_{2.5}$. Section 7 summarizes study results. Section 8 is the bibliography and references. Appendix A lists the minimum detection limits (MDL) for gases, particle mass, filter light transmission (b_{abs}), elemental, ionic, carbon, and non-polar organic species analysis methods applied for this study. Appendix B plots the real-time stack velocity, stack temperature, and pollutant (CO, CO_2, NO, PM_1, $PM_{2.5}$, PM_{10}) concentrations for each test.

2 Stack Sampling Methods

2.1 Certification Test Methods

The most common approach for determining PM emissions from stacks for compliance uses the Alberta Stack Sampling Code Method 5 (Alberta Environment, 1995), or U.S. EPA Method 5 (U.S.EPA, 2000a), or Method 17 (U.S.EPA, 2000b), as illustrated in Figure 2-1. The Alberta Method 5 (Figure 2-1a) is similar to U.S. EPA Method 5. It employs a glass-fiber filter external to the stack, retained at an elevated temperature (120 ± 14 °C), which allows collection of particles independent of stack flue gas temperature and precludes the condensation and collection of water. Some variants of U.S. EPA Method 5 (e.g., Methods 5B and 5F) specify the filter temperature to be at 160 ± 14 °C to minimize the collection of H_2SO_4 (Myers and Logan, 2002). These high temperatures also preclude collection of several organic and inorganic compounds (e.g., sulfates, nitrates, fluorides, and metals) from stack emissions. Therefore, differences in the filter temperature will result in variations in collected mass. U.S. EPA Method 17 (Figure 2-1b) uses an in-stack filter to capture solid and liquid particles present at stack temperature and the mass collection therefore depends on the stack temperature. The filtered stack emissions are sent through a set of solutions contained in impingers immersed in an ice bath that capture condensed PM as well as gases that penetrate the hot filter. This configuration was adequate in the early 1960s when it was developed, since large stacks were uncontrolled and had high emissions of primary fine and coarse particles. The impingers were intended to determine condensable PM, which was expected to be small compared to the large masses of particles captured on the front filter. However, this five-decade old test method does not apply to today's well-controlled industrial processes that are equipped with efficient control devices. The condensable PM is not measured by the hot filter, resulting in an underestimation of PM. The downstream impinger, intended to capture condensable PM, also absorbs gaseous SO_2 and volatile organic compounds (VOCs) from the effluent, thereby overestimating actual PM emissions. The controversy regarding the representativeness of PM measured in the impingers led to the omission of the back-half catch analysis from the U.S. EPA Method 5 in the United States (Corio and Sherwell, 2000). In addition, neither the front glass-fiber filters nor the impinger catches are amenable to the types of chemical analyses that are commonly applied to ambient PM samples and that facilitate receptor-oriented source apportionment.

The promulgation of the U.S. National Ambient Air Quality Standards (NAAQS) (Bachmann, 2007; Chow et al., 2007c) for PM_{10} in 1987 created a need for measurement methods for PM_{10} emissions from stationary sources. To satisfy this need, U.S. EPA introduced Method 201A in 1990, which was further updated in 2010 (U.S.EPA, 2010a). Method 201A uses in-stack PM_{10} and $PM_{2.5}$ cyclones to remove larger particles and an in-stack filter to capture filterable particles. To capture the vapor phase species that would condense upon discharge into ambient air, U.S. EPA added Method 202 (U.S.EPA, 2010b). In the 1990 version of Method 202, the filtered gas was quenched in cold water to condense vapors. The impinger solution was extracted with methylene chloride ($MeCl_2$) to separate the organic and inorganic fractions, which were dried and weighed separately. Similar to Method 5, the impinger methods for condensable PM in Method 202 were subject to several artifacts: 1) dissolution of SO_2 and NO_x into water with subsequent oxidation to PM sulfate and nitrates, respectively, in the impingers; 2) dissolution of soluble organic compounds in water; and 3) gas phase reactions between NH_3 and SO_2 and/or hydrogen chloride (HCl) in the impingers(Richards et al., 2005; Corio and Sherwell, 2000).

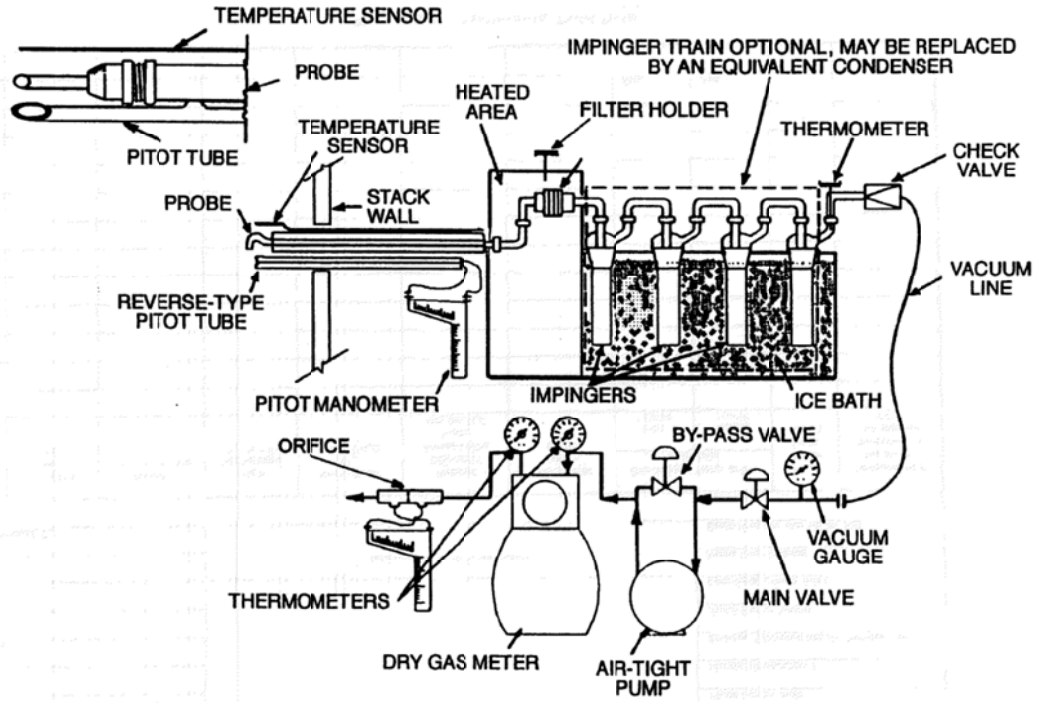

(a)

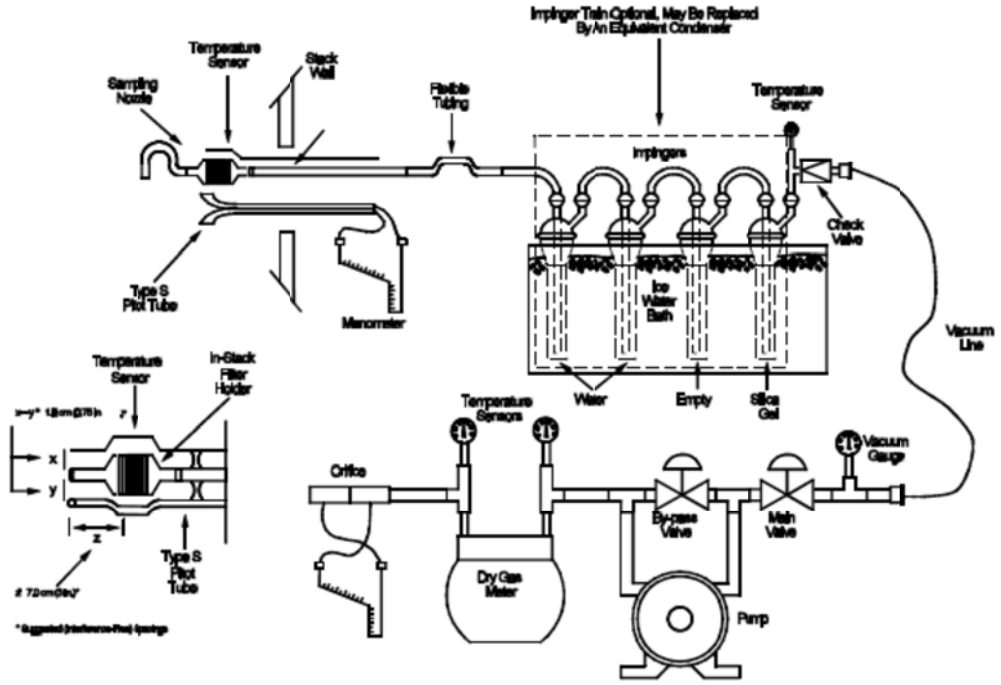

(b)

Figure 2-1. Sampling system for measuring total suspended particulate (TSP) compliance emissions from stationary sources using: (a) Alberta Method 5 (Alberta Environment, 1995) and (b) U.S. EPA Method 17 (U.S.EPA, 2000b).

Since gas phase reactions between NH_3, SO_2, and other atmospheric components take place over time during plume transport, these gases should not be included as part of the primary PM emissions. As $(NH_4)_2SO_4$ and/or ammonium chloride (NH_4Cl) mass are formed in the impingers, the mass added to the front filter would result in overestimation of PM emissions. Although optional provisions such as allowing for purging of the absorbed SO_2 from the impinger water for one hour after sampling to minimize positive bias, the effectiveness of purging is directly related to the pH of the solution which varies from stack to stack (Corio and Sherwell, 2000). Method 202 was also criticized for a lack of precision (Myers and Logan, 2002). In 2010, U.S. EPA revised Methods 201A and 202 (Figure 2-2) with the intent to reduce sampling artifacts and increase precision.

Most gases are measured by compliance methods using wet chemistry (i.e., pulling the gas through absorbing solutions with subsequent laboratory analyses). U.S. EPA Methods 6 and 7 measure SO_2 and NO_x, respectively, as shown in Figure 2-3. For Method 6, SO_2 and sulfur trioxide (SO_3) are adsorbed in impinger solutions and SO_2 is analyzed by the barium-thorin titration method. In Method 7, a grab sample is collected in an evacuated flask containing a dilute H_2SO_4-hydrogen peroxide (H_2O_2) absorbing solution. The NO_x, except nitrous oxide (N_2O), is measured colorimetrically using the phenoldisulfonic acid (PDS) procedure. A complete list of Code of Federal Register (CFR) Promulgated Test Methods can be found at the U.S. EPA website: http://www.epa.gov/ttn/emc/promgate.html. These wet chemical methods are costly and easily contaminated in an industrial environment. They were abandoned many years ago for ambient sampling and were not considered for mobile source emissions testing. It is only tradition and their inclusion in the U.S. Code of Federal Regulations that encourages their use in the U.S. Unfortunately, many other countries not subject to U.S. rules have adopted these antiquated methods instead of leapfrogging ahead to more cost effective and real-world methods (Chow and Watson, 2008; 2010a).

2.2 Dilution Sampling Methods

To achieve a more realistic representation of actual PM emissions and chemical compositions, it is necessary to simulate the diluting, cooling, and aging of the hot exhaust under conditions that simulate plume discharge to the atmosphere (Hildemann et al., 1989; Watson, 2002). Dilution sampling methods are widely used to simulate ambient conditions and are the standard reference method (SRM) for automotive emissions (e.g. ISO 8178). This concept is readily adaptable to stack tests. Stack dilution sampling systems have long been used to obtain source profiles for receptor modeling studies (Heinsohn et al., 1980; Huynh et al., 1984; Harris, 1986; Sousa et al., 1987; Olmez et al., 1988; Cooper et al., 1989; Hildemann et al., 1989; Hueglin et al., 1997; England et al., 1998b; England et al., 1998a; England et al., 2007a; Zielinska et al., 1998; Corio and Sherwell, 2000; Lee et al., 2000; McDonald et al., 2000; Watson et al., 2001a; Watson et al., 2002; Watson and Chow, 2001; Lipsky et al., 2002; Seames et al., 2002; Maguhn et al., 2003; Chang et al., 2004b; Chang and England, 2004a; Chang et al., 2004a; Chang et al., 2005; Chow et al., 2004b; Lee et al., 2004; Lipsky et al., 2004; Jimenez and Ballester, 2005; Lipsky and Robinson, 2005; Yi et al., 2006; Budd et al., 2007; Sheya et al., 2008; Tsukada et al., 2008; England et al., 2007a; 2007b; England et al., 2000). The American Society for Testing and Materials (ASTM) was developing a dilution sampling guidance for stationary source certification that better reconciles the current discrepancy between stationary or mobile source emissions and ambient PM measurements (ASTM International, 2010).

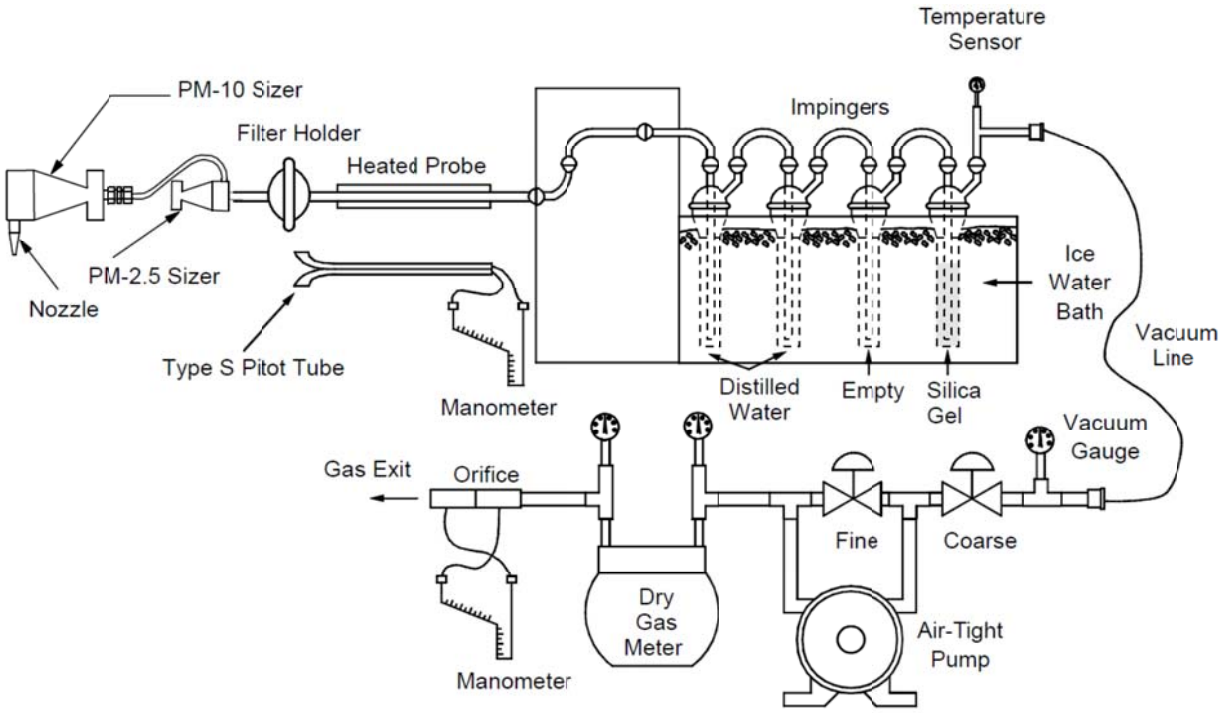

Figure 2-2. Sampling system for measuring filterable PM_{10} compliance emissions from stationary sources using U.S. EPA Methods 201A and 202 (U.S.EPA, 2010a; U.S.EPA, 2010b).

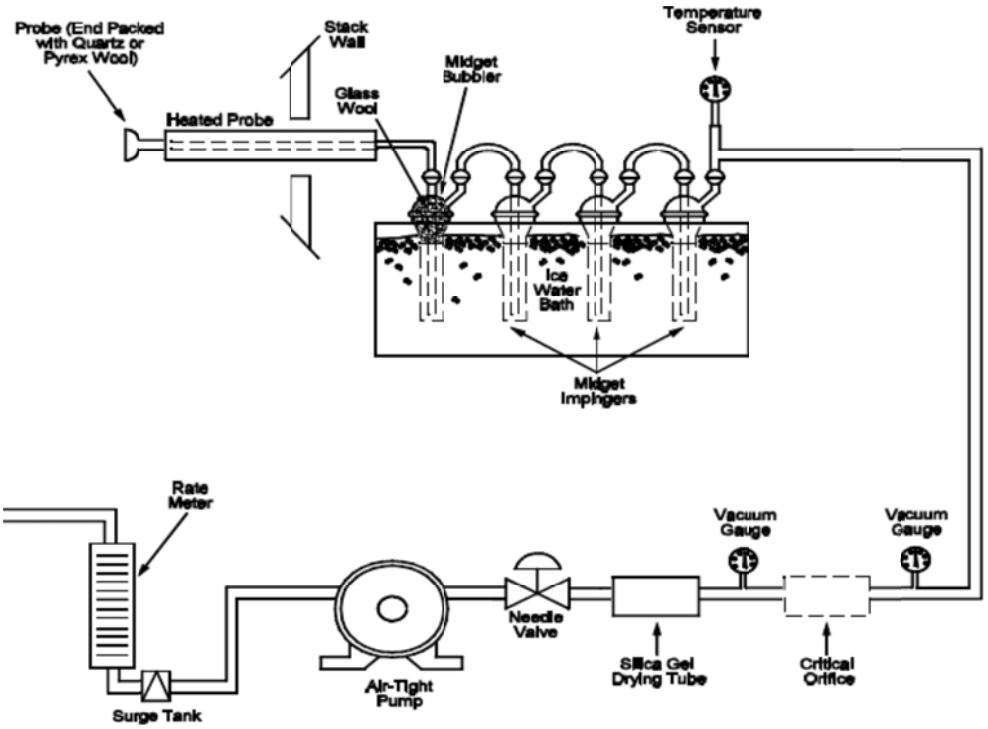

(a)

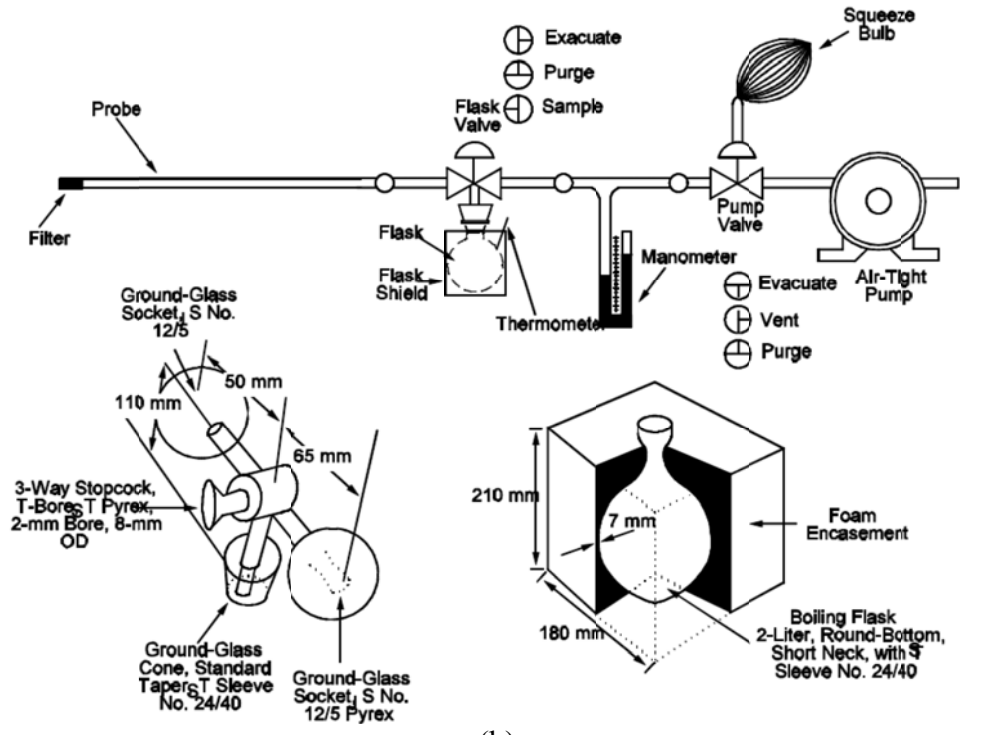

(b)

Figure 2-3. Sampling systems for: (a) SO_2 by U.S. EPA Method 6 (U.S.EPA, 2000c) and (b) NO_x by U.S. EPA Method 7 (U.S.EPA, 2000d).

The Emission Measurement Center of the U.S. EPA's Office of Air Quality Planning and Standards (OAQPS) is also developing a Federal Reference Method (FRM) to better characterize the source emissions of both filterable and condensable PM based on the dilution sampling method (Myers and Logan, 2002). The U.S. EPA Conditional Test Method (CTM) 039 uses dilution sampling method to measure $PM_{2.5}$ and PM_{10} (U.S.EPA, 2004). If the dilution sampling method is adopted, the historic PM emission factors for stationary sources will require retesting and updating (England et al., 2007a).

In a dilution sampling system, as illustrated in Figure 2-4, gases are extracted at stack temperatures by a probe similar to the one used in Method 5. The stack effluent enters a dilution chamber where it is mixed with clean filtered air to bring the emissions to ambient temperatures. The diluted mixture is then routed to a residence chamber where rapid chemical reactions, particle nucleation, condensation, and coagulation can take place, and the gas-particle partitioning can reach equilibrium (Hildemann et al., 1989). Continuous monitors and a set of filter packs, cartridges, and canisters can be connected to the residence chamber to measure components in the diluted exhaust. Flow rates of stack air, dilution air, and sampler air are measured to calculate the dilution ratio.

Although the design shown in Figure 2-4 was used in several source apportionment studies, it has several drawbacks. First, it is large and cumbersome, making it time consuming and difficult to move and place on stack sampling platforms. Sometimes, it cannot fit on smaller source testing platforms. Second, the venturi in the sampling probe removes some of the larger particles although all $PM_{2.5}$ will pass into the residence chamber. Furthermore, the venturi is not an accurate flow measurement device, which sometimes causes uncertainties in dilution ratios.

Based on the evolution of the ultrafine and accumulation modes of particle size distributions, the aging time needed to bring the particles into equilibrium for emissions from coal, residual oil, and natural gas combustion were evaluated by Chang et al. (2004b). The completion of immediate particle nucleation, agglomeration, evaporation, and condensation processes are deemed complete when the particle size distribution does not change with further dilution or aging. For the natural gas combustion experiments, Figure 2-5 demonstrates that equilibrium was not achieved at 10:1 dilution ratios, but it was achieved at 20:1 and larger dilution ratios using the dilution sampling system configuration shown in Figure 2-4. Natural gas emissions represent a worst-case situation for equilibrium because there are few larger particles on which cooled gases can condense. Coal and residual oil boilers reached equilibrium even at a 10:1 dilution ratio owing the presence of many primary particles upon which gases could rapidly condense.

Using the dilution sampling system shown in Figure 2-4, Chang et al. (2004b) discovered that the right angle joint between the sampling probe and the U-shaped dilution tunnel did not engender good mixing until the flow reached the end of the U-shaped dilution tunnel (Chang and England, 2004a). By adding a diffuser, Chang et al. (2004b) demonstrated that equilibrium was achieved before entry into the residence chamber, thereby making it unnecessary.

Figure 2-6 compares PM ERs from the hot filter-impinger method (U.S. EPA Method 201A/202) with ERs from the dilution sampling method applied to gas-fired boiler emissions. The mass collected on the in-stack filter by Method 201A/202 was near or below the system detection limit, and was much lower than that measured by the dilution sampling system. Most of the impinger catch consisted of dissolved organic- and sulfur-containing gases, and adding these to the emission rate overestimates actual $PM_{2.5}$ emissions by orders of magnitude. Large

discrepancies were also found for $PM_{2.5}$ emissions between the dilution sampling system and those reported in the U.S. EPA Compilation of Air Pollution Emission Factors (AP42).

In summary, the filterable PM captured on the filter in compliance testing methods underestimates stack emissions since it does not account for the PM that forms after the emissions exit the stack, while the summation of filterable PM and condensable PM overestimates stack emissions due to positive artifacts in the impinger that captures dissolved organic and inorganic gases. A dilution sampling system that simulates ambient dilution processes of stack exhaust most likely provides representative estimates of stack emissions.

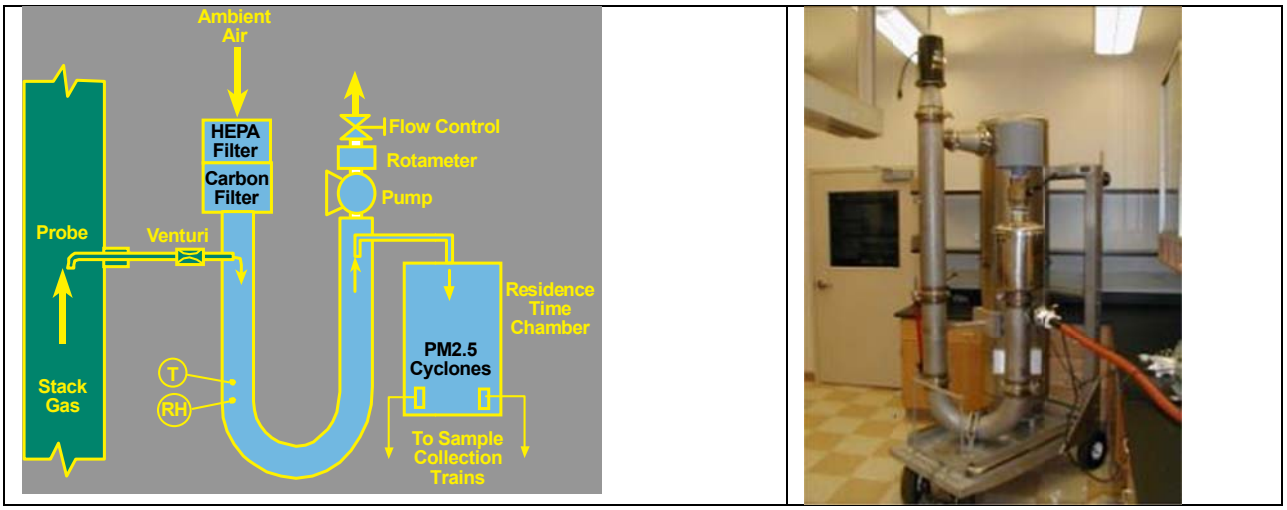

Figure 2-4. Stack dilution sampling system developed for acquiring real-world $PM_{2.5}$ stack emissions and source profiles (Hildemann et al., 1989).

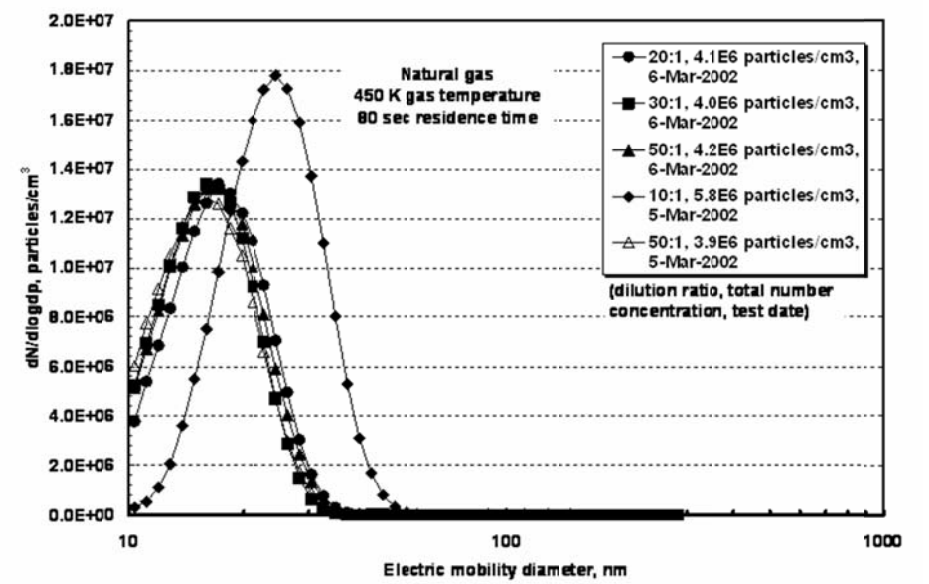

Figure 2-5. Equilibration of the particle size distribution for different dilution ratios when testing emissions from a natural gas boiler (Chang et al., 2004b).

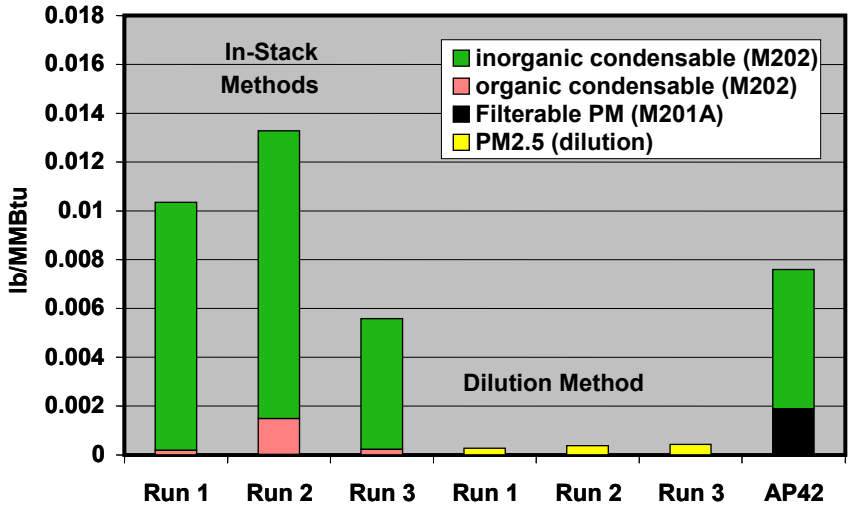

Figure 2-6. Comparison tests between Method 201A/202 and a dilution sampling system for $PM_{2.5}$ samples acquired from natural gas-fired boiler emissions. Condensable PM also includes gaseous emissions captured by the impinge and measured as PM (England et al., 2000) .

3 Experimental Configuration

3.1 Overview

Diluted effluent samples were acquired from three stacks from two AOSR facilities (hereafter referred to as Facilities A and B) during the summer of 2008 (Wang et al., 2012). A sample of the flue gas was drawn from the stack, diluted with filtered ambient air and, and quantified for CO, CO_2, NO, particle size distribution, and size-segregated PM mass concentrations in real time. Integrated filter pack samples were acquired for laboratory analyses of NH_3, H_2S, SO_2, and $PM_{2.5}$ mass, filter light transmission (b_{abs}), and chemical composition. $PM_{2.5}$ chemical compositions included elements, lead isotopes, water-soluble ions, organic and elemental carbon (OC and EC, respectively) in eight thermal fractions, water soluble organic carbon (WSOC), and organic compounds including polycyclic aromatic hydrocarbons (PAHs).

3.2 Stack Emission Sampling and Measurement

3.2.1 Dilution Sampling System

The dilution sampling system is illustrated in Figures 3-1 and 3-2. A sample of ~ 5 L/min flue gas was drawn isokinetically from the stack with a buttonhook sampling probe (Figure 3-3) similar to that used by U.S. EPA Method 5 (U.S.EPA, 2000a) and diluted by clean dilution air. The 2.4 m-long sampling line was heated to 5 °C above the stack temperature to the point where dilution air was introduced. The dilution air was generated by blowing ambient air through an activated charcoal capsule filter followed by a high efficiency particulate air (HEPA) filter to remove volatile gas contaminants and particles, respectively. The dilution flow rate was controlled by a mass flow controller. In these tests, the dilution factor was at least 20:1 to simulate the real-world ambient cooling and dilution. The sample and dilution air were mixed in the dilutor illustrated in Figure 3-4 (England et al., 2007a). The diluted sample passed through a spiral residence chamber (see Figure 3-2) for ~28 seconds, nearly three times longer than the minimum aging time (10 seconds) required to produce stable gas/particle equilibrium (Chang et al., 2004b). The spiral shape of the residence chamber is more compact and portable than the previously-used dilution sampling system shown in Figure 2-4. It offers more flexibility in size and installation as shown in Figure 3-2. The probe was inserted straight into the stack without a bend, and the dilution chamber size can be increased with additional sections when PM levels are low or stack temperatures are high, requiring more aging time. The diluted and well-mixed sample passed through the residence chamber and reached a manifold where it was split into multiple streams for quantification by both real-time instruments (Table 3-1) and integrated filter packs (Figure 3-5). The sampling probe, dilutor, residence chamber, and manifold are made of stainless steel. Downstream of the manifold, Teflon tubing was used for connecting to gas instruments, and flexible conductive tubing was used for connecting to particle instruments. Such arrangement minimized gaseous reactions and particle losses during transport.

Particle losses through the dilution system without the 2.4 m-long sampling probe were evaluated prior to the field measurement using monodisperse polystyrene latex spheres (PSL) of five sizes (0.5, 1.0, 2.5, 5.0, and 10.0 μm) entrained in sample flow heated to 70 °C and diluted by a factor of ~20. The measured transmission efficiencies were ~100% for 0.5–5 μm PSL and 86.2±18.6% for 10 μm PSL. Particle losses through the 2.4 m sampling probe were estimated for

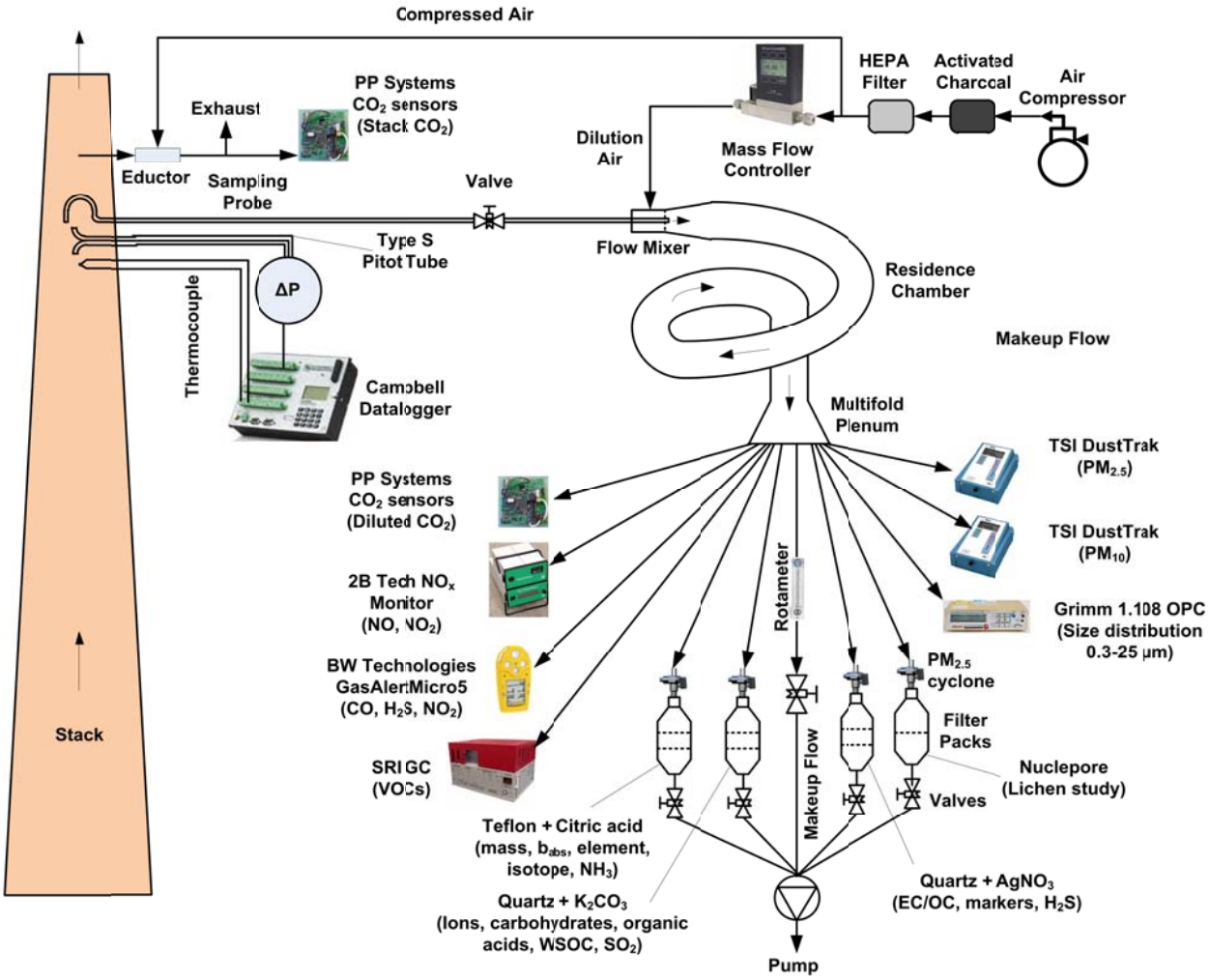

Explanation of abbreviations:

Abbreviation	Parameter	Abbreviation	Parameter/Instrument
ΔP	differential pressure	NH_3:	ammonia
$AgNO_3$:	silver nitrate	NO:	nitrogen oxide
b_{abs}:	filter light transmission, surrogate for black carbon	NO_2:	nitrogen dioxide
CO:	carbon monoxide	OC:	organic carbon
CO_2:	carbon dioxide	OPC	optical particle counter
EC:	elemental carbon	$PM_{2.5}$	particles with aerodynamic diameter <2.5 µm
H_2S:	hydrogen sulfide	PM_{10}	particles with aerodynamic diameter <10 µm
GC:	gas chromatography	VOCs	volatile organic compounds
K_2CO_3:	potassium carbonate	WSOC:	water-soluble organic carbon

Figure 3-1. Schematic diagram of dilution sampling system.

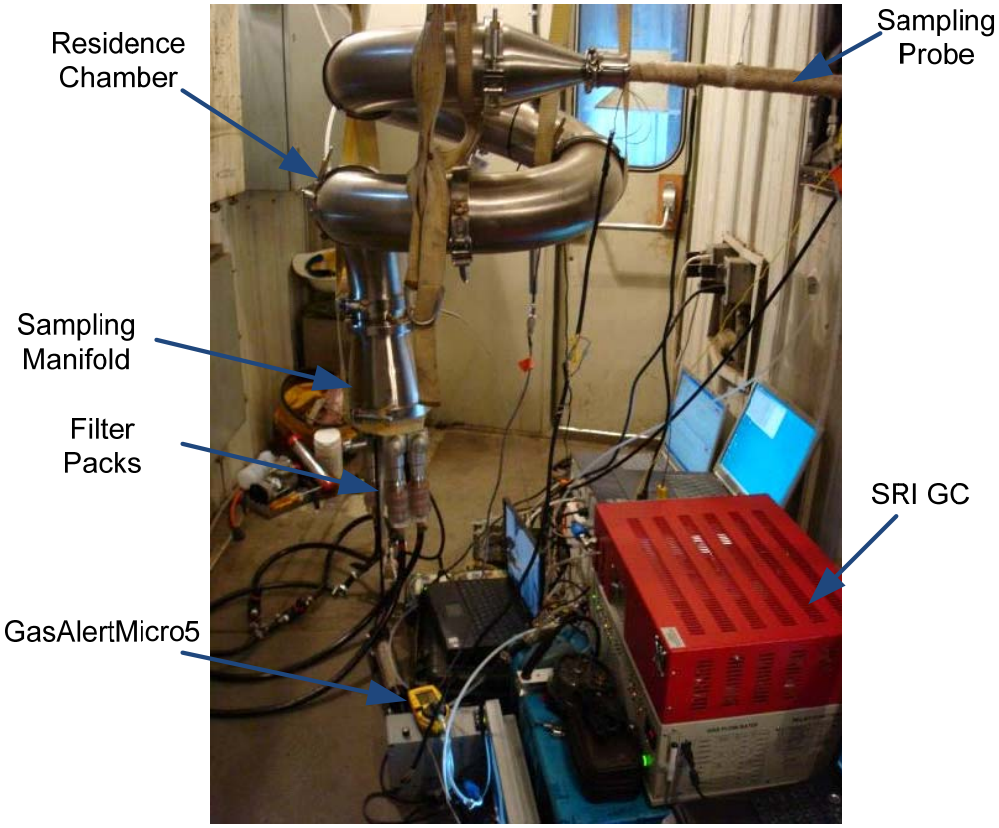

Figure 3-2. Dilution sampling system operating in a stack from Facility A at AOSR.

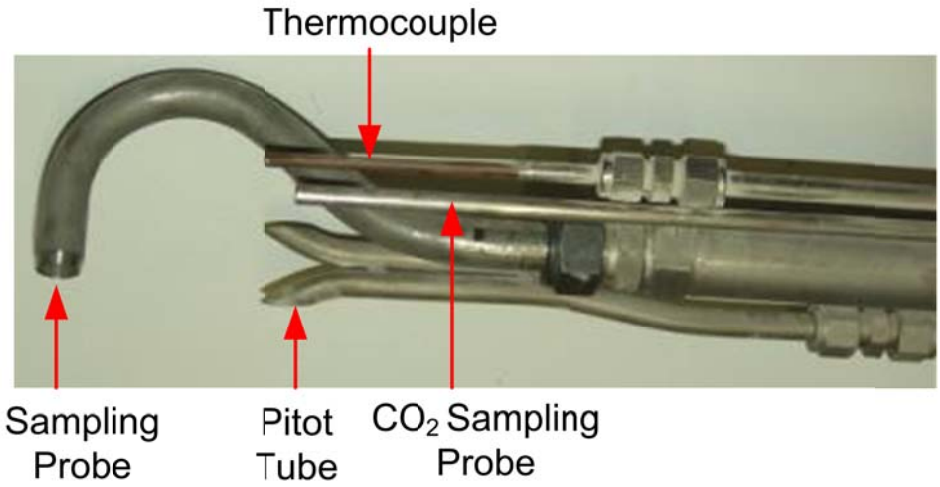

Figure 3-3. In-stack sampling probe, pitot tube, thermocouple, and CO_2 sampling probe.

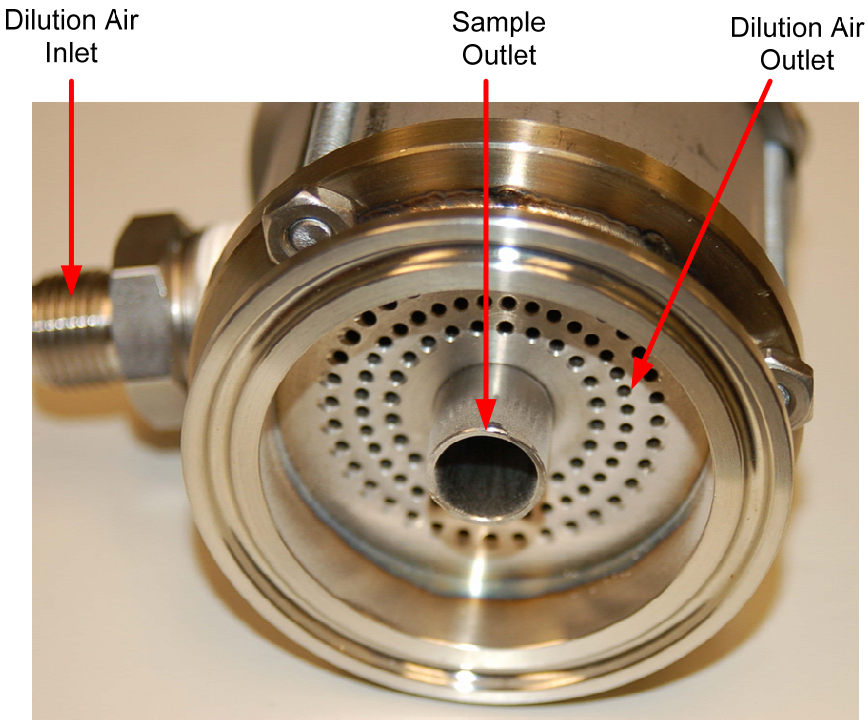

Figure 3-4. Dilution and mixing system. The flue gas sample is introduced in the center and dilution air is introduced from the diffuser plate with holes. Turbulence generated downstream of the holes helps mixing of the flue gas sample and dilution air.

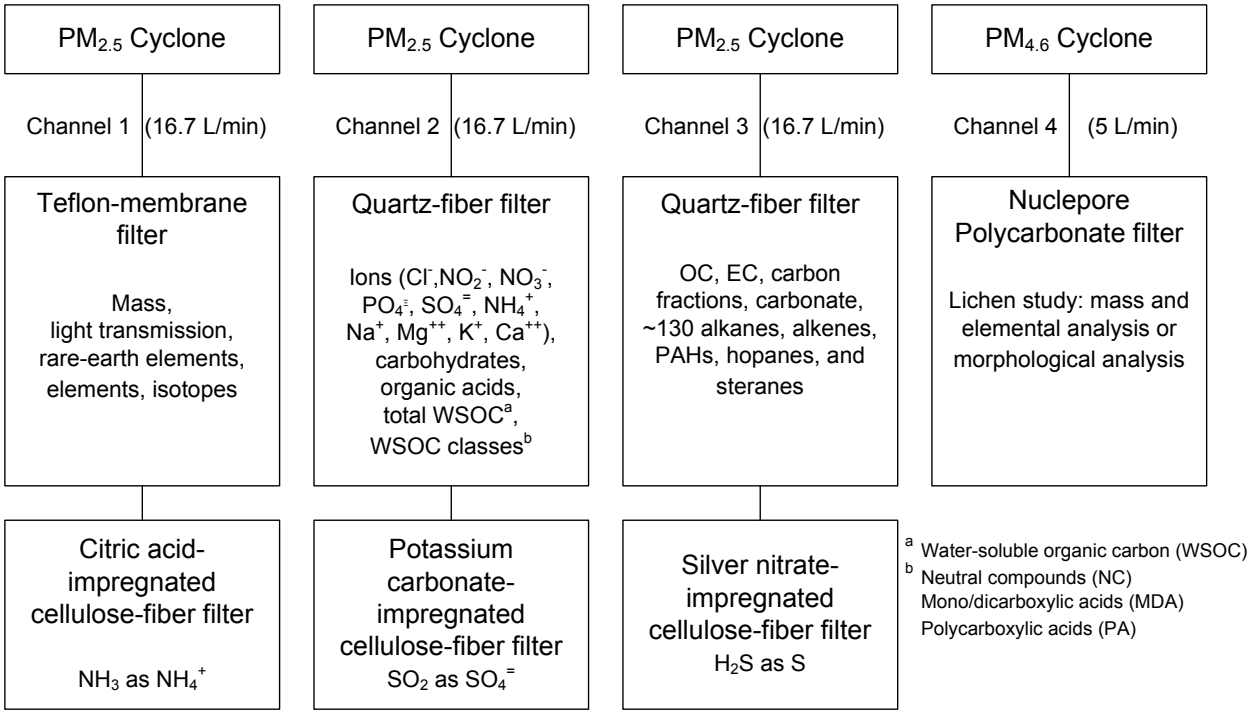

Figure 3-5. Four-channel filter pack sampling configuration that accompanies the DRI dilution sampling system for AOSR stationary source characterization.

Table 3-1. Real-time instruments applied to the stack emission testing at AOSR.

Instrument	Parameter of Interest and Measurement Principles	Measurement Range	Time Resolution	Nominal Precision/Accuracy
PP System CO_2 analyzers Model SBA-4	CO_2 by non-dispersive infrared (NDIR) Stack gas stream Diluted sample stream	0-20,000 ppm 0-5,000 ppm	~1.5 s	<1% of span concentration
2B Tech NO Monitor and NO_2 Converter Model 400 and 401[a]	NO, NO_2, NO_x by reaction with O_3	2-2000 ppbv	10 s	Higher of 3 ppbv or 3% of reading
BW Technologies Multi-Gas Detector Model GasAlertMicro 5[b]	O_2 by electrochemical sensor CO by electrochemical sensor H_2S by electrochemical sensor NO_2 by electrochemical sensor Combustible gases lower explosive limit (LEL) by catalytic bead sensor	O_2: 0-30% CO: 0-500 ppm H_2S: 0-500 ppm NO_2: 0-99.9 ppm LEL: 0-100%	30 s	O_2: 0.1% CO: 1.0 ppm H_2S: 1.0 ppm NO_2: 1.0 ppm LEL: 1%
SRI Portable GC Model 8610C	Volatile organic compound (VOC) by GC separation and detection	Species dependent	20 min	PID[c] for aromatics: 10 ppb FID[c] for hydrocarbons: 1 ppm DELCD[c] for halogens: 10 ppb
TSI DustTrak Model 8520	PM mass concentration by light scattering ($PM_{2.5}$ or PM_{10})	Size: ~ 0.1-2.5 µm or 0.1-10 µm Mass: 0.001-100 mg/m^3	1 min[d]	±20% (for calibration aerosol)
Grimm Optical Particle Counter (OPC) Model 1.108	Particle size distribution by light scattering	Size: 0.23-25 µm Number: 0.001 to 2,000 particle/cm^3 Mass: 0.0001 to 100 mg/m^3	1 min[e]	±2.5%
Pitot tube	Stack velocity	1-100 m/s	1 min	±2.5%
Thermocouple	Stack temperature	-200 to 1250°C	1 min	Greater of 2.2°C or 0.75%

a. The 2B Tech NO_2 converter did not work in this study. Therefore, only NO was measured.

b. Only CO was accurately measured by the Model GasAlertMicro 5.

c. PID: photoionization detector; FID: flame ionization detector; DELCD: dry electrolytic conductivity detector.

d. Data were recorded as 1 minute average in this study., but a 1 second average can be achieved

e. Data were recorded as 1 minute average in this study, but a 6 second average can be achieved

Brownian diffusion and gravimetric setting under stack sampling conditions (Kulkarni *et al.*, 2011). The overall transmission efficiencies are estimated to be ~100% for 0.1–1 μm, 96–98% for 2.5 μm, 46–56% for 10 μm, and 0% for ≥18 μm.

Parallel to the sampling probe, a type S pitot tube (see Figures 3-1 and 3-3) measures the pressure difference (ΔP) between the two openings, from which the stack flow velocity and flow rate can be calculated according to U.S. EPA (2011) Method 2. The stack temperature (T) is measured by a type K thermocouple. The ΔP and T are recorded by a data logger (Model 21X, Campbell Scientific, Logan, Utah). In an initial setup during sampling from Stack A at Facility A, the stack CO_2 concentration was measured by a CO_2 analyzer (Model SBA-4, PP Systems, Amesbury, MA) connected directly to the sampling probe upstream of the dilution gas introduction. During the first run, excess water vapor in the flue gas caused the CO_2 analyzer to malfunction after 30 minutes. For the remaining Stack A tests, the flow rate from the sampling probe was measured, and the dilution ratio was calculated from the dilution and sample flow rates. For sampling of the other two stacks, the stack CO_2 measurement was switched to the configuration shown in **Error! Reference source not found.**, where the flue gas was extracted from the stack by an eductor pump and diluted by a factor of 21.4 with filtered air, thus reducing water vapor concentrations to levels permitted by the CO_2 analyzer.

Compliance stack sampling typically requires traversing multiple sampling points across the stack cross section (Alberta Environment, 1995). The sampling point was fixed at a radial location in this study. A velocity traverse measurement in Stack A showed that the velocity at the sampling point (1.5 m from the stack wall) was only 3% different from the average stack velocity. Since $PM_{2.5}$ disperses with flow due to its low inertia, it was assumed that velocity and concentrations at the sampling point represent the average values.

3.2.2 Real-time Gas Measurement Instruments

Specifications for real-time gas monitoring instruments are provided in Table 3-1. The instruments included: 1) PP System CO_2 Analyzer (Model SBA-4, Amesbury, MA), 2) 2B Tech NO Monitor and NO_2 Converter (Models 400 and 401, Boulder, CO), 3) BW Technologies Multi-Gas Detector (Model GasAlertMicro 5, Arlington, TX), and 4) SRI Gas Chromatographs (Model 8610C, Torrance, CA). Most of these instruments are miniaturized for source and aircraft sampling. Table 3-1 also details some instrument malfunctions during sampling.

3.2.2.1 PP System CO_2 Analyzer:

The PP System CO_2 analyzer is based on non-dispersive infrared (NDIR) measurement techniques to quantify CO_2. It automatically zeros every 20 minutes to account for the sensor drift by passing the sample air through a soda lime CO_2 scrubber. For this study, two CO_2 analyzers were used: one sampled the stack gas stream (with a measurement range of 0 - 20,000 ppm), and the other measured the diluted sample stream (with a measurement range of 0 - 5000 ppm).

3.2.2.2 2B Tech NO Monitor and NO_2 Converter:

The 2B Tech NO monitor quantitatively measures NO by its reaction with ozone (O_3):

$$NO + O_3 \rightarrow NO_2 + O_2 + h\nu \tag{3-1}$$

Instead of measuring radiation emitted from the reaction as in chemiluminescence NO analyzers, the 2B Tech NO monitor quantifies NO by gas-phase titration, measuring the decrease

in O_3. This is accomplished by producing a known amount of O_3 (4 ppm) and measuring the remaining O_3 after it reacts with NO using an ultraviolet (UV) lamp (low pressure mercury, 254 nm) and a photodiode detector. The NO_2 converter uses a molybdenum catalyst heated to 325 °C to reduce NO_2 to NO. The reduced air stream is then passed into the NO monitor to measure NO_x with contributions from both NO in the original sample stream and NO converted from NO_2. The NO_2 converter can switch between allowing the sample air stream pass through the molybdenum catalyst to measure NO_x (in the NO analyzer) or to bypass the catalyst to measure NO. The difference between NO_x and NO is NO_2 assuming the concentration is stable between the switching. For this study, the switching between analyzing NO and NO_x was set to every 5 minutes and the concentration measurement range is 2 – 2000 ppbv. Unfortunately, it was found that NO_2 converter did not perform adequately in this study showing near zero NO_2 concentrations, and only NO is reported in this report.

3.2.2.3 BW Technologies Multi-Gas Detector:

The BW Technologies Multi-Gas Detector measures five gases: O_2, CO, H_2S, NO_2, and combustible gases (Lower Explosive Limit [LEL]). It uses four different sensors: O_2 by a capillary controlled concentration electrochemical cell; CO and H_2S by a twin plug-in electrochemical cell; NO_2 by a single plug-in electrochemical cell; and combustible gases by a plug-in catalytic bead sensor.

3.2.2.4 SRI Gas Chromatographs:

The portable SRI Gas Chromatograph traps VOCs on Tenax-GR and Carbon Molecular Sieve traps, purging them onto a 60 m capillary column (5.0 μ DB-1 Type MXT-1) with detection of: 1) hydrocarbons by flame ionization detector (FID); 2) aromatics and molecules with double carbon bonds by photoionization detector (PID); and 3) halogens by dry electrolytic conductivity detector (DELCD) in series. This instrument requires frequent calibration with standards to account for retention time drift. The GC was calibrated before and after the field study with EPA-TO14 calibration standards (Scott Special Gases, Plumsteadville, PA). Because some VOCs co-elute, ultimate species identifications require a companion canister sample to be analyzed by gas chromatography/mass spectrometry (GC/MS).

3.2.3 Real-time Particle Measurement Instruments

Two real-time continuous particle measurement instruments were used: 1) TSI DustTrak (Model 8520, Shoreview, MN), and 2) Grimm Dust Monitor (Model 1.108, Douglasville, GA) to acquire $PM_{2.5}$, PM_{10}, and particle size distribution (0.23 – 25 μm) with one-minute averages. Instrument specifications are listed in Table 3-1, and more detailed descriptions are given below:

3.2.3.1 TSI DustTrak:

The TSI Model 8520 DustTrak measures the amount of light scattered by particles illuminated by a laser beam (wavelength 780 nm). Two DustTraks equipped with PM_{10} or $PM_{2.5}$ impactor inlets were operated in parallel. Each DustTrak was calibrated by the manufacture prior to the field study with Arizona Road Dust (ARD). When the aerosol being measured differs from ARD in composition and size, custom calibration factors are used to scale the indicated concentration to be equivalent with gravimetric concentrations.

3.2.3.2 Grimm Dust Monitor:

The Grimm Model 1.108 Dust Monitor is an optical particle counter (OPC). It acquires PM size distribution in 0.23 – 25 μm range by measuring the amount of light scattered by individual particles, which is converted to the geometric particle diameter. Particles are assigned to one of 16 size bins based on the scattered pulse height. The instrument can report the size distribution in either number or mass mode assuming spherical particle shape and certain density. The Grimm OPC is calibrated at the factory using a three-step process: 1) verify against a standard unit for proper size classification; 2) verify gravimetric mass concentration for fine particles using stearin-acidity aerosol; and 3) verify gravimetric mass concentration for coarse particles using spherical glass beads. For this study, the instrument was set to report mass distributions.

3.2.4 Integrated Filter Sampling

Integrated gaseous and PM samples are collected on filter packs. **Error! Reference source not found.** depicts the filter pack assembly and analysis parameters of the four parallel sampling channels. Each filter pack is preceded by a very sharp cut $PM_{2.5}$ cyclone (Model VSCCA, BGI Inc., Waltham, MA). The filter holders are 47 mm Swin-Loks (Model 420400, GE Healthcare Life Sciences, Piscataway, NJ). Flow rates of 16.7 L/min were drawn through the Teflon®-membrane and quartz-fiber filters and 5 L/min were drawn through the Nuclepore polycarbonate-membrane filter (the cyclone cut size was ~4.6 μm at 5 L/min). Lower flows rates were used for the Nuclepore polycarbonate-membrane filter to minimize particle overloading for morphological analysis. The flow rates were set at the beginning of the experiment by adjusting the valves while referencing a calibrated rotameter, and verified after sampling to ensure flow-rate stability was within ±10% of pre-set values. Flow rates at the beginning and end of tests were averaged for sample volume calculation.

3.3 Stack Information and Sampling Conditions

The stacks selected for testing were identified by Clearstone Engineering Ltd. (2006) as among the largest stationary source emitters in the AOSR. Emissions were measured at the main stack and a flue gas desulfurization (FGD) stack from Facility A (i.e., Stacks A and B, respectively), and from an FGD stack from Facility B (i.e., Stack C). Key parameters for the three stacks are listed in Table 3-1. The Stack A configuration is shown in Figure 3-6a. Overhead gas from two fluid coker burners, effluent from three utility boilers, ammonia overhead stream (~94 molar percent NH_3 and <0.5 mole percent H_2S) from the sour water plant, and sometimes effluent from the sulfur recovery units are incinerated in two CO boilers. The CO boilers are fired primarily on coker burner overhead gas with <5% refinery gas. During startup the CO boiler is fired with natural gas, but this did not occur during these tests. The boiler effluent then passes through two electrostatic precipitators (ESP) to remove most solid PM before being routed through Stack A and into the atmosphere. NH_3 in the gas stream enhances performance of the ESPs and partially neutralizes H_2SO_4 in the flue gas.

Figure 3-6b shows the block diagram of the FGD Stack B. The overhead gas from a fluid coker burner is first sent to a CO boiler to recover energy. The CO boilers also incinerate tail gas from Claus sulfur recovery units, which converts sulfur in the form of H_2S preprocessed in the amine plants to elemental liquid sulfur. Most particles in the boiler effluent are removed by an ESP. The hot off-gas exiting the ESP enters a spray tower where it is in contact with a diluted slurry of $(NH_4)_2SO_4$ containing an excess of NH_3. The SO_2 in the flue gas reacts with NH_3 and

produces a slurry, which drains into the tower sump. Air is added to the tower sump to produce crystalized $(NH_4)_2SO_4$, which is further processed to form a fertilizer grade granular $(NH_4)_2SO_4$ by-product. The treated flue gas is released via the FGD Stack B. The Stack B FGD process is designed to remove >90% SO_2. The actual SO_2 removal efficiency was 80-85% during the test period due to high sulfites from an initial excursion in May 2008.

Figure 3-7 shows that the FGD Stack C in Facility B receives flue gas from three coke-fired boilers. The coke feedstock contains 76–80% carbon, 6–9% moisture, and 5.6–5.9% sulfur (S). During these tests, the Coker Boiler 2 was offline. Flue gas from the boilers passes through three ESPs to remove particles, then enters a jet bubbling reactor (JBR), which is the heart of the FGD plant where SO_2 is scrubbed. Water, oxidation air and limestone slurry ($CaCO_3$) are added to the JBR to react with the flue gas. Adsorption takes place as SO_2 reacts with dissolved limestone and is oxidized to calcium sulfate ($CaSO_4$) which then crystalizes. The crystallization of the $CaSO_4$ produces a gypsum slurry that is drawn-off from the JBR and pumped to a sedimentation pond for dewatering. The recovered water from the gypsum pond is directed back to the FGD plant for reuse. Flue gas enters the FGD plant at a rate of ~1557 tonnes/hr at a temperature of ~307 °C, which is then cooled to ~63 °C by raw water spray and gypsum slurry spray. The FGD plant has an SO_2 removal efficiency up to 95%.

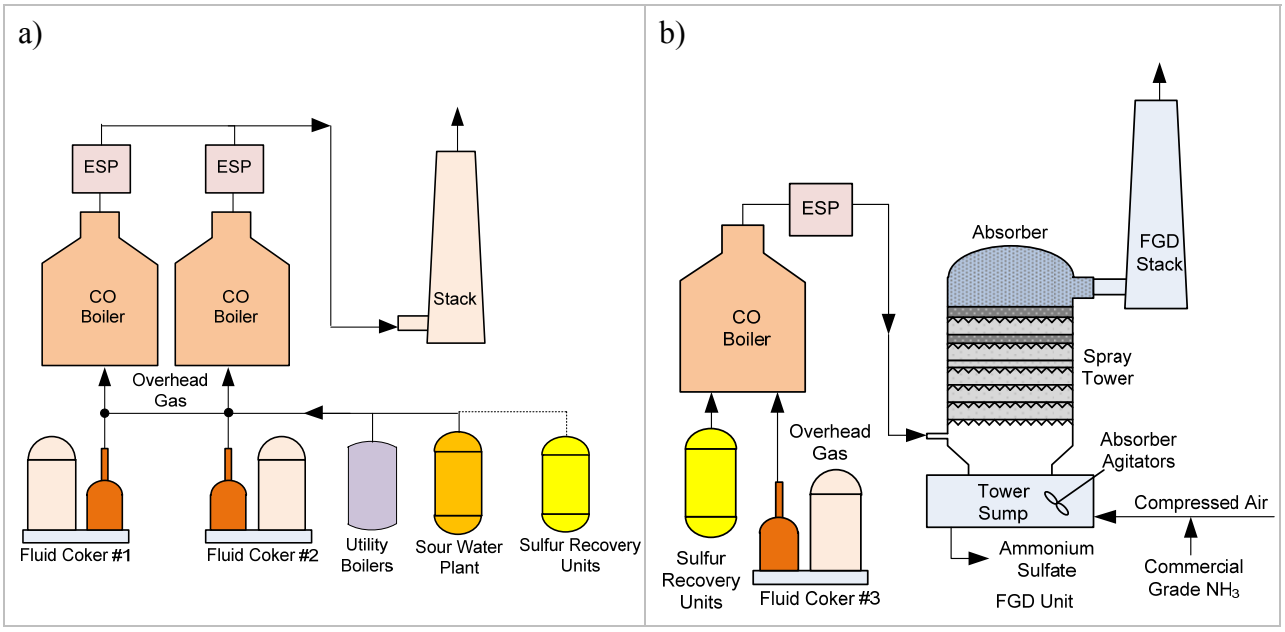

Figure 3-6. Configurations of: a) Stack A and b) FGD Stack B in Facility A.

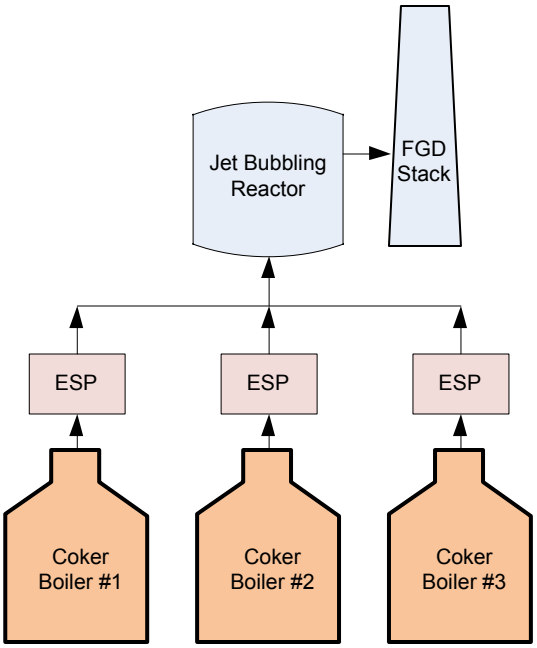

Figure 3-7. Block diagram of the flue gas contributing to the FGD Stack C in Facility B.

Table 3-2. Physical and operating parameters of the three stacks related to stack emission testing.

Stack Physical Characteristics	**Facility A**		**Facility B**
	Stack A	**Stack B**	**Stack C**
Stack inside diameter	7.94 m	6.10 m	7.01 m
Stack Height	183 m	94 m	91 m
Sampling point: Distance (in number of diameters) downstream from last bend	10.5	3.6	3.6
Distance (in number of diameters) upstream from stack outlet	9	3.8	3.8
Stack Operating Characteristics			
Typical velocity	26 m/s	17 m/s	12 m/s
Stack temperature at the sampling port	250 ^{o}C	74 ^{o}C	75 ^{o}C
Moisture content in percent volume	22%	34%	16%
Stack gauge pressure in inches of water column draft	28 "	29 "	29 "
Average ambient relative humidity- August 2007	80%	80%	80%
Sampling Port Characteristics			
Sampling Port Size	10.2 cm	10.2 cm	10.2 cm
Elevation of Sampling Port from Sampling Platform	1.5 m	1.1 m	1.5 m
Elevation of Sampling Platform above ground level	91 m	70 m	61 m
Ground level elevation above mean sea level	304 m	305.6 m	251 m

3.4 Test Procedures

Test procedures are summarized in Table 3-3. Background gas and PM concentrations were checked by sampling only dilution air to make sure the system was leak tight and instruments had reasonable background readings. Flow rates for unexposed and exposed filter packs were verified before and after sampling, respectively. Filter packs along with the field data sheet were packaged individually in an airtight container and stored cold in the sampling cooler.

A total of 19 sample runs were conducted and three field blanks were collected from 8/9/2008 to 8/20/2008, as shown in Table 3-4. Sample durations ranged from 120 to 180 minutes per run and dilution factors varied from 22:1 to 50:1 with ~25:1 dilutions for most runs. The ambient temperature ranged 9.0–32.7 °C with an average of 18.7 °C during the sampling period.

Table 3-3. Procedures for field testing of stack emission with the dilution sampling and measurement system.

	Procedures
Before Run	• Connect all tubing. • Power on instruments. • Synchronize time stamps of all continuous instruments, perform zero and span checks, and start running and recording data. • Close the valve on the stack sampling line, and set dilution flow to the total flow under normal stack sampling conditions. • Install test filters on the filter sampler and set the flow rate of the filter packs to the specified 16.7 or 5 L/min. Adjust the makeup flow to reach flow balance. • If this is the first run of the day, conduct a 10-minute background run sampling only dilution air. Note down the background sampling start time, check that all instruments readings are within specification with background concentrations, and record the background sampling stop time. • Change the test filters to acceptance tested and unexposed filter packs and set to correct flow rates. • Turn on the stack sample flow and adjust the dilution flow to desired value. Record the filter sampling start time.
During Run	• Examine the file directory and make sure that data from every instrument is being logged. • Examine the measured values to ensure that they are within the limits of specified operating ranges. Ensure that the filter flows do not reduce >10% during the run due to particle loading or clogging. • At the end of the run, turn off valve on the sampling probe to stop the sample flow, and turn off the pump that draws flow through filter packs. • Record filter stop time.
After Run	• Record final flow rate of each filter pack. • Unload the four sampled filter packs, and replace with new, unexposed filters. • Download data from instruments and clear internal memory if necessary. • Clean the cyclone. • Check soda lime on CO_2 analyzers.
End of the Day	• Download data and verify data validity for each of the real-time instruments. • Clear internal memory in real-time instruments. • Clean the sampling inlets and sampling line. • Power down all instruments.

3.5 Laboratory Analysis

Table 3-5 and Figure 3-8 summarize analyses performed on each filter for the four-channel filter pack sampling configuration in Figure 3-5. Analyzed species are intended to serve as the basis (i.e., source profiles) for lichen and/or aerosol sample source apportionment studies. The minimum detection limits (MDLs) for gases, particle mass, b_{abs}, elements, ions, carbon, carbohydrates, organic acids, WSOC, and non-polar organic species analysis methods that were applied for this study are documented in Appendix A. Teflon®-membrane filters were analyzed for mass by gravimetry, b_{abs} by densitometer, 51 elements by x-ray fluorescence (i.e., sodium, magnesium, aluminum, silicon, phosphorous, sodium, chlorine, potassium, calcium, scanadium, titanium, vanadium, chromium, manganese, iron, cobalt, nickle, copper, zinc, gallium, arsenic, selenium, bromine, rubidium, strontium, yttrium, zirconium, niobium, molybdenum, palladium, silver, cadmium, indium, tin, antimony, caesium, barium, lanthanum, cerium, samarium, europium, terbium, hafnium, tantalum, tungsten, iridium, gold, mercury, thallium, lead, and uranium), and 14 rare-earth elements (i.e., lanthanum, cerium, praseodymium, neodymium, samarium, europium, gadolinium, terbium, dysprosium, holmium, erbium, thulium, ytterbium, and lutetium), as well as cesium, barium, and four lead isotopes (i.e., Pb-204, Pb-206, Pb-207, and Pb-208) by inductively coupled plasma/mass spectrometry (ICP/MS) (Chow and Watson, 2012).

Table 3-4. Summary of experimental parameters for each run.

Stack	Run ID	Date	Time	Sampling Duration (min)	Dilution Factor	CO_2 Analyzers (CO_2, pressure)	NO_x Monitor (NO)	GasAlertMicro5 (CO)	DustTrak ($PM_{2.5}$, PM_{10})	OPC (0.23-25 µm)	Filter ID
A	A-1	8/9/2008	16:13:55 - 18:13:55	120	21.8	X	X	X	X	X	2
	A-2	8/10/2008	11:57:30 – 14:57:30	180	44.2	X	X	X	X	X	3
	A-3	8/10/2008	15:37:10 - 17:37:10	120	24.9	X	X	X	X	X	4
	A-4	8/11/2008	10:45:10 - 12:45:10	120	26.3	X	X	X	X	X	5
	A-5	8/11/2008	13:19:20 - 15:19:20	120	22.3	X	X	X	X	X	6
	A-6	8/11/2008	15:50:00 - 17:50:00	120	22.7	X	X	X	X	X	7
	A-7	8/11/2008	Blank	-	NA	NA	NA	NA	NA	NA	8
B	B-1	8/14/2008	14:05:25 - 16:05:25	120	25.0	X	X	X	X	X	9
	B-2	8/14/2008	16:29:25 - 18:29:25	120	26.6	X	X	X	X	X	10
	B-3	8/15/2008	10:02:30 - 12:03:40	121	25.3	X	X	X	X	X	11
	B-4	8/15/2008	12:18:15 - 14:18:15	120	20.7	X	X	X	X	X	12
	B-5	8/15/2008	14:29:15 - 16:29:15	120	25.5	X	X	X	X	X	13
	B-6	8/16/2008	9:54:00 - 11:54:00	120	50.4	X	X	X	X	X	14
	B-7	8/16/2008	12:05:20 – 14:05:20	120	32.6	X	X	X	X	X	15
	B-8	8/16/2008	Blank	-	NA	NA	NA	NA	NA	NA	16
C	C-1	8/19/2008	11:48:02 – 13:48:05	120	33.1	X	X	X	X	X	17
	C-2	8/19/2008	14:20:20 – 16:20:20	120	21.9	X	X	X	X	X	19
	C-3	8/19/2008	16:32:30 – 18:32:30	120	26.7	X	X	X	X	X	20
	C-4	8/20/2008	9:38:40 – 11:38:40	120	24.7	X	X	X	X	X	21
	C-5	8/20/2008	11:51:30 – 13:51:30	120	23.1	X	X	X	X	X	22
	C-6	8/20/2008	14:03:35 – 16:03:35	120	24.0	X	X	X	X	X	23
	C-7	8/20/2008	Blank	-	NA	NA	NA	NA	NA	NA	24

Table 3-5. Sampling and analysis matrix for gases and particles from integrated filter samples.

Sampling Method	Gases and Chemical Species	Analysis Method/ Instruments
Teflon®-membrane filter (2 µm pore size; Teflo PTFE-membrane with polymethylpropylene support ring; Pall Sciences, Port Washington, NY, USA)	$PM_{2.5}$ mass concentration	Gravimetry
	Filter light transmission	Tobias TBX-10 Densitometer
	Elements	XRF
	Cs, Ba, Rare-earth elements, Pb isotopes	ICP/MS
Quartz-fiber filter 1 (Tissuquartz 2500 QAT-UP; (Pall Sciences, Port Washington, NY, USA)	Ions (Cl^-, NO_2^-, NO_3^-, $PO_4^{\equiv}$, $SO_4^{=}$, NH_4^+, Na^+, Mg^{++}, K^+, Ca^{++})	IC, AC, AAS
	Total WSOC, WSOC classes	TOC
	OC/EC, carbon fractions, carbonate	TOR/TOT Carbon Analyzer
	Carbohydrate, organic acids	IC
Quartz-fiber filter 2 (Tissuquartz 2500 QAT-UP; Pall Sciences, Port Washington, NY, USA)	Alkanes, alkenes, PAH, hopanes, steranes	TD-GC/MS
Nuclepore Track-etch polycarbonate filter (0.4 µm pore size; Whatman, Inc., Fairfield, CT, USA)	Elements affecting lichen	ICP
Citric acid- impregnated cellulose-fiber filter (31 ET, 0.5 mm thickness, Whatman, Inc., Fairfield, CT, USA) behind Teflon®-membrane filter (Pall Sciences, Port Washington, NY, USA)	NH_3	AC
K_2CO_3 - impregnated cellulose-fiber filter (31 ET, 0.5 mm thickness, Whatman, Inc., Fairfield, CT, USA) behind quartz-fiber filter (Pall Sciences, Port Washington, NY, USA)	SO_2	IC
$AgNO_3$ impregnated cellulose-fiber (31 ET, 0.5 mm thickness, Whatman, Inc., Fairfield, CT, USA) filter behind quartz-fiber filter (Pall Sciences, Port Washington, NY, USA)	H_2S	XRF

AAS atomic absorption spectrophotometry by Varian Model Spectro880 (Varian, Walnut Creek, CA, USA)
AC automated colorimetry by Astoria Model 302A (Astoria, Astoria OR, USA)
EC elemental carbon by DRI Model 2001 thermal/optical carbon analyzer (DRI, Reno, NV, USA)
GC/MS gas chromatography/mass spectrometry by Agilent Model 6890N/5973 (Agilent Technology, Foster City, CA, USA)
IC ion chromatography by Dionex Model ICS-3000 (Dionex, Sunnyvale, CA, USA)
ICP inductively coupled plasma by Thermo X Series (Thermo Scientific, Madison, WI, USA)
OC organic carbon by DRI Model 2001 thermal/optical carbon analyzer (DRI, Reno, NV, USA)
TOC total organic carbon by Shimadzu TOC Analyzer Model VCSH (Shimadzu, Columbia, MD, USA)
TOR thermal/optical reflectance by DRI Model 2001 thermal/optical carbon analyzer (DRI, Reno, NV, USA)
TOT thermal/optical transmittance by DRI Model 2001 thermal/optical carbon analyzer (DRI, Reno, NV, USA)
WSOC water soluble organic carbon by TOC Analyzer
XRF X-ray fluorescence by PANalytical Model Epsilon 5 (PANalytical, Almelo, the Netherlands)

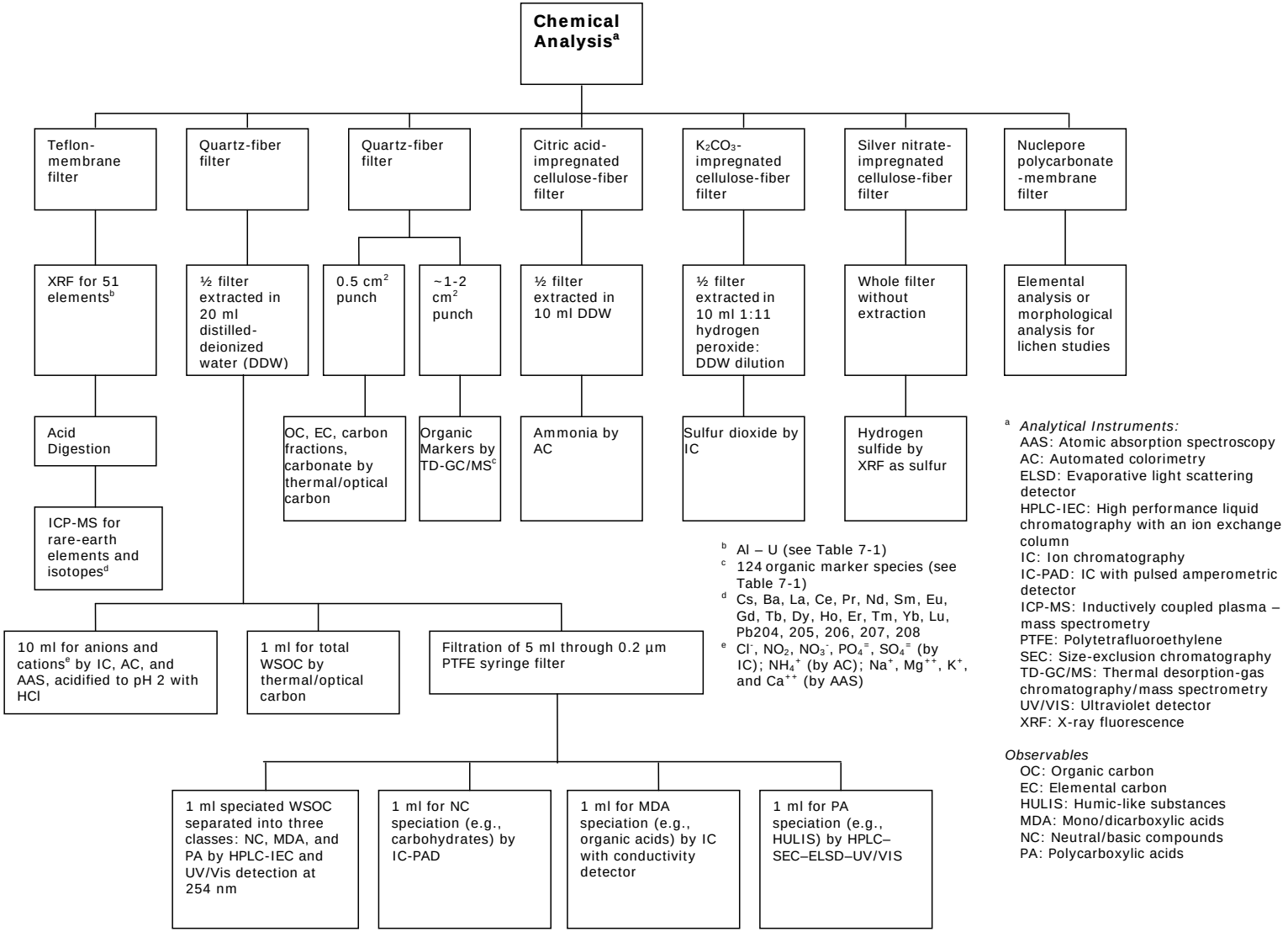

Figure 3-8. Chemical analyses on each filter substrate.

Half of the quartz-fiber filters were extracted in distilled deionized water (DDW) and analyzed for chloride (Cl^-), nitrite (NO_2^-), nitrate (NO_3^-), phosphate ($PO_4^{\equiv}$) and sulfate ($SO_4^=$) by ion chromatography (IC; Chow and Watson, 1999). Water-soluble sodium (Na^+), potassium (K^+), magnesium (Mg^{++}) and calcium (Ca^{++}) were determined by atomic absorption spectroscopy (AAS), and ammonium (NH_4^+) was measured by automated colorimetry (AC). Total water soluble organic carbon (WSOC) and three WSOC classes (i.e., neutral, mono-/di-carboxylic acids, and polycarboxylic acids) were measured from the water extract by high performance liquid chromatograph (HPLC) and total organic carbon analyzer (TOC). Thirteen carbohydrates (i.e., glycerol, inositol, erythritol, xylitol, levoglucosan, sorbitol, mannosan, mannitol, arabinose, glucose, galactose, trehalose, and mannitol) and nine organic acids (i.e., oxalic acid, malonic acid, succinic acid, glutaric acid, lactic acid, acetic acid, formic acid, maleic acid, and methanesulfonic acid) were measured by IC. OC, EC, and eight thermal fractions (OC1-OC4, pyrolyzed carbon [OP], EC1-EC3) were quantified by the IMPROVE_A thermal/optical protocol on the pre-fired quartz-fiber filter samples (Chow et al., 1993; 2001; 2004a; 2005; 2007a). The second half of the quartz-fiber filters were analyzed for 113 non-polar speciated organic carbon compounds including *n*-alkanes, iso/anteiso-alkanes, hopanes, steranes, other alkanes, one alkene, cyclohexanes, and PAHs by thermal desorption-gas chromatography/mass spectrometry (TD-GC/MS; Chow et al., 2007b; Ho and Yu, 2004). Citric acid-impregnated cellulose-fiber filters behind the Teflon®-membrane front filters were analyzed for NH_3 by AC. The backup potassium carbonate (K_2CO_3)-impregnated cellulose-fiber filters behind the quartz-fiber front filters were analyzed for SO_2 by IC and the backup silver nitrate-impregnated cellulose-fiber filters behind the quartz-fiber front filters were analyzed for H_2S by x-ray fluorescence (XRF).

The K_2CO_3-impregnated cellulose filters were designed for ambient measurements, with an average K_2CO_3 impregnation and maximum SO_2 holding capacity of 728±42 μmol/filter. This capacity was exceeded during sampling from Stack A. Therefore, Stack A SO_2 concentration and emission rates were flagged and reported as their lower-bound values.

4 Analytical Specifications and Stack Data Validation

4.1 Analytical Specifications

Every measurement consists of: 1) a value; 2) a precision; 3) an accuracy; and 4) a validity (Watson et al., 2001b). The measurement methods described in Section 3 are used to obtain the *"value"*. Performance testing via regular submission of standards, blank analysis, and replicate analysis can be used to estimate the *"precision"*. The submission and evaluation of independent standards through quality audits are used to estimate *"accuracy"*. *"Validity"* applies both to the measurement method and to each measurement taken with that method. The validity of the methods was evaluated by tests described in Section 4.3.

4.2 Definitions of Measurement Attributes

Precision, accuracy and validity of the aerosol measurements are defined as follows :

- A **measurement** is an observation at a specific time and place which possesses: 1) value – the center of the measurement interval; 2) precision – the width of the measurement interval; 3) accuracy – the difference between measured and reference values; and 4) validity – the compliance with assumptions made in the measurement method.
- A **measurement method** is the combination of equipment, reagents and procedures which provide the value of a measurement. The full description of the measurement method requires substantial documentation. For example, two methods may use the same sampling systems and the same analysis systems. These are not identical methods, however, if one performs acceptance testing on the filter media while the other does not. Seemingly minor differences between methods can result in major differences between measurement values.
- **Measurement method validity** is the identification of measurement method assumptions, the quantification of effects of deviations from those assumptions, the evaluation that deviations are within reasonable tolerances for the specific application, and the creation of procedures to quantify and minimize those deviations during a specific application.
- **Sample validation** is accomplished by procedures that identify deviations from measurement assumptions and the assignment of flags to individual measurements for potential deviations from assumptions.
- **Equivalence:** The only equivalence criteria found is for U.S. EPA $PM_{2.5}$ compliance network mass concentrations, in that U.S. EPA (1997) requires Federal Equivalent Methods (FEM) to meet the following requirements when collocated with an Federal Reference Method (FRM): 1) collocated precision of 2 $\mu g/m^3$ or 5% (whichever is larger); 2) linear regression slope of 1 ± 0.05; 3) linear regression intercept of 0 ± 1 $\mu g/m^3$; and 4) linear regression correlation coefficient (r) of ≥ 0.97. Although these criteria are specific to $PM_{2.5}$ mass equivalence, they can also be used for chemical composition equivalence to maintain consistency.
- **Comparability:** Within stated precision intervals, the criteria for comparability (Watson et al., 1998) are met when: 1) the slope (by either ordinary least squares [OLS] or effective variance [EV] weighting) equals unity within three standard errors, or average ratios (Y/X) equal unity within one standard deviation; 2) the intercept does not significantly differ from zero within three standard errors; and 3) the correlation

coefficient exceeds 0.9. This is a less demanding definition than equivalence because it considers the reported precisions of the two measurements being compared.

- **Predictability:** Some measures, such as light scattering by TSI DustTrak (St. Paul, MO, USA) as a PM surrogate can be correlated with filter-based $PM_{2.5}$ or PM_{10} even though they measure different properties. The criterion for predictability (Watson et al., 1998) between two measurements is met when the correlation coefficient exceeds 0.9, although the slope may substantially deviate from unity and the intercept from zero. Predictability may be qualified, especially when there is high correlation for all but a few outlier measurements. The regression equation is used to estimate mass concentrations from the measured observable.
- **Completeness** measures how many environmental measurements with specified values, precisions, accuracies, and validities were obtained out of the total number attainable. It measures the applicability of the selected measurement processes throughout the measurement period. Databases which have excellent precision, accuracy and validity may be of little use if they contain so many missing values that data interpretation is impossible

4.3 Data Validation

Data acquired from source sampling is subjected to four data validation levels. Level 0 and Level I are completed by the sampler operators and laboratory analysts. Level II and III validation are performed by analysis and research personnel.

- Level 0 sample validation: This is applied to data as they come off the instrument. This process ascertains that the field or laboratory instrument is functioning.
- Level I sample validation: 1) flags samples when significant deviations from measurement assumptions have occurred; 2) verifies computer file entries against data sheets; 3) eliminates values for measurements that are known to be invalid because of instrument malfunctions; 4) replaces data from a backup data acquisition system in the event of failure of the primary system; and 5) adjusts the values for quantifiable calibration or interference biases. Tables 4-1 and 4-2 summarize field and laboratory validation flags, respectively.
- Level II sample validation: Applies consistency tests to the assembled data based on known physical relationships between variables. Level II validation tests and results are described in the following sections. Level II data validation tests for physical consistency, such as sum of species to mass ratio, $SO_4^=$ to sulfur ratio, and anion to cation balances. Data outliers are flagged as suspect in the validated database.
- Level III sample validation: This is part of the data interpretation process. The first assumption upon finding a measurement inconsistent with physical expectations is the unusual value results from a measurement error. If nothing unusual is found upon tracing the path of the measurement, the value can be assumed to be a valid result of an environmental cause. Unusual values are identified during the data interpretation process as: 1) extreme values; 2) values which would otherwise normally track the values of other variables in a time series; and 3) values for observables which would normally follow a qualitatively predictable spatial or temporal pattern.

The following sub-sections document procedures for both field and laboratory data validation.

Table 4-1 Field data validation flags.

Validation Flag	Sub Flag	Description
A		Sampler adjustment or maintenance.
	A1	Sampler audit during sample period.
	A2	Sampler cleaned prior to sample period.
	A3	Particle size cut device regreased or replaced prior to sample period.
B		Field Blank.
D		Sample dropped.
	D1	Sample dropped after sampling.
	D2	Filter dropped during unloading.
	D3	Sample dropped before sampling
F		Filter damaged or ripped.
	F1	Filter damaged in the field.
	F2	Filter damaged when removed from holder.
	F3	Filter wrinkled.
	F4	Filter torn due to over-tightened filter holder.
	F5	Teflon membrane separated from support ring.
	F6	Pinholes in filter.
G		Filter deposit damaged.
	G1	Deposit scratched or scraped, causing a thin line in the deposit.
	G2	Deposit smudged, causing a large area of deposit to be displaced.
	G3	Filter returned to laboratory with deposit side down in Petri slide.
	G4	Part of deposit appears to have fallen off; particles on inside of Petri slide.
	G5	Finger touched filter in the field (without gloves).
	G6	Finger touched filter in the laboratory (with gloves).
H		Filter holder assembly problem.
	H1	Filter misaligned in holder - possible air leak.
	H2	Filter holder loose in sampler - possible air leak.
	H3	Filter holder not tightened sufficiently - possible air leak.
	H4	Filter support grid upside down.
	H5	Two substrates loaded in place of one.
	H6	Filter pack not used, broken during shipment.
I		Inhomogeneous sample deposit.
	I1	Evidence of impaction - deposit heavier in center of filter.
	I2	Random areas of darker or lighter deposit on filter.
	I3	Light colored deposit with dark specks.
	I4	Non-uniform deposit near edge - possible air leak.
L		Sample loading error.
	L1	Teflon and quartz filters were loaded reversely in SFS.
	L3	Fine and Coarse filters were loaded reversely in dichotomous sampler.
	L4	Filter loaded in wrong port.
M		Sampler malfunction.

Table 4-1. Continued		
Validation Flag	**Sub Flag**	**Description**
N		Foreign substance on sample.
	N1	Insects on deposit, removed before analysis.
	N2	Insects on deposit, not all removed.
	N3	Metallic particles observed on deposit.
	N4	Many particles on deposit much larger than cut point of inlet.
	N5	Fibers or fuzz on filter.
	N6	Oily-looking droplets on filter.
	N7	Shiny substance on filter.
	N8	Particles on back of filter.
	N9	Discoloration on deposit.
O		Sampler operation error.
	O1	Pump was not switched on after changing samples.
	O2	Timer set incorrectly.
	O3	Dichotomous sampler assembled with virtual impactor 180° out of phase; only PM_{10} data reported.
P		Power failure during sampling.
Q		Flow rate error.
	Q1	Initial or final flow rate differed from nominal by > ±10%.
	Q2	Initial or final flow rate differed from nominal by > ±15%.
	Q3	Final flow rate differed from initial by > ±15%.
	Q4	Initial or final flow rate not recorded, used estimated flow rate.
	Q5	Nominal flow rate assumed.
R		Replacement filter used.
	R1	Filter that failed flow rate or QC checks replaced with spare.
	R2	Filter sampling sequence changed from order designated on field data sheet.
S		Sample validity is suspect.
T		Sampling time error.
	T1	Sampling duration error of > ±10%.
	T2	Sample start time error of > ±10% of sample duration.
	T3	Elapsed time meter reading not recorded or recorded incorrectly. Sample duration estimated based on readings from previous or subsequent sample.
	T4	Nominal sample duration assumed.
	T5	Sample ran during prescribed period, plus part of next period.
	T6	More than one sample was run to account for the prescribed period.
U		Unusual local particulate sources during sample period.
	U1	Local construction activity.
	U2	Forest fire or slash or field burning.
V		Invalid sample (Void).
W		Wet Sample.
	W1	Deposit spotted from water drops.
	W2	Filter damp when unloaded.
	W3	Filter holder contained water when unloaded.
X		No sample was taken this period, sample run was skipped.

[a]Samples are categorized as valid, suspect, or invalid. Unflagged samples, or samples with any flag except 'S' or 'V' indicate valid results. The 'S' flag indicates samples of suspect validity. The 'V' flag indicates invalid samples. Field data validation flags are all upper case.

Table 4-2. Validation flags applied at DRI's EAF.

Validation Flag	Sub Flag	Description
b		Blank.
	b1	Field/dynamic blank.
	b2	Laboratory blank.
	b3	Distilled-deionized water blank.
	b4	Method blank.
	b5	Extract/solution blank.
	b6	Transport blank.
c		Analysis result reprocessed or recalculated.
	c1	XRF spectrum reprocessed using manually adjusted background.
	c2	XRF spectrum reprocessed using interactive deconvolution
d		Sample dropped.
f		Filter damaged or ripped.
	f1	Filter damaged, outside of analysis area.
	f2	Filter damaged, within analysis area.
	f3	Filter wrinkled.
	f4	Filter stuck to Petri slide.
	f5	Teflon membrane separated from support ring.
	f6	Pinholes in filter.
g		Filter deposit damaged.
	g1	Deposit scratched or scraped, causing a thin line in the deposit.
	g2	Deposit smudged, causing a large area of deposit to be displaced.
	g3	Filter deposit side down in Petri slide.
	g4	Part of deposit appears to have fallen off; particles on inside of Petri slide.
	g5	Ungloved finger touched filter.
	g6	Gloved finger touched filter.
h		Filter holder assembly problem.
	h1	Deposit not centered.
	h2	Sampled on wrong side of filter.
	h4	Filter support grid upside down- deposit has widely spaced stripes or grid pattern.
	h5	Two filters in Petri slide- analyzed separately.
i		Inhomogeneous sample deposit.
	i1	Evidence of impaction - deposit heavier in center of filter.
	i2	Random areas of darker or lighter deposit on filter.
	i3	Light colored deposit with dark specks.
	i4	Non-uniform deposit near edge - possible air leak.
m		Analysis results affected by matrix effect.
	m1	Organic/elemental carbon split undetermined due to an apparent color change of non-carbon particles during analysis; all measured carbon reported as organic.
	m3	A non-typical, but valid, laser response was observed during TOR analysis. This phenomena may result in increased uncertainty of the organic/elemental carbon split. Total carbon measurements are likely unaffected.
	m4	FID drift quality control failure
	m2	Non-white carbon punch after carbon analysis, indicative of mineral particles in deposit.

Table 4-2. Continued.

Validation Flag	Sub Flag	Description
n		Foreign substance on sample.
	n1	Insects on deposit, removed before analysis.
	n2	Insects on deposit, not all removed.
	n3	Metallic particles observed on deposit.
	n4	Many particles on deposit much larger than cut point of inlet.
	n5	Fibers or fuzz on filter.
	n6	Oily-looking droplets on filter.
	n7	Shiny substance on filter.
	n8	Particles on back of filter.
	n9	Discoloration on deposit.
q		Standard.
	q1	Quality control standard.
	q2	Externally prepared quality control standard.
	q3	Second type of externally prepared quality control standard.
	q4	Calibration standard.
r		Replicate analysis.
	r1	First replicate analysis on the same analyzer.
	r2	Second replicate analysis on the same analyzer.
	r3	Third replicate analysis on the same analyzer.
	r4	Sample re-analysis.
	r5	Replicate on different analyzer.
	r6	Sample re-extraction and re-analysis.
	r7	Sample re-analyzed with same result, original value used.
s		Suspect analysis result.
	s1	Failed Level I data validation
	s2	Failed sum of species to mass ratio test (outside of 0.6-1.4 range)
	s3	Failed sulfate to sulfur ratio test (outside of 1-4 range)
v		Invalid (void) analysis result.
	v1	Quality control standard check exceeded ± 10% of specified concentration range.
	v2	Replicate analysis failed acceptable limit specified in SOP.
	v3	Potential contamination.
	v4	Concentration out of expected range.
w		Wet Sample.
	w1	Deposit spotted from water drops.
y		Data normalized
	y1	X-ray fluorescence (XRF) data normalized to a sulfate/sulfur ratio of three
	y2	Each species reported as a percentage of the measured species sum
	y3	Minimum detection limit used as uncertainty

4.3.1 Field data Validation

Data collected from source testing by field operators includes: date, time, site, sampling duration, flow rates and site temperature and barometric pressure. From these data the volume for each sample is calculated and reported in site actual cubic meters. Flow rates are set prior to sampling and verified at the end of the sampling period using a calibrated rotameter. Rotameters are calibrated by the DRI QA laboratory using a NIST traceable rotameter. Field data validation flags, shown in Table 4-1, are applied during the validation and calculation of the sampling volumes. Volume uncertainties are estimated to be 5% of the sampling volume.

4.3.2 Laboratory Data Validation

Laboratory data validation is conducted to ensure the internal consistency of $PM_{2.5}$ mass and chemical composition. Physical consistency is tested for: 1) sum of measured species versus gravimetric mass, 2) $SO_4^=$ versus total sulfur (S); 3) Cl^- versus chlorine (Cl); 4) K^+ versus total K; 5) calculated versus measured NH_4^+; and 6) anion and cation balance.

The sum of species should be less than or equal to the corresponding gravimetric PM mass loading, since unmeasured species such as oxygen (O) and hydrogen (H) are not included. Figure 4-1a and b show that the regression between the sum of species and gravimetric mass from Teflon®-membrane filters have slopes of 0.69 and 1.00 for Stacks A and B, respectively, with correlation coefficient (R^2) of 0.97 and 0.99, respectively. This is quite typical for aerosol samples. Stack C (Figure 4-1c) has a lower slope (0.52) with $R^2 = 0.93$, indicating more unidentified species at this site. Concentrations from all three stacks have slopes less or equal to one, which validates both the chemical and mass measurements.

$SO_4^=$ is measured by IC on quartz-fiber filter extracts while total S is measured by XRF on Teflon-membrane® filters. The ratio of $SO_4^=$ to S is expected to equal to three if all of the S is present as $SO_4^=$. Water-soluble $SO_4^=$ should not exceed three times the S concentration, within precision estimates. Figure 4-2a and b show that Stacks A and B have slopes of 3.01 and 3.33, and R^2 of 0.98 and 0.97, respectively, indicating reasonable agreement with expectations. Stack C, however, has a slope of 4.97 and R^2 of only 0.81 (Figure 4-2c). Some volatile sulfur was measured by IC that may have been vaporized under the vacuum and higher temperature environment of the XRF analysis chamber. The IC $SO_4^=$ therefore is believed to be more accurate for this case.

PM Cl^- by IC on quartz-fiber filter extracts should be less than or equal to total Cl by XRF on Teflon®-membrane filters. However, Cl^- is close to the distilled water blank and is subject to high measurement uncertainties in IC analysis, and some volatile Cl may be lost in the vacuum during XRF analysis. Similarly, PM K^+ measured by AAS on the quartz-fiber filter extract should be equal to or less than total K measured by XRF on the Teflon®-membrane filter. Figure 4-3a shows that the chloride/chlorine plot for Stack A has a slope of 1.30 and $R^2 = 0.99$. The higher than unity slope is not uncommon and indicates some volatile Cl compounds may have been lost in the XRF vacuum. The slope and R^2 are 0.94 and 0.92, respectively, for Stack B as shown in Figure 4-3b. Cl^- concentrations from Stack C were below detection limit, so a regression is not possible (Figure 4-3c). Figure 4-4 show that soluble versus total potassium slopes are 0.36, 0.70, and 0.59 at Stacks A, B, and C, respectively, indicating that soluble K^+ is always less than total K as expected.

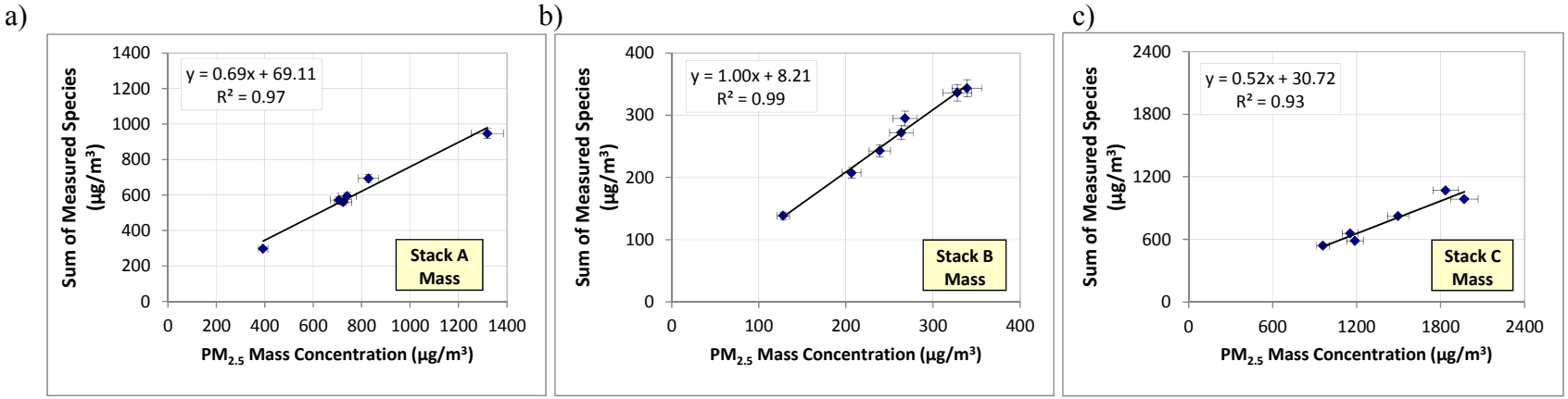

Figure 4-1. $PM_{2.5}$ mass concentration by gravimetry from the Teflon®-membrane filters versus sum of measured species mass concentrations for Stacks a) A, b) B, and c) C.

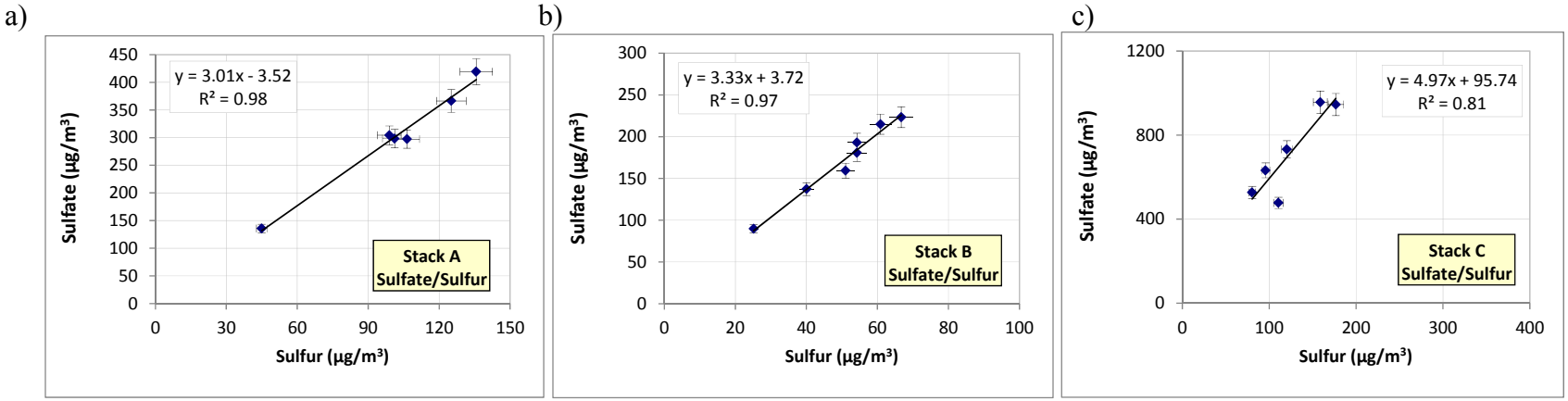

Figure 4-2. Water soluble sulfate ($SO_4^{=}$) on quartz-fiber filter by ion chromatographic (IC) analysis versus total sulfur (S) on Teflon®-membrane filters by x-ray fluorescence (XRF) analysis for Stacks a) A, b) B, and c) C.

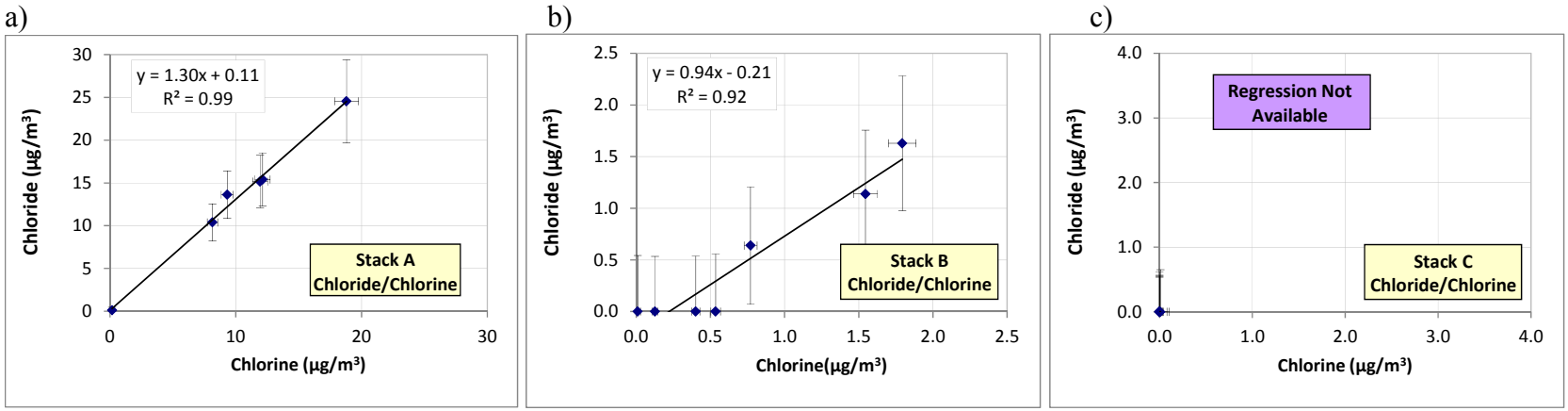

Figure 4-3. Water soluble chloride (Cl^-) on quartz-fiber filter by ion chromatographic (IC) analysis versus total chlorine (Cl) on Teflon®-membrane filters by x-ray fluorescence (XRF) analysis for Stacks a) A, b) B, and c) C.

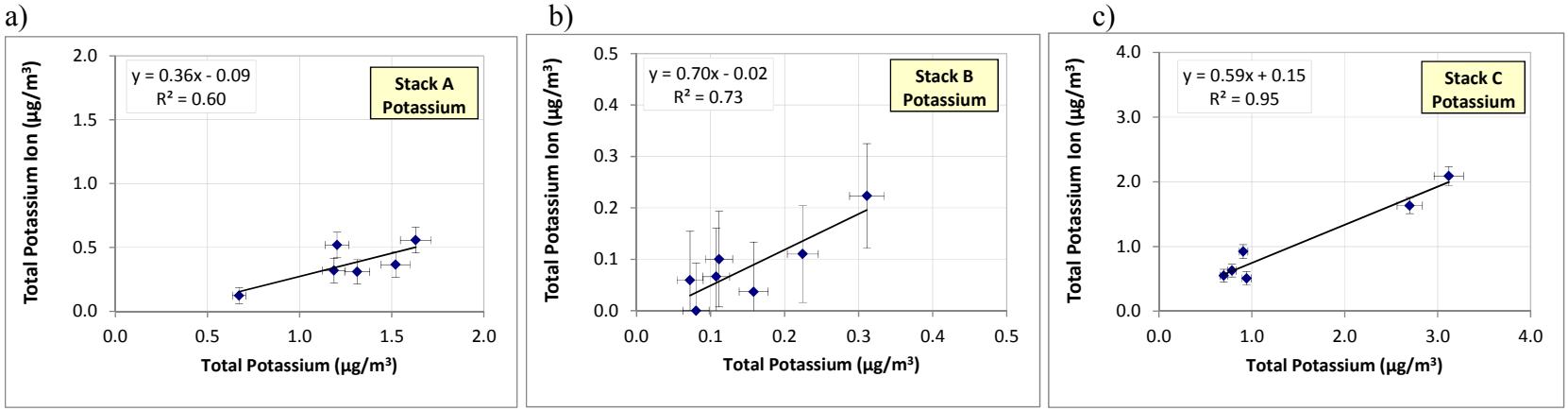

Figure 4-4. Water soluble potassium (K^+) on quartz-fiber filter by atomic absorption spectrophotometry (AAS) analysis versus total potassium (K) on Teflon®-membrane filters by x-ray fluorescence (XRF) analysis for Stacks a) A, b) B, and c) C.

To further evaluate ion measurements, calculated versus measured NH_4^+ are compared. NH_4^+ is directly measured by AC analysis of the quartz-fiber filter extract. NH_4^+ is found in the chemical forms of NH_4NO_3, $(NH_4)_2SO_4$, and ammonium bisulfate (NH_4HSO_4). Ammonium chloride (NH_4Cl) concentration is low and not included in the calculations. Assuming full neutralization, measured NH_4^+ can be compared with calculated NH_4^+, which is the sum of NH_4NO_3 with either $(NH_4)_2SO_4$ ($0.29 \times NO_3^- + 0.38 \times SO_4^=$), or $(NH_4)HSO_4$ ($0.29 \times NO_3^- + 0.192 \times HSO_4^-$).

Figure 4-5 shows that the calculated and measured NH_4^+ have high correlations (R^2=1.00) for samples from Stacks A and B. However, this is not the case for samples from Stack C, with negative slopes and correlations of about 0.26. The calculated NH_4^+ from the high $SO_4^=$ on these samples greatly overestimates the measured NH_4^+, indicating that the $SO_4^=$ is highly acidic.

The anion and cation balance compares the sum of Cl^-, NO_2^-, NO_3^-, $PO_4^{\equiv}$, and $SO_4^=$ to the sum of NH_4^+, Na^+, Mg^{++}, K^+, and Ca^{++} in μeq/m^3, the product of mass concentration (in μg/m^3) divided by the atomic weight of the chemical species divided by the species' charge. Therefore:

$$\mu eq/m^3 \text{ for anions} = \left(C_m \frac{Cl^-}{35} + C_m \frac{NO_2^-}{46} + C_m \frac{NO_3^-}{62} + C_m \frac{PO_4^{\equiv}}{95/3} + C_m \frac{SO_4^=}{98/2} \right) \quad (4\text{-}1)$$

$$\mu eq/m^3 \text{ for cations} = \left(C_m \frac{NH_4^+}{18} + C_m \frac{Na^+}{23} + C_m \frac{Mg^{++}}{24.3/2} + C_m \frac{K^+}{39.1} + C_m \frac{Ca^{++}}{40.1/2} \right) \quad (4\text{-}2)$$

Figure 4-6a and 4-6b show that the ion balances for Stacks A and B are in agreement with a slope near unity (1.05 and 0.98, respectively), and $R^2 \sim 1.00$. Stack C has a negative slope (-4.69) and low correlation (0.30) which again indicates high sulfate being present without a measured cation to balance it. This indicates that sulfate is probably present primarily as H_2SO_4, which is also more volatile than $(NH_4)_2SO_4$ and may evaporate during heating and vacuum in the XRF analysis chamber.

4.4 Precision Calculations and Error Propagation

Measurement precisions are propagated from precisions of volumetric measurements, chemical composition measurements, and field blank variability (Watson et al., 2001b). The following equations are used to calculate the precision associated with filter-based measurements:

$$C_i = \frac{M_i - B_i}{V} \quad (4\text{-}3)$$

$$V = Q \times t \quad (4\text{-}4)$$

$$B_i = \frac{1}{n} \sum_{o=1}^{n} B_{io} \quad \text{for } B_i > \sigma_{B_i} \quad (4\text{-}5)$$

$$B_i = 0 \quad \text{for } B_i < \sigma_{B_i} \quad (4\text{-}6)$$

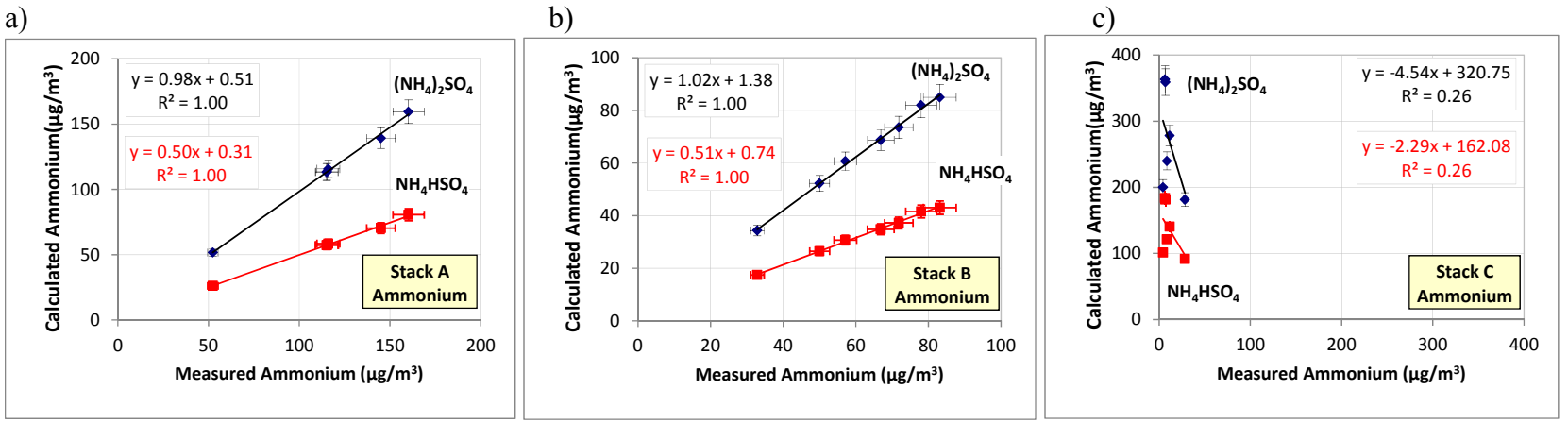

Figure 4-5. Calculated ammonium by summing ammonium ions in NH_4NO_3 with either $(NH_4)_2SO_4$ ($0.29 \times NO_3^- + 0.38 \times SO_4^=$; blue symbols) or $(NH_4)HSO_4$ ($0.29 \times NO_3^- + 0.192 \times HSO_4^-$; red symbols) versus ammonium measured directly by automated colorimetry (AC).

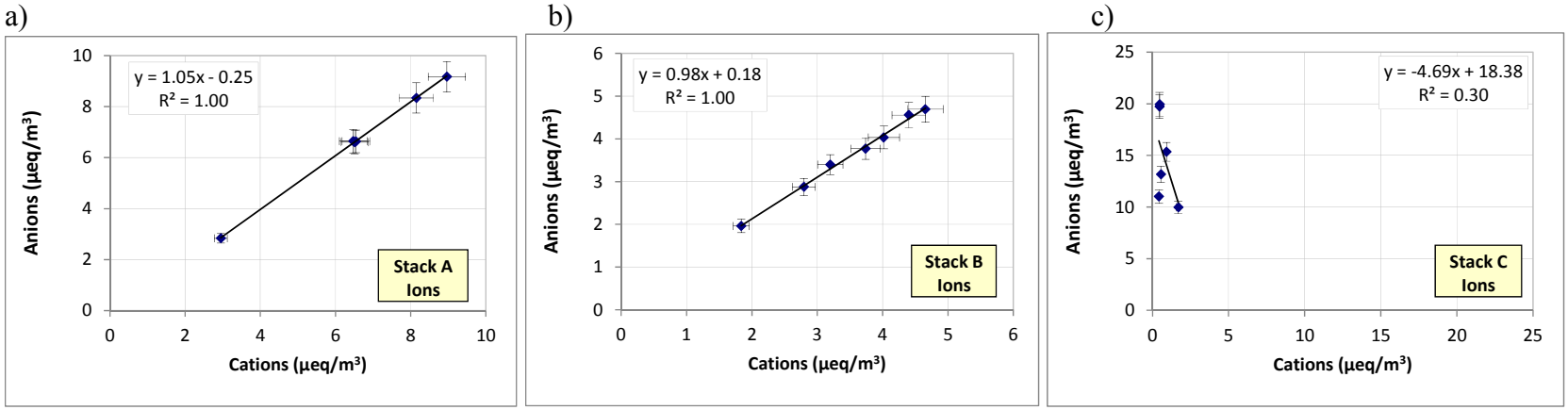

Figure 4-6. Total anions versus cations for Stacks a) A, b) B, and c) C.

$$\sigma_{B_i} = STD_{B_i} = \left[\frac{i}{n-1} \sum_{o=1}^{n} \left(B_{io} - B_i \right)^2 \right]^{\frac{1}{2}} \quad for\ STD_{B_i} > SIG_{B_i} \tag{4-7}$$

$$\sigma_{B_i} = SIG_{B_i} = \left[\frac{i}{n} \sum_{o=1}^{n} \left(\sigma_{B_{io}} \right)^2 \right]^{\frac{1}{2}} \quad for\ STD_{B_i} \le SIG_{B_i} \tag{4-8}$$

$$\sigma_{C_i} = \left[\frac{\sigma_{M_i}^2 + \sigma_{B_i}^2}{V^2} + \frac{\sigma_V^2 \left(M_i - B_i \right)^2}{V^4} \right]^{\frac{1}{2}} \tag{4-9}$$

$$\sigma_{RMSi} = \left(\frac{1}{n} \sum_{o=}^{n} \sigma_{C_i}^2 \right)^{\frac{1}{2}} \tag{4-10}$$

$$\frac{\sigma_V}{V} = 0.05 \tag{4-11}$$

$$F_{ij} = \frac{\sum_{i=1}^{I} C_i}{mass} \tag{4-12}$$

$$\sigma_{F_{ij}} = \left[\left(\frac{\left[\sigma \sum_{i=1}^{I} C_i \right]^2}{mass^2} \right) + \left(\frac{\left[\sum_{i=1}^{I} C_i \right]^2 \times \sigma mass^2}{mass^4} \right) \right]^{\frac{1}{2}} \tag{4-13}$$

where:

B_i = average amount of species *i* on field blanks
B_{io} = the amount of species *i* found on field blank *o*
C_i = the source concentration of species *i*
Q = flow rate throughout sampling period
M_i = amount of species *i* on the substrate
n = total number of samples in the sum
SIG_{B_i} = the root mean square error (RMSE), the square root of the averaged sum of the squared $\sigma_{B_{io}}$
STD_{B_i} = standard deviation of the blank
σ_{B_o} = blank precision for species *i*
$\sigma_{B_{io}}$ = precision of the species *i* found on field blank *j*
σ_{C_i} = propagated precision for the concentration of species *i*
σ_{M_i} = precision of amount of species *i* on the substrate
σ_{RMSi} = root mean square precision for species *i*
σ_V = precision of sample volume

t = sample duration
V = volume of air sampled.

The uncertainty of the measured value and the average uncertainty of the field blanks for each species are used to propagate the overall precision for each blank subtracted concentration value. The final value is propagated by taking the square root of the sum of the squares of the calculated uncertainty and the average field blank uncertainty for each measurement.

5 Pollutant Concentrations and Emission Rates

5.1 Emission Rate Calculation

Emission Rates (ERs) from stationary sources are expressed in mass emitted per unit of time or in mass of pollutant per mass of dry or wet air emitted by the stack. The time-based ERs are calculated from species concentrations, dilution ratio, average stack velocity, and stack diameter as:

$$ER_i = 3600 \times C_i \times V_{Stk} \times CSA \times \frac{T_{std}}{T_{Stk}} \times \frac{P_{Stk}}{P_{std}} \quad (5\text{-}1)$$

where:

i = pollutant i,
ER_i = emission rate of pollutant i in µg/hr,
C_i = wet basis stack concentration of the pollutant i in µg/m^3 under standard temperature (T_{std} = 298.15 Kelvin [K]) and pressure (P_{std} = 101,325 pascal [Pa]) conditions,
V_{Stk} = average stack velocity in m/s,
CSA = stack cross section area in m^2,
T_{Stk} and P_{Stk} = stack temperature in K and stack pressure in Pa, respectively.

For pollutants measured after dilution, the measured concentrations ($C_{i,Dil}$ in µg/m^3) need to be corrected by the dilution ratio (DR):

$$C_i = C_{i,Dil} \times DR \quad (5\text{-}2)$$

The DR is calculated using measured stack, diluted, and background CO_2 concentrations by:

$$DR = \frac{CO_{2,Stk} - CO_{2,Bkg}}{CO_{2,Dil} - CO_{2,Bkg}} \quad (5\text{-}3)$$

where:

$CO_{2,Stk}$ = undiluted CO_2 stack concentration in ppm,
$CO_{2,Dil}$ = diluted CO_2 concentration in ppm,
$CO_{2,Bkg}$ = CO_2 background concentration in ppm.

The average stack velocity (V_{Stk}) is determined following U.S. EPA Method 2 (U.S.EPA, 2011):

$$V_{Stk} = K_p \times C_S \times \left(\Delta P \times \frac{T_{Stk} + 273}{MW \times P_{Stk}} \right)^{\frac{1}{2}} \quad (5\text{-}4)$$

where:

K_p = stack velocity constant (34.97),
C_s = pitot tube constant (0.84),
ΔP = velocity head of stack gas in millimeters of water (mmH_2O),
T_{Stk} = stack temperature in degrees Celsius (°C),
MW = molecular weight of the stack gas in g/mol (assumed to be 29.9 g/mol based on previous measurements of flue gas composition from Stack A)
P_{Stk} = absolute stack pressure in mm mercury (mmHg)

The uncertainty of the emission rate ($\sigma_{ER,p}$ in µg/hr) is calculated as:

$$\sigma_{ER,i} = 3600 \times CSA \times \frac{T_{std}}{T_{Stk}} \times \frac{P_{Stk}}{P_{std}} \times \left(\sigma_{C_i}^2 \times V_{Stk}^2 + \sigma_{V_{Stk}}^2 \times C_i^2\right)^{\frac{1}{2}} \quad (5\text{-}5)$$

where:

σ_{C_i} = stack mass concentration uncertainty from pollutant i in $\mu g/m^3$,

$\sigma_{V_{Stk}}$ = stack velocity uncertainty in m/s (estimated to be 5% of the measured stack velocity).

For pollutant concentration measured after dilution, σ_{C_i} is calculated as:

$$\sigma_{C_i} = \left(\sigma_{C_{i,Dil}}^2 \times DR^2 + \sigma_{DR}^2 \times C_{i,Dil}^2\right)^{\frac{1}{2}} \quad (5\text{-}6)$$

where:

$\sigma_{C_{i,Dil}}$ = diluted pollutant concentration uncertainty,

σ_{DR} = dilution ratio uncertainty,

$C_{i,Dil}$ = diluted concentration of pollutant i.

σ_{DR} is calculated as:

$$\sigma_{DR} = \left[\frac{\sigma_{Stk,Diff}^2}{(CO_{2,Dil} - CO_{2,Bkg})^2} + \frac{(CO_{2,Stk} - CO_{2,Bkg})^2 \times \sigma_{Dil,Diff}^2}{(CO_{2,Dil} - CO_{2,Bkg})^4}\right]^{\frac{1}{2}} \quad (5\text{-}7)$$

where:

$\sigma_{Stk,Diff}$ = uncertainty of the difference between the undiluted CO_2 concentration and the background CO_2 concentration,

$\sigma_{Dil,Diff}$ = uncertainty of the difference between the diluted CO_2 concentration and the background CO_2 concentration, both determined from Eq. 5-8 in ppm as:

$$\sigma_{Diff} = \left(\sigma_{CO2}^2 + \sigma_{Bkg}^2\right)^{\frac{1}{2}} \quad (5\text{-}8)$$

where:

σ_{Diff} = $\sigma_{Stk,Diff}$ or $\sigma_{Dil,Diff}$,

σ_{CO2} = uncertainty of the undiluted or diluted CO_2 concentration in ppm,

σ_{Bkg} = uncertainty of the background CO_2 concentration in ppm.

The uncertainty of the CO_2 measurements is 1% of the span concentration.

5.2 Data Reduction

The following steps were taken to analyze the real-time data:

- Raw data files from each real-time instrument from each test were combined into a single Excel worksheet.
- Average stack effluent velocities (V_{Stk}) were calculated from pitot tube differential pressures using Eq. 5-4. The average stack velocity, flow rate under standard conditions (25°C and 101,325 Pa), and stack temperature are listed in Table 5-1. Note that the flow rate of Stack A (645 m^3/s) was more than twice of those for the other two stacks, and its recorded gas temperature (258°C) was 3-5 times higher than temperatures in the FGD stacks.
- DRs for 10 s, 30 s, 60 s, and entire test durations were calculated using Eq. 5-3.

- Measured pollutant concentrations ($C_{i,Dil}$) were multiplied by DR, and PM concentrations in mg/m^3 under dilution chamber conditions were converted to wet basis mg/m^3 under standard conditions.
- Real-time concentrations were averaged to obtain test-average concentrations.
- ERs were calculated using Eq. 5-1.

Table 5-1. Stack velocity, temperature, and flow rate under standard conditions (25°C, and 101,325 Pa). Data were reported as average ± standard error of multiple runs.

Parameter	Stack A	Stack B	Stack C
Stack Velocity (m/s)	24.7±0.3	12.7±0.1	9.6±0.2
Stack Flow Rate (m^3/s)	645.1±6.9	295.8±2.7	316.4±5.7
Stack Temperature (°C)	258.3±0.6	79.6±0.2	54.5±0.1

In ER calculations, species with concentrations below MDLs were replaced by 3 times the analytical uncertainty and used for calculating the average concentrations and emission rates. If the species was below the MDL during any of the runs at each sampling condition, the average value was flagged by the "<" sign. In source profile calculations, species with concentrations below MDLs were set to zero, and the uncertainty value takes the larger of standard deviation and uncertainty of average of multiple runs.

5.3 VOC Concentrations and Emission Rates

The SRI portable GC was not part of the original test plan, but its availability at the time of these tests allowed for an initial assessment of VOC emissions. Figure 5-1 illustrates GC chromatograms for VOCs from the three stacks. Note that chromatogram patterns are consistent among multiple measurements in each stack, and some peaks are present in all chromatograms from the three stacks (e.g. retention time 587.8 s). Peaks occurring before the 400 s retention time are difficult to deconvolute and quantify. The presence of the large peak between 417 and 443 s in the Stack A chromatograms and its absence in Stacks B and C indicate that compounds corresponding to this peak were probably removed by the FGD process, although its species information does not correspond with peaks from the EPA-TO14 calibration standards (Scott Special Gases, Plumsteadville, PA). Based on calibration standards analyzed using the same portable GC program, major VOC (benzene, toluene, ethylbenzene, and xylenes; BTEX) concentrations and ERs were quantified. Benzene and 1,2,4-Trimethylbenzene were at measurable concentrations in all three stacks, with Stack B having the highest concentrations (1.7 and 2.8 times for benzene, and 6.7 and 3.2 times for 1,2,4-Trimethylbenzene of those in Stacks A and C, respectively). Stacks B and C also emitted measurable amounts of toluene (19.6 and 2.8 kg/day, respectively) and o-Xylene (2.8 and 1.0 kg/day, respectively). Most other VOCs species in the diluted sample were present at levels less than the 0.2 ppbv detection limits. More complete and lower concentration VOC concentrations would be available from canister samples with laboratory GC/MS analysis in future studies.

5.4 Particle Optical Properties and Mass Distributions

$PM_{2.5}$ mass concentrations by gravimetry from the Teflon®-membrane filters are compared to those reported by the TSI DustTrak and the Grimm OPC from light scattering measurement in Figure 5-2. The three measurements are correlated ($R^2 > 0.81$) in $PM_{2.5}$ for Stacks A and B. As shown in Figure 5-2a-b, the filter $PM_{2.5}$ and optical instruments have higher

correlations for stack B (R^2 = 0.95 between filter and TSI DustTrak, and R^2 = 0.99 between filter and OPC), and lower correlation for Stack A (R^2 = 0.88 and 0.81 between filter $PM_{2.5}$ and TSI DustTrak and Grimm OPC, respectively). The $PM_{2.5}$ by TSI DustTrak and the Grimm OPC have high correlations ($0.92 \leq R^2 \leq 0.95$) as shown in Figure 5-2c.

Table 5-2. Wet basis concentration and ER of VOCs measured by the SRI portable GC. (Cells with "<" indicate the compound is below the portable GC minimum detection limit (0.2 ppbv) in diluted sample in at least one test. Data were averaged from five runs for Stacks A and C and four runs for Stack B)

VOCs/Air Toxics Compound	MW	Stack Concentration (ppb)			Emission Rate (g/hr)		
		A	B	C	A	B	C
Benzene	78.1	11.5	19.4	7.0	84.1	65.2	25.3
Toluene	92.1	<38.8	205.4	27.8	<336.0	815.2	117.9
Ethylbenzene	106.2	<5.5	13.2	<4.1	<54.5	60.2	<20.1
m+p-Xylene	106.2	<2.2	<2.2	<2.9	<21.9	<10.1	<14.3
Styrene	104.2	<1.7	<0.6	<2.9	<16.2	<2.8	<14.0
o-Xylene	106.2	<8.2	25.5	8.7	<81.9	116.7	42.7
4-EthylToluene	120.2	<0.0	<0.0	<2.9	<0.0	<0.0	<16.2
1,3,5-Trimethylbenzene	120.2	<2.7	<5.8	<2.9	<30.9	<29.9	<16.2
1,2,4-Trimethylbenzene	120.2	19.7	131.9	41.5	222.2	682.9	229.9

Despite high correlations, the TSI DustTrak readings using the factory Arizona Road Dust calibration are twice those of the Grimm OPC as indicated by the regression slopes (2.21 and 2.05 for Stacks A and B, respectively). This is due to different calibration factors that convert light scattering signal to particle mass and illustrates why a corresponding filter measurement needs to be taken alongside the continuous optical measurements. Correlations were low for Stack C. Emissions from Stack C probably consist of large quantities of H_2SO_4-H_2O droplets (See Section 6). These particles absorb or lose water at different RHs (Seinfeld and Pandis, 1997), resulting in changes of mass concentration with RH. Since the Teflon®-membrane filter was equilibrated at ~30 ± 5% RH and 21.5 ± 1.5 °C before gravimetric analysis while the TSI DustTrak and Grimm OPC may have different internal temperature and RH during in-situ measurement, the particle-bound water content will be different among the three measurement methods, contributing to the poor correlations.

Filter light transmission (b_{abs}) on Teflon®-membrane filter by densitometer (Tobias TBX-10; Ivyland, PA) has been used as a surrogate for light absorption by EC derived from TOR carbon analysis on quartz-fiber filters following the IMPROVE_A protocol (Chow et al., 2007a). Figure 5-3a shows that b_{abs} is highly correlated with EC (R^2 = 0.94) for Stack A, has found elsewhere (Chow et al., 2010b), but the correlation is poor for the other two stacks. This is due to higher EC abundance (7.16% of $PM_{2.5}$ mass) in Stack A. The mass absorption efficiency (i.e., the slope of b_{abs} vs. EC) is 17.44 m^2/g, much higher than the ~10 m^2/g typically assumed to convert b_{abs} to EC. $PM_{2.5}$ b_{abs} is also reasonably correlated ($0.63 < R^2 < 0.88$) with gravimetric $PM_{2.5}$ mass from Teflon®-membrane filters and those acquired by the TSI DustTrak and Grimm OPC (Figure 5-3b to Figure 5-3d). Particles from the two FGD stacks (B and C) contain only a small fraction of light absorbing EC in $PM_{2.5}$ mass (2.15 ± 0.16%, and 0.42 ± 0.13% for Stack B and Stack C, respectively). As expected, there is no relationship between b_{abs} and $PM_{2.5}$ mass measurements.

The mass calibration factor for the DustTrak was obtained by taking the ratio of the $PM_{2.5}$ mass concentration by gravimetric analysis of the Teflon®-membrane filter to that by the DustTrak for each run. For the OPC, the mass concentration for particles smaller than 2.5 μm were first summed to obtain $PM_{2.5}$ mass concentration, and the calibration factor was calculated as the ratio of the Teflon® $PM_{2.5}$ concentration to the OPC $PM_{2.5}$ concentration. The $PM_{2.5}$ concentration was measured following the reference method (filter), and the $PM_{2.5}$ calibration factors were applied to all size fractions. The OPC sizes particles according to light scattering, and therefore the reported geometric particle diameters differ from aerodynamic particle diameters. The optical sizes were assumed to be close to aerodynamic sizes. The calibration factor-corrected particle size distributions measured by the OPC were grouped into PM_1, $PM_{2.5}$, PM_{10}, and PM_{25} and used for reporting size segregated PM ERs.

Figure 5-4 shows the particle mass distribution measured by the Grimm OPC, and Figure 5-5 depicts the cumulative mass percentage as a function of particle size. The mass median diameters (MMD) are 1.15, 0.70, and 0.34 μm for Stacks A, B, and C, respectively. Although the PM mass concentration from Stack A is higher, particles from Stacks A and B have similar bimodal mass distributions, peaking at 0.5 – 0.6 μm for the submicron mode and 1.5 – 2.5 μm for the surpermicron mode. The cumulative size distributions in Figure 5-5 show ~50% mass in PM_1, ~30% in $PM_{1\text{-}2.5}$, and ~20% in $PM_{2.5\text{-}10}$. On the other hand, particles from Stack C are much smaller, with a single mode peaking at 0.45 μm. Figure 5-5 shows 96% of mass in PM_1 and ~99% of mass in $PM_{2.5}$. High vapor-phase sulfur compounds levels from the coker and the sulfur recovery unit tail gas, some fraction of which will be H_2SO_4, reasonably could be expected at the scrubber inlet. Scrubbers can cause H_2SO_4 to condense as submicron aerosols due to rapid temperature decrease in the quench section. Removal efficiencies of submicron aerosols across the spray tower/absorber and mist eliminators are often low (~30-50%). Thus, the predominance of both high unbalanced "sulfate" (Section 4.3.2) and submicron aerosols after the scrubber is consistent with a H_2SO_4 composition. The two FGD stacks (i.e., Stack B and C) for Facility A and B show a difference in particle size distributions even though Table 3-2 shows comparable stack physical parameters and Table 5-1 shows that stack operation parameters such as velocity, flow rate, and temperature are similar between the stacks. Differences in flue gas desulfurization process (Stack B uses saturated ammonia and Stack C uses limestone slurry as scrubbing agent) and fuel composition are probably the cause these size distribution differences.

5.5 Real-time Emission Concentrations

Figure 5-6 illustrates real-time data from one test at each stack (Run ID A-3, B-4, and C-5, respectively), including stack velocity, stack temperature, and gaseous (i.e., CO, CO_2, and NO) and PM concentrations (i.e., PM_1, $PM_{2.5}$, and PM_{10}) under standard conditions in the stack. Real-time data for individual tests are plotted in Figures B-1 to B-19 of Appendix B. Stack parameters were relatively stable over the test periods, with occasional spikes in PM concentration. For Stack C, the PM spikes happen simultaneously with NO spikes, probably due to process variability. There are few NO spikes corresponding with PM spikes for Stack A. Real-time measurements not only provide average emission concentrations and rates, but also detect short-duration stack emission changes due to process variations.

5.6 Stack Concentrations and Emission Rates of Gases and PM

Table 3-5 lists the average inorganic gas and PM concentrations under standard conditions with ERs are reported in kg/hr. Average ERs (kg/hr) for the three stacks are plotted in Figure 5-7. The ratios of pollutant concentrations and ERs among the three stacks are listed in

Table 5-4, using the lowest value in each comparison as the reference (1). CO concentrations in Stacks A and B are 1.5 and 2.1 times of those found at Stack C, respectively. After accounting for flue gas flow rate (see Table 5-1), the CO ERs from Stacks A and B are 3.1 and 2.0 times of that from Stack C, respectively. CO_2 concentrations in Stacks B and C are 1.5 and 2.1 times those in Stack A. Stacks A and C have similar CO ERs, both ~1.5 times of that from Stack B. NO concentrations are similar among the three stacks (123-164 mg/m^3).Large variations are found in NH_3 concentrations and ERs. Stack C has 1-2 orders of magnitude lower NH_3 ERs, only 1.1% and 0.2% of levels in Stacks A and B, respectively. Stack B has the highest NH_3 concentrations and ER, probably it injects NH_3 as the FGD scrubbing agent. The NH_3 in Stack A originates from the stream from the Sour Water Plant which contains 94 molar percent of NH_3.

Table 5-3. Average gas and PM wet basis concentrations (under standard conditions: 25°C and 101,325 Pa) and emission rates for the three stacks.

Measured Species		Concentration (mg/m^3)			Emission Rates (kg/hr)		
		Stack A	**Stack B**	**Stack C**	**Stack A**	**Stack B**	**Stack C**
Gases	CO	686±26	915±42	443±73	1599±54	982±45	500±73
	CO_2	(1.12±0.02)×10^5	(1.65±0.00)×10^5	(2.36±0.03)×10^5	(2.61±0.05)×10^5	(1.77±0.02)×10^5	(2.70±0.05)×10^5
	NO	126±3	123±2	164±10	295±11	133±2	187±11
	NH_3	7.2±1.0	80.6±20.9	0.16±0.01	16.6±2.4	86.4±22.9	0.18±0.01
	SO_2	>453[a]	677±120	174±22	>1050[a]	727±132	201±28
	H_2S	0.017±0.008	0.007±0.002	0.004±0.001	0.038±0.017	0.007±0.002	0.005±0.002
PM	PM_1	13.0±1.1	5.5±0.1	36.1±2.7	30.5±2.7	5.9±0.1	41.3±3.4
	$PM_{2.5}$	21.1±2.1	7.5±0.3	37.4±3.0	49.4±5.1	8.0±0.3	42.7±3.8
	PM_{10}	29.3±3.4	10.0±1.1	37.5±3.1	68.6±8.2	10.8±1.3	43.0±4.0
	PM_{25}	29.4±3.4	10.2±1.3	37.7±3.2	68.8±8.2	11.0±1.5	43.2±4.1

[a]The K_2CO_3-impregnated filter capacity was exceeded during Stack A sampling. Therefore, Stack A SO_2 concentration and emission rates were underestimated.

Table 5-4. Average ratio of gas and PM wet basis concentrations and emission rates for Stacks A, B, and C.

Parameter		Ratio of Stack A: B: C	
		Concentration	**Emission Rate**
Gases	CO	1.5 : 2.1 : 1.0	3.1 : 2.0 : 1.0
	CO_2	1.0 : 1.5 : 2.1	1.5 : 1.0 : 1.5
	NO	1.0 : 1.0 : 1.3	2.2 : 1.0 : 1.4
	NH_3	46 : 513 : 1	92 : 480 : 1
	SO2	>2.6 : 3.9 : 1.0	>5.2 : 3.6 : 1.0
	H_2S	5.7 : 1.7 : 1.0	12.7 : 1.7 : 1.0
PM	PM_1	2.4 : 1.0 : 6.6	5.2 : 1.0 : 7.0
	$PM_{2.5}$	2.8 : 1.0 : 5.0	6.1 : 1.0 : 5.3
	PM_{10}	3.0 : 1.0 : 3.9	6.5 : 1.0 : 4.1
	PM_{30}	3.0 : 1.0 : 3.9	6.4 : 1.0 : 4.1

a)

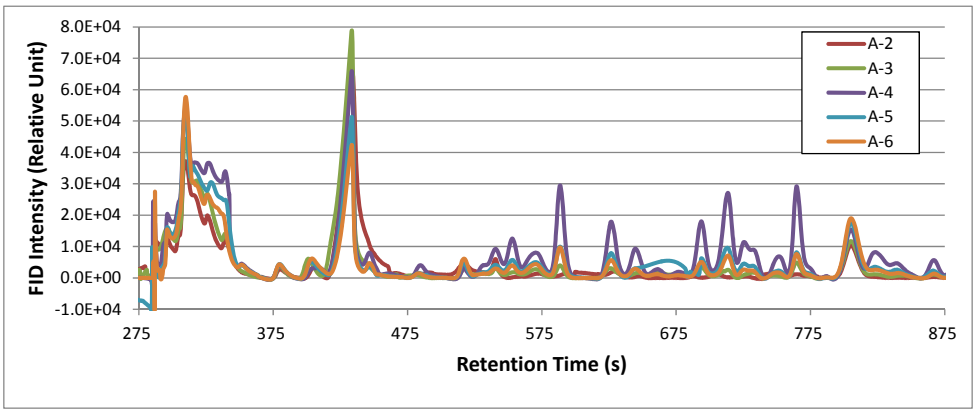

b)

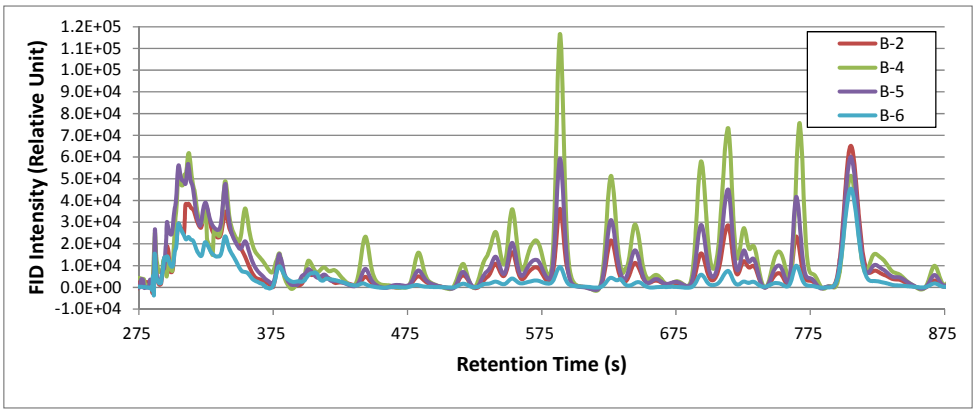

c)

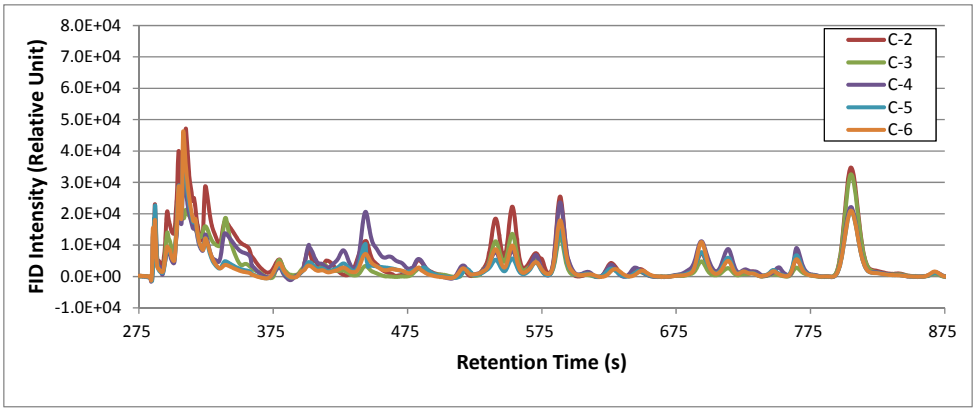

Figure 5-1. Superposition of all valid VOC chromatograms measured by the SRI portable GC from a) Stacks A, b) B, and c) C.

a)

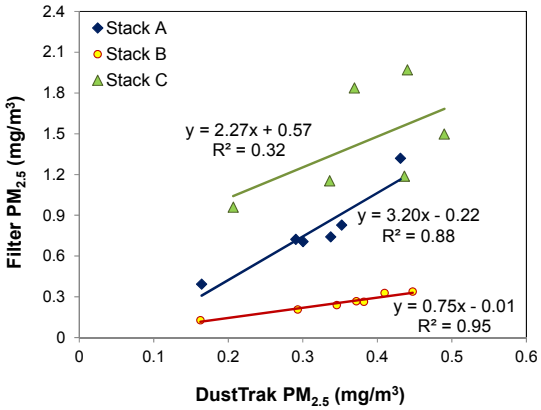

b)

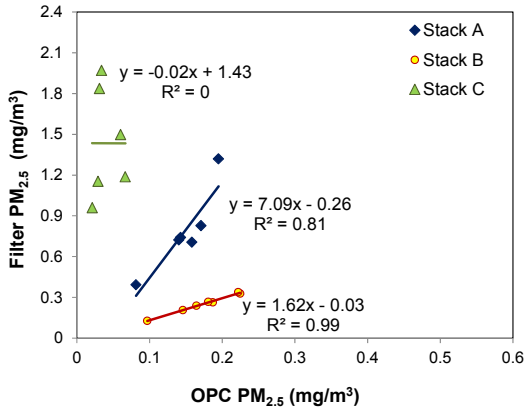

c)

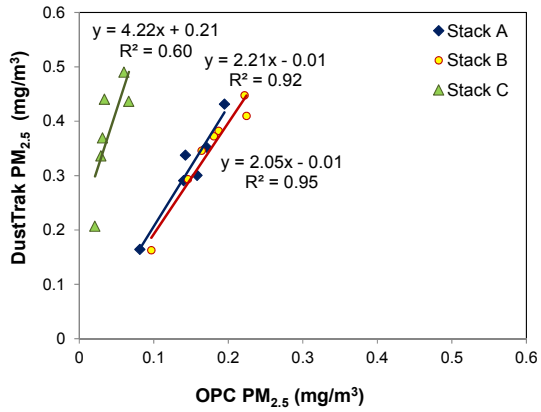

Figure 5-2. Correlations between $PM_{2.5}$ concentration before dilution correction: a) gravimetric filter vs. TSI DustTrak; b). gravimetric filter vs. Grimm optical particle counter (OPC); and 3) TSI DustTrak vs. Grimm OPC. The reported concentrations by the TSI DustTrak and Grimm OPC were derived with their internal calibration factors set by manufacturers (i.e., without correction by custom calibration factors for the stack aerosols).

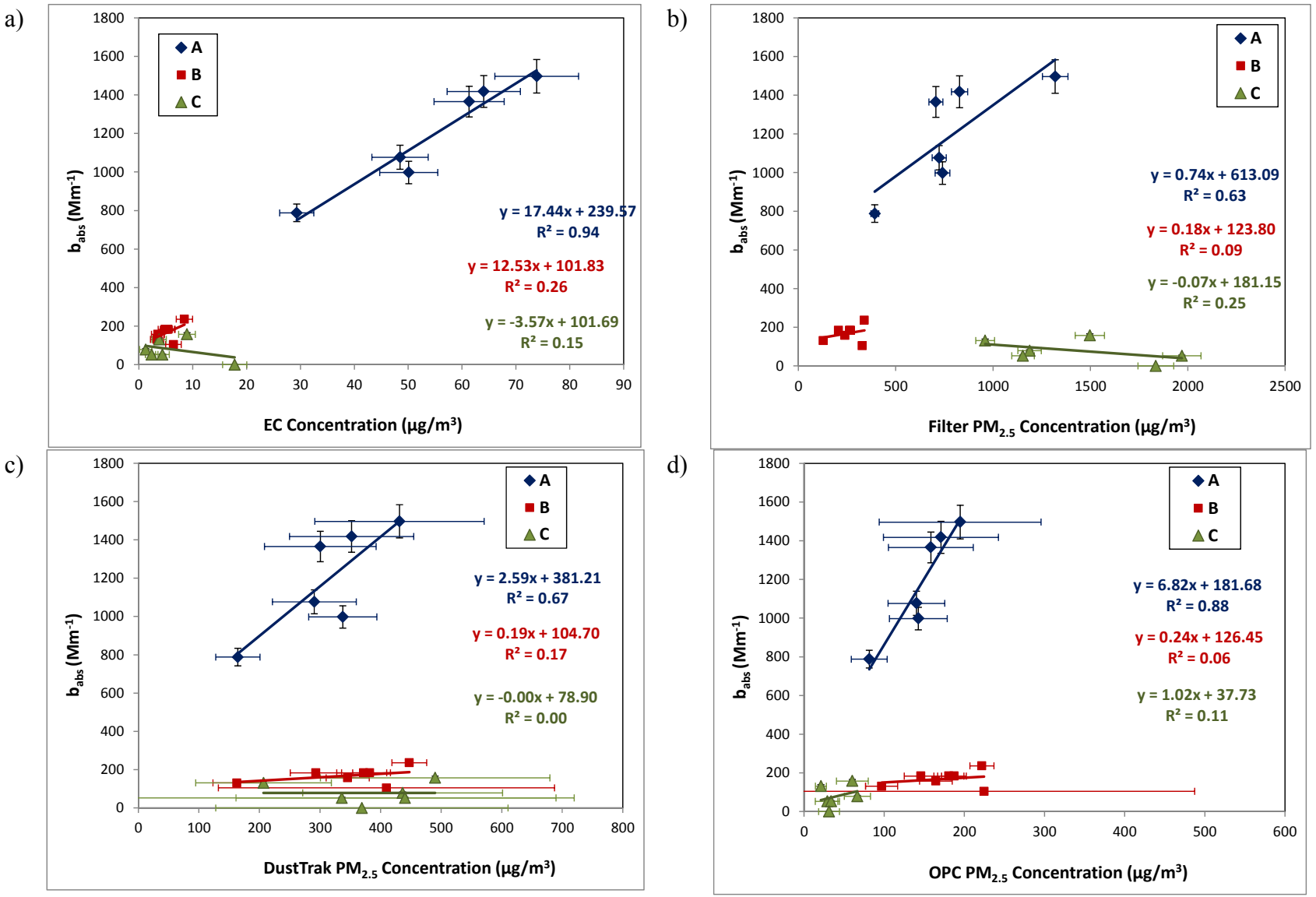

Figure 5-3. Correlation between filter light transmission coefficient (b_{abs}) and: a) quartz-fiber filter elemental carbon (EC) following the IMPROVE_A thermal/optical reflectance method(Chow et al., 2007a), b) Teflon®-membrane filter gravimetric $PM_{2.5}$, c) TSI DustTrak $PM_{2.5}$, and d) Grimm optical particle counter (OPC) $PM_{2.5}$ mass concentrations.

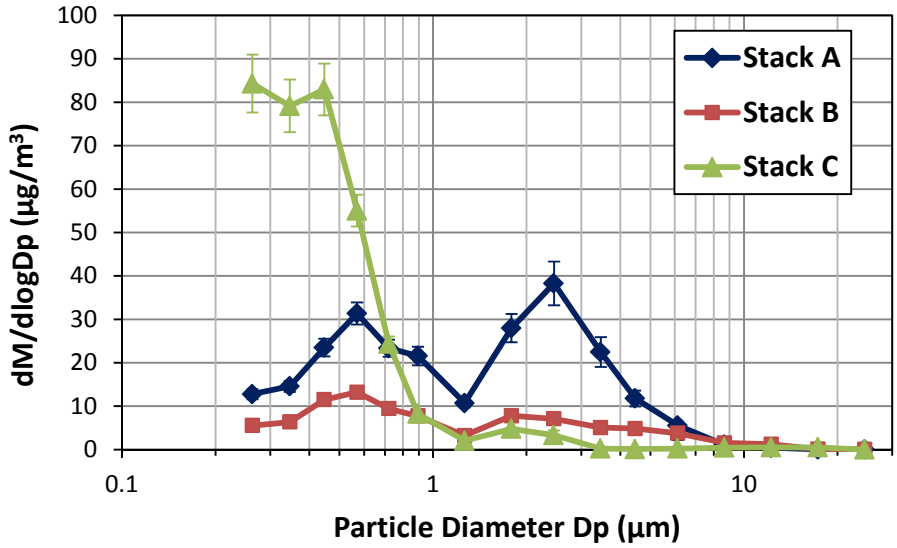

Figure 5-4. Particle mass distribution measured by the Grimm optical particle counter (OPC). The mass concentrations were scaled by the $PM_{2.5}$ concentrations from Teflon®-membrane filter, and are expressed in concentrations under standard conditions (i.e., 101,325 Pa and 25 °C). The error bar represents standard error from multiple measurements (an average of six runs each from Stacks A and C, and seven runs for Stack B).

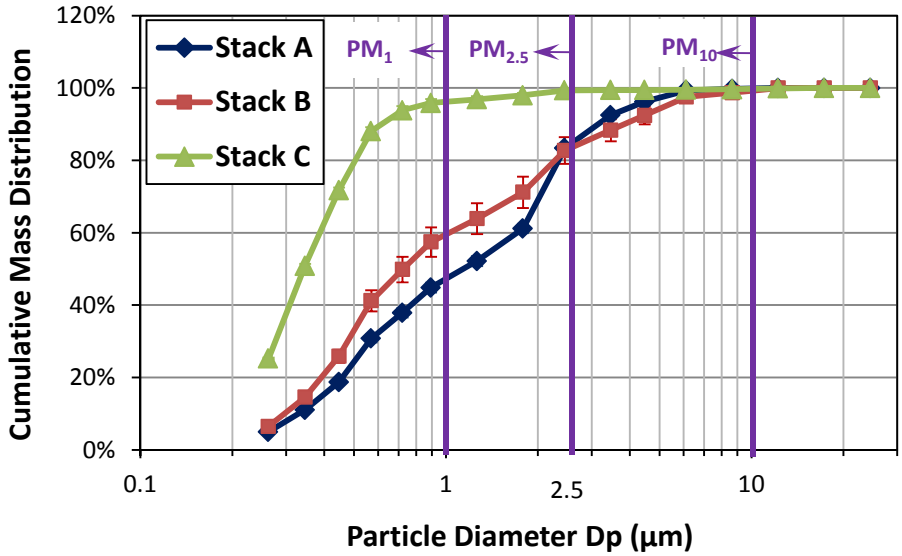

Figure 5-5. Cumulative particle mass distribution measured by the Grimm OPC. The error bar represents standard error from multiple measurements (an average of six runs each from Stacks A and C, and seven runs for Stack B).

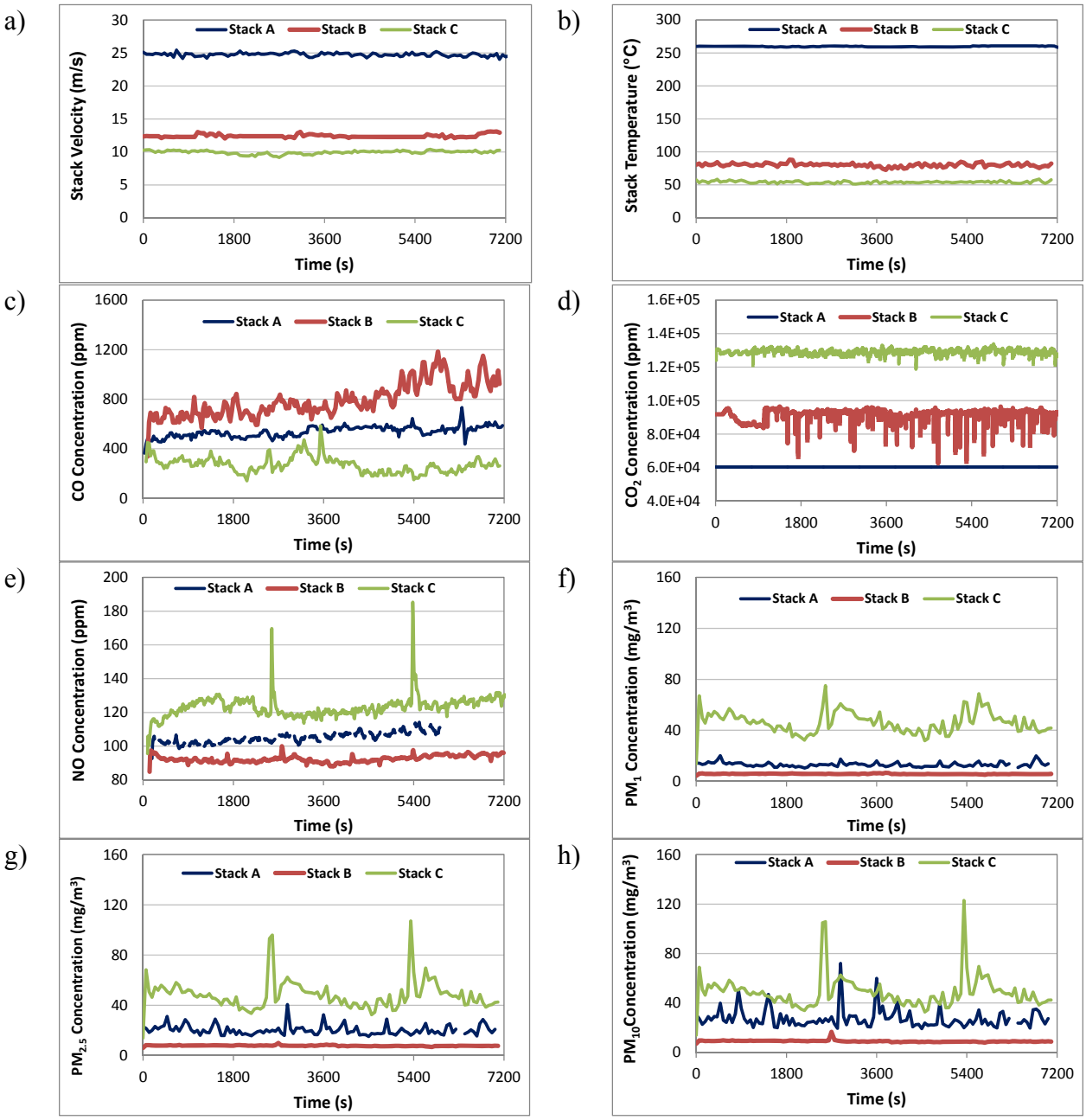

Figure 5-6. Examples of real-time data for stack parameters (stack velocity and temperature; Figures 5-6a– b), gas (CO, CO_2, and NO; Figures 5-6c – e, respectively) concentrations, and PM (PM_1, $PM_{2.5}$, and PM_{10}) concentrations (Figure 5-6f – h, respectively).

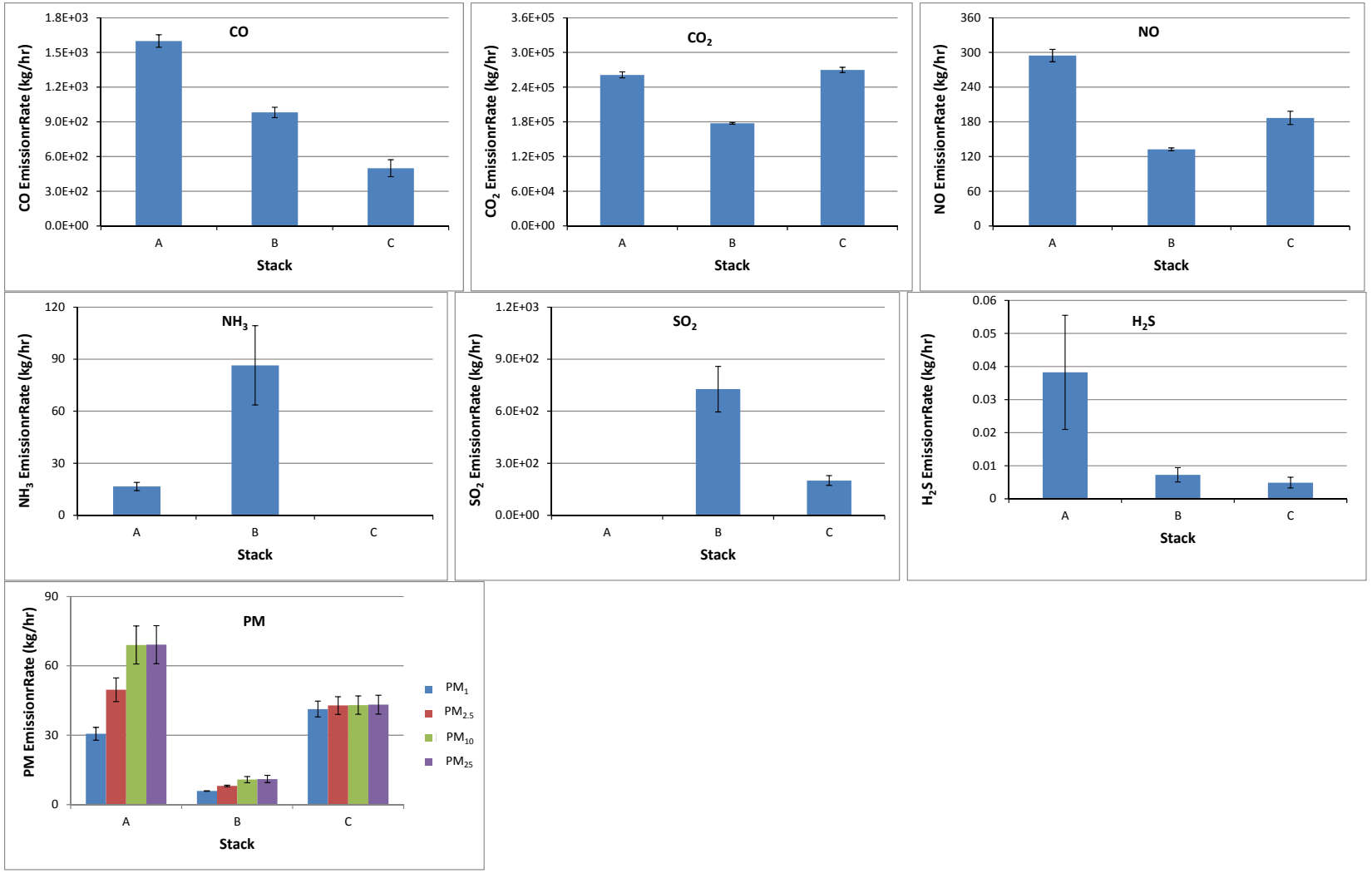

Figure 5-7. Averaged emission rates (ERs) of gases and PM. Data are the same as the ER (kg/hr) in Table 5-3. Error bar indicates the standard error from multiple tests. The actual Stack A SO_2 emission rate is higher than shown due to filter saturation.

SO_2 concentrations in Stacks A and B are >2.6 and 3.9 times of those found at Stack C, respectively. SO_2 ERs from Stacks A and B are >5.2 and 3.6 times of that from Stack C, respectively. Facility A noted that the SO_2 removal efficiency was 80-85% during the test period, likely due to high sulfites from initial excursion in May 2008. This is probably the cause for higher SO_2 concentrations in Stack B than Stack C. All three Stacks exhibit low H_2S ERs (5–38 g/hr). Stack C has the lowest H_2S ERs, only 7.9% and 60% of the Stacks A and B, respectively. Stack B has the lowest PM ERs, ~14-20% of the other two stacks. As mentioned in Section 4.3, although ~100% of particles are in the PM_{10} size fraction for all three stacks, Stack C different size distributions differ from those of from Stacks A and B. For Stacks A and B, ~50% particles are PM_1 and ~80% are $PM_{2.5}$, while for Stack C, ~96% particles are PM_1 and ~99% are $PM_{2.5}$.

Table 5-5 compares the NO_x, SO_2, and TSP ERs measured on Stack A from compliance tests conducted in 2007 and dilution sampling of this study in 2008. The compliance tests followed the Alberta Stack Sampling Code (Alberta Environment, 1995), which is similar to the U.S. EPA Methods 1-8 for stationary source testing (http://epa.gov/ttn/emc/promgate.html). The NO_x, SO_2, and TSP ERs from dilution sampling were 52%, >12%, and 17%, respectively, of those from compliance tests. Some of these differences are due to actual emission differences between the test periods, and some are due to the differences in sampling methodology. As discussed in Section 2.1, TSP measured by U.S. EPA Method 5 includes filterable PM collected on the heated glass-fiber filter, the condensable PM and dissolved gases collected by the impinger, and those collected by washing the sampling lines. It typically overestimates TSP due to positive artifacts from gas reactions and dissolution (Corio and Sherwell, 2000; Richards et al., 2005; England et al., 2000).

Table 5-6 compares the particle size distribution measured from an in-stack survey test conducted on Stack A during 2002 and from the dilution sampling applied in this study. The in-stack sampling followed a setup modified from the U.S. EPA Method 201A by installing both a PM_{10} and $PM_{2.5}$ in-stack cyclones (U.S.EPA, 2010a). The condensable fraction captured in the impingers was not accounted for in these in-stack test data. The PM_{10} ER by the two methods differs by <15%. However, the $PM_{2.5}$ ER from this study is 2.7 times higher than the in-stack survey, while the TSP is only 66% of the in-stack survey. As discussed earlier, the in-stack hot filter does not collect particles that would nucleate and grow upon cooling and will underestimate fine particle concentration. This is probably the reason why the hot filter $PM_{2.5}$ is so much lower than the dilution sampling. The >10 μm fraction in the in-stack measurement was recovered by washing the sampling probe and cyclone with acetone (U.S.EPA, 2010a). This procedure causes uncertainties in the TSP data. On the other hand, particle losses (especially those of larger sizes) in the dilution sampling method were not accounted for, and the OPC only measures particles ~<25 μm. These factors, along with the different stack operating conditions, may have contributed to the differences in TSP ERs.

Table 5-7 compares the ERs from compliance tests in 2007 with the dilution sampling in this study for Stack B. The average NO_x ER from dilution sampling was 45% higher than compliance tests, while ERs for SO_2 by dilution sampling and compliance tests are very similar (727±132 and 741±239 kg/hr, respectively). The TSP ER by dilution sampling (estimated by the Grimm OPC PM_{25}) was only ~3% of the TSP or 21% of the filterable PM from compliance tests, which does not include the condensable PM fraction collected by impingers.

Table 5-5. Comparison of emission rates (ER) from compliance tests conducted in 2007 (data from the 2007 AENV Air Emission Report by Facility A), the present study, and the permitted ER limit for Stack A.

Test ID		Test Date	NO_x (as NO_2, kg/hr)[a]	SO_2 ER (kg/hr)	TSP (kg/hr)[c]
Compliance Tests	07-1	3/13/2007	-	9800	630
	07-1-R1	5/8/2007	680	8700	280
	07-2	6/5/2007	-	10600	320
	07-3	7/4/2007	1010	7500	340
	07-4	8/21/2007	900	7500	300
	07-5	9/18/2007	890	8600	380
	07-6	10/16/2007	-	9200	500
	Average		870±69	8843±431	392±48
Present study	A-1	8/9/2008	449	>999[b]	109
	A-2	8/10/2008	523	>843	62
	A-3	8/10/2008	457	>863	63
	A-4	8/11/2008	452	>1397	66
	A-5	8/11/2008	394	>1183	60
	A-6	8/11/2008	437	>1018	52
	Average		452±17[a]	>1050	69±8[b]
Emission Limits		-	1500	16400	600

[a]In this study, only NO was measured. The NO ER was converted to NO_2 ER based on the ratio of molecular weight by ER (NO_2) = ER (NO) × 46/30.
[b]The K_2CO_3-impregnated filter capacity was exceeded during Stack A sampling. Therefore, Stack A SO_2 concentration and emission rates were underestimated.
[c]The listed TSP concentration of this study is the PM_{25} measured by the Grimm OPC.

Table 5-6. Comparison of particle size distribution measured from Stack A from an in-stack survey test and the dilution sampling in this study.

Test Name	Test Date	$PM_{2.5}$ ER (kg/hr)	PM_{10} ER (kg/hr)	TSP ER (kg/hr)
In-stack Survey	5/1/2002 – 5/2/2002	18±2	58±10	103±27
This Study	8/9/2008 – 8/11/2008	49±5	69±8	69±8

Table 5-8 compares the TSP ERs measured on Stack C from compliance tests conducted in 2010 and dilution sampling of this study in 2008. The TSP ER from dilution sampling was 16% lower than the compliance test.

It should be noted that the PM_{25} measured by the Grimm OPC may not represent TSP, and significant losses for particles >10 μm in dilutions sampling may cause underestimation of TSP. Particles in Stacks A and B have a larger fractions of mass in >2.5 μm size fractions (Figure 5-5) and while those in Stack C are predominantly <1 μm. These size distribution differences may partially cause the larger differences between dilution sampling and compliance tests in Stacks A and B, but smaller differences in Stack C.

5.7 Emission Rates of PM Constituents

Table 5-9 lists concentrations and ERs for $PM_{2.5}$ constituents (soluble ions, carbon fractions, and elements). Soluble $SO_4^=$ is the component that has the highest concentration and ER among all $PM_{2.5}$ constituents for all three stacks, accounting for 39-68% of the $PM_{2.5}$ emissions. A more detailed examination of the different chemical species and source profile will be discussed in Section 6.

Concentrations and ERs for Cs, Ba, rare earth elements, and Pb in $PM_{2.5}$ measured by ICP/MS are listed in Table 5-10. Ce is the rare earth element that have the highest ERs for all three stacks.

Table 5-11 lists ERs for 113 non-polar organic carbon compounds. These organic compounds are grouped into nine categories (i.e., PAHs, n-alkanes, iso- and anteiso-alkanes, hopanes, steranes, methyl-alkanes, branched alkanes, cyclo-alkanes, and alkenes). Cells with "<" indicate that the levels are below detection limits. Overall the particulate non-polar compounds ERs are low for all three stacks. Stack A has the highest ER, while C has the lowest ERs. n-Alkanes have the highest ERs among all compounds. Most PAHs, all hopanes, and all steranes are below MDL for Stack C.

Table 5-12 lists concentrations and ER for carbohydrates, organic acids, and three WSOC classes (i.e., neutral, mono-/di-carboxylic acids, and polycarboxylic acids) and total WSOC. Most carbohydrates and organic acids are below the MDLs. WSOCs from all three stacks were below or only slightly above the MDLs except for neutral compounds.

Table 5-7. Comparison of emission rates (ER) from compliance tests conducted in 2007 (data from the 2007 AENV Air Emission Report by Facility A), the present study, and the permitted ER limit for Stack B.

Test ID		Test Date	NO_x (as NO_2, kg/hr)[a]	SO_2 ER (kg/hr)	Filterable PM (kg/hr)	TSP (kg/hr)[b]
Compliance Tests	07-1	1/10/2007	80	420	30	150
	07-1b	5/2/2007	-	480	-	-
	07-2	6/20/2007	60	490	70	287
	07-3	8/14/2007	190	580	70	370
	07-4	9/11/2007	160	180	90	558
	07-5	10/16/2007	180	690	50	454
	07-6	11/13/2007	140	730	15	450
	07-7	11/27/2007	170	2360	40	377
	Average	-	140±19	741±239	52±10	378±50
Present Study	B-1	8/14/2008	210	433	-	20.2
	B-2	8/14/2008	205	262	-	8.9
	B-3	8/15/2008	205	641	-	9.6
	B-4	8/15/2008	182	742	-	9.6
	B-5	8/15/2008	199	653	-	9.4
	B-6	8/16/2008	211	1151	-	9.6
	B-7	8/16/2008	209	1208	-	9.8
	Average	-	203±4[a]	727±132	-	11.0±1.5[b]
Emission Guideline		-	-	-	-	250[c]

[a]In this study, only NO was measured. The NO ER was converted to NO_2 ER based on the ratio of molecular weight by ER (NO_2) = ER (NO) × 46/30.

[b]The listed TSP concentration of this study is the PM_{25} measured by the Grimm OPC.

[c]The emission guideline was 0.20 g/kg of dry effluent (adjusted to 50% excess air) for TSP. It was converted to emission rate of 250 kg/hr by taking the average dry flue gas flow rate of 1250 tonnes/hr measured by compliance tests in 2007.

Table 5-8. Comparison of NO_x and TSP emission rates (ER) from compliance tests conducted in 2010 (data provided by Facility B), the present study, and the permitted ER limits for Stack C.

Test Name	Test Date	NO_x (as NO_2, kg/hr)a	TSP ER (kg/hr)b
Compliance Tests	2010	-	51.09
This Study	8/19/2008 – 8/20/2008	284±17[a]	43.2±4.1[b]
Emissions guidance	-	1800	340[c]

[a]In this study, only NO was measured. The NO ER was converted to NO_2 ER based on the ratio of molecular weight by ER (NO_2) = ER (NO) × 46/30.
[b]The listed TSP concentration of this study is the PM_{25} measured by the Grimm OPC.
[c]The emission guideline was 0.20 g/kg of dry effluent (adjusted to 50% excess air) for TSP. It was converted to emission rate of 340 kg/hr by taking the average dry flue gas flow rate of 1703 tonnes/hr measured by a compliance tests in 2010.

Table 5-9. PM constituent (ions, carbon fractions, and elements) wet basis concentrations (under standard conditions) and emission rates for the three stacks. (Cells with "<" indicate the compound is below instruments' minimum detection limit (MDL[a]) in at least one test. Data were reported as average ± standard error of multiple runs [b].)

Chemical Species	Stack Concentration (µg/m^3)			Emission Rate (kg/hr)		
	A	B	C	A	B	C
Cl^-	330.1±76.8	<46.144	<43.811	0.760±0.173	<0.050	<0.050
NO_2^-	<27.705	<32.038	<24.720	<0.064	<0.034	<0.028
NO_3^-	13.9±2.5	17.5±3.9	<12.919	0.032±0.006	0.019±0.004	<0.015
PO_4^{3-}	<25.754	<44.979	<29.680	<0.060	<0.048	<0.033
$SO_4^=$	8134±499	5070±152	18539±1529	18.9±1.2	5.440±0.195	21.2±2.0
NH_4^+	3143±192	1859±58	322.7±136.0	7.296±0.447	1.995±0.073	0.364±0.150
Na^+	10.5±1.2	<5.833	12.4±3.6	0.024±0.003	<0.006	0.014±0.004
Mg^{++}	4.3±0.5	3.2±0.2	10.5±1.2	0.010±0.001	0.003±0.000	0.012±0.001
K^+	9.7±1.3	<3.696	27.3±6.4	0.023±0.003	<0.004	0.031±0.007
Ca^{++}	22.8±3.2	8.4±2.1	<32.158	0.053±0.008	0.009±0.002	<0.036
OC1[c]	541.6±310.2	<93.803	<64.126	1.271±0.734	<0.100	<0.072
OC2[c]	588.5±89.7	270.9±18.9	<44.622	1.374±0.216	0.290±0.021	<0.051
OC3[c]	<83.545	49.4±5.7	<100.653	<0.195	0.053±0.006	<0.116
OC4[c]	108.9±15.0	41.5±4.5	80.7±39.8	0.254±0.037	0.045±0.005	0.093±0.047
OPT[c]	<114.658	79.3±10.1	443.2±214.7	<0.267	0.085±0.011	0.511±0.252
OPR[c]	<34.589	<45.146	291.4±171.5	<0.080	<0.048	0.338±0.201
OCT[c]	1278±394	400.3±31.2	554.9±316.5	2.991±0.938	0.430±0.035	0.640±0.372
OCR[c]	1300±394	356.1±33.1	421.6±273.8	3.042±0.938	0.382±0.037	0.488±0.321
EC1[c]	1349±92	148.6±15.3	389.6±226.1	3.137±0.229	0.159±0.016	0.450±0.265
EC2[c]	139.6±20.2	<48.895	66.9±10.7	0.326±0.049	<0.053	0.076±0.012
EC3[c]	<7.816	<13.035	<6.959	<0.018	<0.014	<0.008
ECT[c]	1533.6±91.9	150.3±10.3	63.7±18.0	3.567±0.235	0.161±0.011	0.073±0.021
EC[c]	1483.3±91.9	160.2±12.3	164.1±61.0	3.450±0.234	0.172±0.014	0.188±0.071
TC[c]	2783±446	516.3±29.0	585.7±331.5	6.493±1.080	0.554±0.034	0.675±0.389
Na	186.5±18.2	119.1±8.0	244.4±26.5	0.432±0.041	0.128±0.009	0.279±0.032
Mg	28.5±3.9	13.2±2.7	37.7±3.4	0.066±0.008	0.014±0.003	0.043±0.004
Al	214.4±25.9	21.2±1.0	94.3±23.2	0.499±0.063	0.023±0.001	0.105±0.024
Si	1037±265	29.2±1.9	362.2±105.0	2.424±0.633	0.031±0.002	0.403±0.111
P	<3.173	<3.112	<3.658	<0.007	<0.003	<0.004
S	2732±152	1486±34	3266±350	6.340±0.351	1.593±0.043	3.732±0.427
Cl	252.0±58.1	19.5±6.5	<1.208	0.580±0.131	0.021±0.007	<0.001
K	34.0±1.2	4.4±0.7	40.1±11.0	0.079±0.003	0.005±0.001	0.045±0.012
Ca	37.2±1.6	10.6±1.2	43.1±6.8	0.086±0.003	0.011±0.001	0.048±0.007
Sc	<0.408	<5.714	<0.224	<0.001	<0.006	<0.000
Ti	95.4±2.6	7.6±0.5	24.1±6.7	0.221±0.006	0.008±0.001	0.027±0.007
V	30.9±1.3	3.1±0.3	102.9±28.5	0.072±0.003	0.003±0.000	0.115±0.030
Cr	<0.387	<1.410	<0.547	<0.001	<0.002	<0.001
Mn	18.1±0.8	2.7±0.4	1.9±0.4	0.042±0.002	0.003±0.000	0.002±0.000
Fe	589.6±21.2	124.2±20.0	90.9±20.4	1.369±0.051	0.134±0.023	0.102±0.021
Co	<0.082	<0.106	<0.089	<0.000	<0.000	<0.000
Ni	16.1±1.9	19.6±7.0	13.3±3.5	0.037±0.004	0.021±0.008	0.015±0.004

Table 5-9. Continued

Chemical Species	Stack Concentration (µg/m^3)			Emission Rate (kg/hr)		
	A	B	C	A	B	C
Cu	5.7±2.4	6.3±3.3	1.2±0.8	0.013±0.006	0.007±0.003	0.001±0.001
Zn	5.0±1.5	4.9±2.3	5.2±0.9	0.012±0.004	0.005±0.002	0.006±0.001
Ga	<1.031	<2.002	<2.584	<0.002	<0.002	<0.003
As	<0.113	<0.105	<1.489	<0.000	<0.000	<0.002
Se	<1.492	<2.310	3.9±0.5	<0.003	<0.002	0.004±0.001
Br	1.4±0.2	<0.441	<1.325	0.003±0.001	<0.000	<0.002
Rb	<0.945	<1.210	<0.579	<0.002	<0.001	<0.001
Sr	2.5±0.1	<0.465	0.7±0.1	0.006±0.000	<0.000	0.001±0.000
Y	0.8±0.1	<0.212	<0.467	0.002±0.000	<0.000	<0.001
Zr	3.6±0.2	<1.013	2.0±0.6	0.008±0.000	<0.001	0.002±0.001
Nb	<1.310	<1.268	<1.372	<0.003	<0.001	<0.002
Mo	2.3±0.1	<1.003	15.4±4.2	0.005±0.000	<0.001	0.017±0.004
Pd	<4.300	<4.447	<3.612	<0.010	<0.005	<0.004
Ag	<1.474	<4.627	<2.808	<0.003	<0.005	<0.003
Cd	<3.419	<3.754	<2.813	<0.008	<0.004	<0.003
In	<2.463	<2.264	<2.421	<0.006	<0.002	<0.003
Sn	<1.946	<1.885	<3.108	<0.004	<0.002	<0.003
Sb	<3.818	<7.123	<5.912	<0.009	<0.008	<0.007
Cs	<1.143	<1.026	<0.697	<0.003	<0.001	<0.001
Ba	<0.563	<0.658	<0.567	<0.001	<0.001	<0.001
La	<0.847	<0.794	<0.843	<0.002	<0.001	<0.001
Ce	<0.884	<1.286	<1.026	<0.002	<0.001	<0.001
Sm	<0.653	<1.184	<1.055	<0.002	<0.001	<0.001
Eu	<6.125	<6.292	<6.060	<0.014	<0.007	<0.007
Tb	<2.145	<2.447	<1.784	<0.005	<0.003	<0.002
Hf	<11.425	<15.680	<8.635	<0.027	<0.017	<0.010
Ta	<11.186	<8.605	<11.071	<0.026	<0.009	<0.013
W	<6.995	<10.661	<3.500	<0.016	<0.011	<0.004
Ir	<1.863	<1.682	<2.899	<0.004	<0.002	<0.003
Au	<1.607	<2.798	<5.146	<0.004	<0.003	<0.006
Hg	<1.665	<2.646	<1.779	<0.004	<0.003	<0.002
Tl	<2.006	<2.751	<2.010	<0.005	<0.003	<0.002
Pb	1.0±0.3	<0.874	<1.762	0.002±0.001	<0.001	<0.002
U	<1.507	<1.542	<2.126	<0.003	<0.002	<0.002
Sum of Species[d]	16441±1297	7762±263	20288±1648	38.2±3.2	8.3±0.3	23.2±2.1

[a] See Tables A-1 and A-2 of Appendix A for analytical MDL for each measurement.

[b] Average of 6 tests for Stacks A and C, and 7 tests for Stack B.

[c] OC1, OC2, OC3, and OC4 are organic carbon evolved at 140, 280, 480, and 580 °C, respectively, in a 100% He atmosphere
EC1, EC2, and EC3 are elemental carbon evolved at 580, 740, and 840 °C, respectively, in a 98% He / 2% O2 atmosphere
OP is pyrolyzed organic carbon by reflectance (OPR) or transmittance (OPT)
OC = (OC1 + OC2 + OC3 + OC4) + OPR
EC = (EC1 + EC2 + EC3) – OPR
TC = OC + EC

[d] Including TC, Na^+, Mg^{++}, K, Cl, Ca, $PO_4^{\equiv}$, and $SO_4^{=}$
Excluding OC and EC fractions, OC, EC, Na, Mg, P, S, $CO_3^{=}$, K^+, Cl^-, and Ca^{++}

Table 5-10. Wet basis concentrations (under standard conditions) and emission rates of Cs, Ba, rare earth elements, and Pb in $PM_{2.5}$ from the three stacks measured by ICP/MS. (Cells with "<" indicate the compound is below instruments' minimum detection limit (MDL[a]) in at least one test. Data were reported as average ± standard error of multiple runs[b].)

Chemical Species	Stack Concentration (μg/m^3)			Emission Rate (g/hr)		
	A	B	C	A	B	C
Cs	<0.0004	<0.0005	<0.0058	<0.001	<0.001	<0.006
Ba	1.6070±0.0511	0.2109±0.0253	0.4693±0.1036	3.7355±0.1429	0.2271±0.0288	0.5255±0.1076
La	0.5793±0.0172	0.0508±0.0043	0.1328±0.0354	1.3464±0.0478	0.0545±0.0048	0.1480±0.0373
Ce	1.1892±0.0334	0.1065±0.0095	0.3292±0.0922	2.7635±0.0933	0.1144±0.0106	0.3665±0.0973
Pr	0.1325±0.0039	0.0118±0.0010	0.0360±0.0098	0.3080±0.0110	0.0127±0.0011	0.0401±0.0104
Nd	0.4975±0.0142	0.0445±0.0038	0.1345±0.0366	1.1562±0.0395	0.0477±0.0042	0.1498±0.0386
Sm	0.0892±0.0025	0.0082±0.0008	0.0241±0.0064	0.2074±0.0068	0.0088±0.0009	0.0268±0.0067
Eu	0.0167±0.0006	<0.0004	0.0037±0.0015	0.0388±0.0014	<0.0005	0.0041±0.0016
Gd	0.0665±0.0018	<0.0005	<0.0109	0.1545±0.0047	<0.001	<0.012
Tb	0.0093±0.0003	0.0009±0.0001	0.0032±0.0009	0.0217±0.0007	0.0010±0.0001	0.0036±0.0009
Dy	0.0472±0.0013	0.0040±0.0004	0.0168±0.0048	0.1097±0.0036	0.0043±0.0004	0.0188±0.0050
Ho	0.0087±0.0003	0.0009±0.0001	0.0033±0.0009	0.0203±0.0006	0.0010±0.0001	0.0037±0.0010
Er	0.0247±0.0009	0.0019±0.0001	0.0088±0.0025	0.0574±0.0023	0.0021±0.0002	0.0097±0.0027
Tm	0.0032±0.0002	<0.0005	0.0011±0.0003	0.0075±0.0004	<0.001	0.0012±0.0003
Yb	0.0197±0.0005	<0.0005	0.0053±0.0018	0.0458±0.0014	<0.001	0.0059±0.0019
Lu	0.0026±0.0001	<0.0005	<0.0009	0.0060±0.0002	<0.001	<0.001
Pb	0.7998±0.0546	0.5705±0.3494	1.6368±0.4560	1.8609±0.1388	0.6105±0.3706	1.8218±0.4812

[a] See Tables A-1 and A-2 of Appendix A for analytical MDL for each measurement.

[b] Average of 6 tests for Stacks A and C, and 7 tests for Stack B.

Table 5-11. Wet basis concentration and ER of non-polar speciated organic carbon compounds analyzed by thermal desorption-gas chromatography/mass spectrometry (TD-GC/MS) from filter samples. (Cells with "<" indicate the compound is below instruments' minimum detection limit (MDL[a]) in at least one test. Data were reported as average ± standard error of multiple runs[b].)

Compound	MW	Stack Concentration (µg/m^3)			Emission Rate (g/hr)		
		A	B	C	A	B	C
PAHs							
acenaphthylene	152	<0.183	<0.208	<0.183	<0.419	<0.220	<0.204
acenaphthene	154	<0.099	<0.113	<0.099	<0.227	<0.120	<0.111
fluorene	166	<0.069	0.007±0.001	<0.069	<0.158	0.007±0.001	<0.077
phenanthrene	178	0.029±0.005	0.004±0.002	<0.033	0.066±0.011	0.004±0.002	<0.037
anthracene	178	0.010±0.002	0.004±0.001	<0.013	0.024±0.005	0.004±0.001	<0.015
fluoranthene	202	0.006±0.001	0.005±0.002	<0.020	0.014±0.002	0.005±0.002	<0.022
pyrene	202	0.019±0.004	<0.036	<0.031	0.045±0.010	<0.038	<0.035
benzo[a]anthracene	228	0.026±0.006	<0.068	<0.060	0.059±0.014	<0.072	<0.066
chrysene	228	0.037±0.009	0.003±0.000	<0.031	0.086±0.022	0.004±0.001	<0.035
benzo[b]fluoranthene	252	<0.064	<0.073	<0.064	<0.147	<0.077	<0.072
benzo[j+k]fluoranthene	252	<0.022	<0.025	<0.022	<0.050	<0.026	<0.024
benzo[a]fluoranthene	252	<0.032	<0.036	<0.032	<0.073	<0.039	<0.036
benzo[e]pyrene	252	<0.069	<0.078	<0.069	<0.158	<0.083	<0.077
benzo[a]pyrene	252	<0.070	<0.080	<0.070	<0.161	<0.085	<0.079
perylene	252	<0.076	<0.086	<0.076	<0.179	<0.091	<0.085
indeno[1,2,3-cd]pyrene	276	<0.033	<0.037	<0.033	<0.075	<0.040	<0.037
dibenzo[a,h]anthracene	278	<0.074	<0.084	<0.074	<0.168	<0.088	<0.082
benzo[ghi]perylene	276	<0.049	<0.055	<0.049	<0.111	<0.058	<0.054
coronene	300	<0.057	<0.065	<0.057	<0.131	<0.069	<0.064
dibenzo[a,e]pyrene	302	<0.022	<0.025	<0.022	<0.050	<0.026	<0.024
9-fluorenone	180	<0.077	0.018±0.005	<0.077	<0.176	0.019±0.005	<0.086
dibenzothiophene	184	0.056±0.006	<0.363	<0.319	0.130±0.014	<0.383	<0.356
1 methyl phenanthrene	192	0.023±0.005	0.035±0.015	<0.035	0.053±0.011	0.038±0.016	<0.039
2 methyl phenanthrene	192	0.007±0.002	0.002±0.001	<0.012	0.016±0.005	0.003±0.001	<0.013
3,6 dimethyl phenanthrene	206	<0.068	<0.077	<0.068	<0.156	<0.082	<0.076
methylfluoranthene	216	<0.022	<0.025	<0.022	<0.050	<0.026	<0.024
retene	219	<0.095	<0.108	<0.095	<0.217	<0.114	<0.106
benzo(ghi)fluoranthene	226	0.033±0.008	0.002±0.000	0.000±0.000	0.077±0.017	0.002±0.000	0.000±0.000
benzo(c)phenanthrene	228	0.003±0.002	0.000±0.000	0.000±0.000	0.006±0.004	0.000±0.000	0.000±0.000
benzo(b)naphtho[1,2-d]thiophene	234	0.007±0.005	0.000±0.000	0.000±0.000	0.016±0.012	0.000±0.000	0.000±0.000
cyclopenta[cd]pyrene	226	<0.022	<0.025	<0.022	<0.050	<0.026	<0.024
benz[a]anthracene-7,12-dione	258	<0.080	<0.091	<0.080	<0.183	<0.096	<0.089
methylchrysene	242	<0.033	<0.037	<0.033	<0.075	<0.040	<0.037
benzo(b)chrysene	278	0.000±0.000	0.000±0.000	0.000±0.000	0.000±0.000	0.000±0.000	0.000±0.000
picene	278	<0.081	<0.093	<0.081	<0.186	<0.098	<0.091
anthanthrene	276	<0.137	<0.156	<0.137	<0.314	<0.165	<0.153

Table 5-11. Continued

Compound	MW	Stack Concentration (ng/m^3)			Emission Rate (g/hr)		
		A	B	C	A	B	C
Alkane/Alkene/Phthalate							
***n*-alkane**							
n-pentadecane (*n*-C15)	212	0.012±0.004	0.017±0.004	0.004±0.001	0.028±0.009	0.018±0.004	0.005±0.001
n-hexadecane (*n*-C16)	226	0.027±0.008	0.135±0.040	0.009±0.001	0.062±0.020	0.146±0.044	0.010±0.002
n-heptadecane (*n*-C17)	240	0.089±0.031	0.078±0.042	0.011±0.002	0.208±0.074	0.083±0.045	0.012±0.002
n-octadecane (*n*-C18)	254	0.139±0.044	0.123±0.049	0.014±0.003	0.324±0.101	0.132±0.053	0.016±0.003
n-nonadecane (*n*-C19)	268	0.146±0.078	0.118±0.026	0.023±0.014	0.336±0.176	0.125±0.028	0.026±0.015
n-icosane (*n*-C20)	282	0.133±0.095	0.025±0.006	0.037±0.003	0.313±0.224	0.027±0.007	0.042±0.003
n-heneicosane (*n*-C21)	296	0.456±0.197	0.059±0.018	0.070±0.010	1.071±0.467	0.063±0.019	0.078±0.010
n-docosane (*n*-C22)	310	0.101±0.032	0.108±0.034	0.083±0.015	0.236±0.077	0.116±0.037	0.093±0.016
n-tricosane (*n*-C23)	324	0.191±0.051	0.175±0.023	0.059±0.010	0.443±0.121	0.187±0.024	0.066±0.010
n-tetracosane (*n*-C24)	338	1.063±0.427	0.435±0.059	0.045±0.007	2.464±0.983	0.465±0.063	0.051±0.007
n-pentacosane (*n*-C25)	352	0.723±0.407	0.241±0.037	0.037±0.005	1.705±0.971	0.257±0.038	0.042±0.005
n-hexacosane (*n*-C26)	366	0.395±0.184	0.190±0.032	0.024±0.004	0.924±0.434	0.203±0.033	0.027±0.004
n-heptacosane (*n*-C27)	380	0.149±0.055	0.152±0.027	0.018±0.005	0.349±0.130	0.162±0.027	0.020±0.006
n-octacosane (*n*-C28)	394	0.029±0.009	0.111±0.015	0.012±0.005	0.067±0.021	0.119±0.015	0.014±0.005
n-nonacosane (*n*-C29)	408	0.031±0.007	0.074±0.010	0.009±0.004	0.073±0.017	0.079±0.010	0.010±0.005
n-triacontane (*n*-C30)	422	0.022±0.004	0.039±0.005	0.004±0.002	0.050±0.010	0.041±0.006	0.005±0.002
n-hentriacotane (*n*-C31)	436	0.020±0.007	0.016±0.002	<0.061	0.046±0.016	0.017±0.002	<0.068
n-dotriacontane (*n*-C32)	450	0.009±0.002	0.005±0.001	<0.070	0.020±0.005	0.005±0.001	<0.079
n-tritriactotane (*n*-C33)	464	0.027±0.009	0.004±0.001	<0.045	0.064±0.021	0.004±0.001	<0.050
n-tetratriactoane (*n*-C34)	478	0.011±0.005	0.003±0.001	<0.052	0.025±0.012	0.003±0.001	<0.058
n-pentatriacontane (*n*-C35)	492	0.017±0.006	<0.064	<0.056	0.040±0.015	<0.068	<0.063
n-hexatriacontane (*n*-C36)	506	<0.067	<0.077	<0.067	<0.154	<0.081	<0.075
n-heptatriacontane (*n*-C37)	521	<0.068	<0.077	<0.068	<0.156	<0.082	<0.076
n-octatriacontane (*n*-C38)	535	<0.068	<0.077	<0.067	<0.156	<0.081	<0.075
n-nonatriacontane (*n*-C39)	549	<0.066	<0.073	<0.065	<0.154	<0.077	<0.073
n-tetracontane (*n*-C40)	563	<0.066	<0.075	<0.066	<0.153	<0.079	<0.073
iso/anteiso-alkane							
iso-nonacosane (iso-C29)	408	0.009±0.004	0.003±0.000	<0.131	0.020±0.009	0.003±0.001	<0.146
anteiso-nonacosane (anteiso-C29)	408	0.007±0.002	0.004±0.001	<0.131	0.017±0.004	0.004±0.001	<0.146
iso-triacontane (iso-C30)	422	0.006±0.001	0.003±0.001	<0.088	0.013±0.003	0.003±0.001	<0.098
anteiso-triacontane (anteiso-C30)	422	0.006±0.002	0.004±0.000	<0.088	0.013±0.004	0.004±0.000	<0.098
iso-hentriacotane (iso-C31)	436	0.005±0.002	0.002±0.001	<0.164	0.012±0.005	0.002±0.001	<0.183
anteiso-hentriacotane (anteiso-C31)	436	0.003±0.001	<0.186	<0.164	0.006±0.002	<0.197	<0.183
iso-dotriacontane (iso-C32)	450	0.016±0.006	<0.175	<0.154	0.038±0.015	<0.185	<0.172
anteiso-dotriacontane (anteiso-C32)	450	0.008±0.002	0.002±0.001	<0.154	0.018±0.006	0.002±0.001	<0.172
iso-tritriactotane (iso-C33)	464	0.003±0.001	<0.139	<0.122	0.007±0.003	<0.147	<0.136
anteiso-tritriactotane (anteiso-C33)	464	0.004±0.001	<0.139	<0.122	0.010±0.002	<0.147	<0.136
hopane							
22,29,30-trisnorneophopane (Ts)	370	0.024±0.007	0.006±0.001	<0.068	0.057±0.017	0.007±0.001	<0.076
22,29,30-trisnorphopane (Tm)	370	0.015±0.004	0.006±0.001	<0.068	0.034±0.009	0.006±0.001	<0.076
αβ-norhopane (C29αβ-hopane)	398	0.035±0.012	0.010±0.001	<0.070	0.081±0.029	0.011±0.001	<0.078
22,29,30-norhopane (29Ts)	398	0.014±0.003	0.009±0.001	<0.070	0.032±0.007	0.009±0.001	<0.078
αα- + βα-norhopane (C29αα- + βα -hopane)	398	0.108±0.042	0.007±0.001	<0.101	0.252±0.100	0.007±0.001	<0.113
αβ-hopane (C30αβ -hopane)	412	0.028±0.008	0.007±0.001	<0.067	0.065±0.020	0.008±0.001	<0.074

Table 5-11. Continued

Compound	MW	Stack Concentration (ng/m^3)			Emission Rate (g/hr)		
		A	B	C	A	B	C
αα-hopane (30αα-hopane)	412	0.011±0.005	<0.090	<0.079	0.025±0.012	<0.095	<0.088
βα-hopane (C30βα -hopane)	412	0.009±0.004	<0.090	<0.079	0.022±0.009	<0.095	<0.088
αβS-homohopane (C31αβS-hopane)	426	0.027±0.010	<0.083	<0.073	0.063±0.023	<0.087	<0.081
αβR-homohopane (C31αβR-hopane)	426	0.014±0.003	<0.096	<0.085	0.033±0.007	<0.102	<0.094
αβS-bishomohopane (C32αβS-hopane)	440	<0.019	<0.022	<0.019	<0.044	<0.023	<0.022
αβR-bishomohopane (C32αβR-hopane)	440	<0.023	<0.026	<0.023	<0.052	<0.027	<0.025
22S-trishomohopane (C33)	454	<0.019	<0.022	<0.019	<0.044	<0.023	<0.022
22R-trishomohopane (C33)	454	<0.023	<0.026	<0.023	<0.052	<0.027	<0.025
22S-tretrahomohopane (C34)	468	<0.019	<0.022	<0.019	<0.044	<0.023	<0.022
22R-tetrashomohopane (C34)	468	<0.023	<0.026	<0.023	<0.052	<0.027	<0.025
22S-pentashomohopane(C35)	482	<0.019	<0.022	<0.019	<0.044	<0.023	<0.022
22R-pentashomohopane(C35)	482	<0.023	<0.026	<0.023	<0.052	<0.027	<0.025
sterane							
ααα 20S-Cholestane	372	<0.046	0.003±0.000	<0.046	<0.106	0.003±0.000	<0.052
αββ 20R-Cholestane	372	0.020±0.015	<0.022	<0.020	0.048±0.036	<0.024	<0.022
αββ 20s-Cholestane	372	0.016±0.011	<0.026	<0.023	0.037±0.025	<0.027	<0.025
ααα 20R-Cholestane	372	<0.023	<0.026	<0.023	<0.052	<0.027	<0.025
ααα 20S 24S-Methylcholestane	386	<0.026	0.002±0.001	<0.026	<0.060	0.002±0.001	<0.029
αββ 20R 24S-Methylcholestane	386	0.002±0.001	<0.030	<0.026	0.005±0.001	<0.032	<0.029
αββ 20S 24S-Methylcholestane	386	0.005±0.001	<0.030	<0.026	0.011±0.003	<0.032	<0.029
ααα 20R 24R-Methylcholestane	386	0.015±0.011	<0.035	<0.031	0.035±0.026	<0.037	<0.034
ααα 20S 24R/S-Ethylcholestane	386	<0.027	<0.029	<0.026	<0.066	<0.031	<0.029
αββ 20R 24R-Ethylcholestane	400	<0.021	<0.023	<0.021	<0.047	<0.025	<0.023
αββ 20S 24R-Ethylcholestane	400	<0.021	<0.023	<0.021	<0.047	<0.025	<0.023
ααα 20R 24R-Ethylcholestane	400	<0.055	<0.062	<0.055	<0.125	<0.066	<0.061
methyl-alkane							
2-methylnonadecane	282	0.152±0.053	0.052±0.005	<0.110	0.355±0.123	0.055±0.005	<0.122
3-methylnonadecane	282	0.087±0.033	0.059±0.009	<0.072	0.203±0.076	0.064±0.010	<0.081
branched-alkane							
pristane	268	0.096±0.016	0.056±0.015	0.027±0.002	0.222±0.036	0.060±0.017	0.030±0.002
phytane	282	0.125±0.027	0.049±0.012	0.021±0.004	0.289±0.059	0.053±0.013	0.023±0.004
squalane	422	0.009±0.002	0.003±0.001	<0.119	0.022±0.006	0.004±0.001	<0.133
cycloalkane							
octylcyclohexane	196	<0.199	<0.227	<0.199	<0.456	<0.240	<0.222
decylcyclohexane	224	<0.170	<0.193	<0.170	<0.388	<0.204	<0.189
tridecylcyclohexane	266	<0.128	<0.146	<0.128	<0.294	<0.155	<0.143
n-heptadecylcyclohexane	322	0.021±0.006	0.010±0.001	0.003±0.000	0.049±0.014	0.010±0.001	0.003±0.000
nonadecylcyclohexane	350	0.011±0.004	0.005±0.001	0.001±0.000	0.026±0.009	0.006±0.001	0.001±0.000
alkene							
1-octadecene	252	0.293±0.102	0.264±0.052	<0.308	0.680±0.233	0.282±0.055	<0.344
Sum of categories							
PAHs		0.544±0.216	0.142±0.034	0.083±0.044	1.276±0.517	0.152±0.037	0.091±0.048
n-alkane		4.143±0.989	2.149±0.188	0.543±0.140	9.677±2.345	2.297±0.190	0.610±0.152
iso/anteiso-alkane		0.066±0.019	0.022±0.003	0.001±0.001	0.154±0.045	0.024±0.003	0.001±0.001
hopane		0.328±0.103	0.051±0.005	<0.249	0.767±0.244	0.054±0.005	<0.278
sterane		0.145±0.069	0.015±0.003	<0.105	0.342±0.165	0.016±0.003	<0.117

Table 5-11. Continued							
Compound	**MW**	**Stack Concentration (ng/m^3)**			**Emission Rate (g/hr)**		
		A	**B**	**C**	**A**	**B**	**C**
methyl-alkane		0.240±0.082	0.111±0.012	0.013±0.004	0.558±0.191	0.119±0.013	0.015±0.005
branched-alkane		0.231±0.024	0.108±0.027	0.048±0.006	0.533±0.050	0.117±0.030	0.054±0.006
cycloalkane		0.039±0.010	0.023±0.005	0.004±0.001	0.090±0.022	0.025±0.005	0.005±0.001
alkene		0.293±0.102	0.264±0.052	0.001±0.001	0.680±0.233	0.282±0.055	0.001±0.001
Sum of all non-polar species		6.028±1.249	2.884±0.238	0.693±0.163	14.076±2.983	3.086±0.243	0.776±0.174

[a] See Tables A-1 and A-2 of Appendix A for analytical MDL for each measurement.
[b] Average of 6 tests for Stacks A and C, and 7 tests for Stack B.

Table 5-12. Wet basis concentration and ER of carbohydrates, organic acids and WSOC from $PM_{2.5}$ particles collected on the quartz filters. (Cells with "<" indicate the compound is below instruments' minimum detection limit (MDL[a]) in at least one test. Data were reported as average ± standard error of multiple runs[b].)

Compound	MW	Stack Concentration (ug/m^3)			Emission Rate (g/hr)		
		A	B	C	A	B	C
Carbohydrates							
Glycerol (C3H8O3)	92	<0.996	<0.937	2.162±0.486	<2.353	<1.013	2.479±0.589
Inositol (C6H12O6)	180	<1.633	<1.925	<1.621	<3.798	<2.068	<1.842
Erythritol (C4H10O4)	122	<2.450	<2.888	<2.431	<5.697	<3.102	<2.764
Xylitol (C5H12O5)	152	<5.913	<1.925	<1.621	<13.84	<2.068	<1.842
Levoglucosan (C6H10O5)/Arabitol (C5H12O5)	162	<6.904	<3.851	<3.242	<16.18	<4.136	<3.685
Sorbitol (C6H14O6)	182	<4.084	<4.813	18.62±0.95	<9.495	<5.170	21.19±1.04
Mannosan (C6H10O5)	162	<2.450	<2.888	<2.431	<5.697	<3.102	<2.764
Trehalose (C12H22O11)	342	<3.267	<3.851	<3.242	<7.596	<4.136	<3.685
Mannitol (C6H14O6)	182	<2.450	<2.888	<2.431	<5.697	<3.102	<2.764
Arabinose (C5H10O5)	150	<2.450	<2.888	<2.431	<5.697	<3.102	<2.764
Glucose (C6H12O6)/Xylose (C5H10O5)	180	<3.070	<1.925	<1.621	<7.184	<2.068	<1.842
Galactose (C6H12O6)	180	<3.267	<3.851	<3.242	<7.596	<4.136	<3.685
Maltitol (C12H24O11)/Fructose (C6H12O6)	344	<4.084	<4.813	<4.052	<9.495	<5.170	<4.606
Organic Acids							
Lactic acid (C3H6O3)	90	8.981±5.181	<2.970	<4.835	21.21±12.37	<3.211	<5.591
Acetic acid (C2H4O2)	60	<5.053	<5.313	<4.854	<11.74	<5.687	<5.507
Formic acid (CH2O)	46	<4.891	<5.776	<4.863	<11.37	<6.204	<5.527
Methanesulfonic acid (CH4SO3)	96	40.91±2.17	<26.12	<3.242	95.07±5.39	<27.86	<3.685
Glutaric acid (C5H8O4)	132	<4.076	<4.813	<4.052	<9.475	<5.170	<4.606
Succinic acid (C4H6O4)	118	<3.261	<3.851	<3.242	<7.580	<4.136	<3.685
Malonic acid (C3H4O4)	104	<4.891	<5.776	<4.863	<11.37	<6.204	<5.527
Maleic acid (C4H4O4)	116	<4.076	<4.813	<4.052	<9.475	<5.170	<4.606
Oxalic acid (C2H2O4)	90	2.732±0.325	<2.769	<3.397	6.350±0.782	<2.975	<3.857
WSOC							
Neutral compounds		11.95±3.16	20.90±6.08	14.73±0.91	27.93±7.63	22.50±6.59	16.77±1.02
Mono-/di- carboxylic acids		<14.57	<17.02	<19.51	<34.36	<18.05	<22.25
Polycarboxylic acids (including HULIS)		<71.63	<93.41	<79.60	<165.88	<100.80	<91.05
Sum of speciated WSOC		22.34±5.66	32.32±8.16	25.34±6.04	52.28±13.58	34.62±8.70	28.58±6.57
Total WSOC		<287.94	62.02±11.91	<143.95	<665.68	66.27±12.58	<163.83

[a] See Tables A-1 and A-2 of Appendix A for analytical MDL for each measurement.

[b] Average of 6 tests for Stacks A and C, and 7 tests for Stack B.

6 Source Profiles

This section reports chemical source profiles for gases and $PM_{2.5}$. As described in Section 2, $PM_{2.5}$ was collected on Teflon®-membrane and quartz-fiber filters for comprehensive laboratory chemical analysis. Source profiles reported in this section are normalized by $PM_{2.5}$ mass measured from the Teflon®-membrane filter. Organic constituents of $PM_{2.5}$ are also normalized by total OC mass from IMPROVE_A carbon analysis of the quartz-fiber filters. Mass abundances (relative to $PM_{2.5}$ mass) for NH_3, SO_2, and H_2S measured from backup filters are listed in Table 6-1. Stack B has the highest abundance of NH_3 and SO_2 (1025±637% and 9205±4662% of $PM_{2.5}$, respectively), while Stack C has the lowest abundance of NH_3 and SO_2 (0.43±0.27% and 472±152% of $PM_{2.5}$, respectively). H_2S has low abundances in all three stacks (<0.038%).

Table 6-1. Source profile abundances for NH_3, SO_2, and H_2S measured from backup filters. Data are expressed as a percentage of the Teflon® filter $PM_{2.5}$ mass concentration.

Chemical Species	A	B	C
NH_3	34.2±10.5	1025±637	0.43±0.27
SO_2	>2226[a]	9205±4662	472±152
H_2S	0.038±0.041	0.026±0.042	0.008±0.006

[a] Potassium carbonate-impregnated filters were saturated with SO_2 in 2008 measurement, causing the SO_2 abundance biased low.

Average $PM_{2.5}$ chemical abundances for the three stacks are summarized in Table 6-2, and the most abundant species (>0.1%) are plotted in Figure 6-1. Figure 6-2 shows the fractions of $PM_{2.5}$ grouped into the following categories: 1) geological materials (including Al_2O_3, SiO_2, CaO, Fe_2O_3, and TiO_2 estimated from XRF measurements of Al, Si, Ca, Fe, and Ti respectively); 2) organics (= OC x 1.2); 3) soot (= EC); 4) $SO_4^=$ 5) NH_4^+; 6) other water soluble ions (Cl^-, NO_2^-, NO_3^-, $PO_4^{\equiv}$, Na^+, Mg^{++}, K^+, and Ca^{++}); 7) other elements (all elements measured by XRF in Table 6-2 from P to U, excluding S, Ca, Fe, and Ti); and 8) unidentified species. Soluble $SO_4^=$ is by far the most abundant species, constituting 39.2 ± 4.9%, 67.9 ± 2.5%, and 49.7 ± 3.6% to $PM_{2.5}$ mass for Stacks A, B, and C, respectively. NH_4^+ is the main identified cation for Stacks A and B, where it accounts for 15.1± 2.0% and 24.9 ± 1.1% of $PM_{2.5}$. NH_4^+ only accounts 0.9± 1.0% of $PM_{2.5}$ in Stack C. 6.1% and 43.1% of $PM_{2.5}$ is unidentified for Stacks A and C, respectively, while the sum of species for Stack B is 103.9% when geological materials or organics are omitted (Table 6-2) and 108.2% when they are included. The slight overestimate is probably due to positive sampling artifacts (Chow et al., 2010c) and measurement uncertainties. 100±10% deviations are common for mass closure measurements (Watson et al., 2012a).

These results are consistent with the major chemical $PM_{2.5}$ component from Stack C being H_2SO_4 droplets in the form of [$H_2SO_4 \cdot xH_2O$]. The major unidentified mass is hydrogen ion and water. As shown Figure 4-6c and discussed in Section 4.3.2, measured anions and cations are out of balance for samples from Stack C, with anions (in μeq/m^3) being ~17 times higher than cations. H^+, a common cation in some stack exhaust, was not quantified in the analytical methods. The Stack C flue gas temperature was ~55°C, below the typical H_2SO_4 dew point (100-150°C), which facilitates formation of H_2SO_4 mist. The NH_4^+ abundance is low from Stack C, insufficient to neutralize H_2SO_4 in the exhaust. The compounds that contain $SO_4^=$ from Stack C are volatile. If most of the sulfur exits in the form of sulfate, the $SO_4^=$/S ratio should be close to 3, as is the case for Stacks A and B (Figure 4-2 a and b). However, this ratio is ~5.0 for Stack C

(Figure 4-2c), indicating that some sulfate species were stable in solution and were quantified by the IC, but evaporated under the vacuum and sample heating of the XRF (1-2 Pa).

Table 6-3 compares $PM_{2.5}$ mass on the Teflon® filters before and after XRF measurements. There was little change for filters from Stacks A and B (7% and 1% losses, respectively). However, the filters from Stack C lost 77% of the mass, on average, after exposure to the XRF vacuum chamber. H_2SO_4 is hygroscopic, absorbing large amounts of water even at low humidities. Under the conditions of DRI's filter conditioning room (21.5 ± 5 °C and 30 ± 5% RH), a 1 μm spherical droplet of H_2SO_4 and H_2O would have equilibrium mole fractions of ~15% H_2SO_4 and 85% of H_2O (Seinfeld and Pandis, 1997), which is equivalent to mass fraction of 49% H_2SO_4 and 51% of H_2O. Water will evaporate quickly under the vacuum of XRF (1-2 Pa) due to its higher vapor pressure, causing major losses of mass. If the filter is in the vacuum long enough to reach the azeotrope of H_2SO_4 solution (98.479% H_2SO_4 and 1.521% of H_2O) (Richardson et al., 1986), H_2SO_4 and H_2O will start to evaporate at the same rate, causing the loss of S measured by XRF as observed in this study. H_2O probably accounts for the large unidentified $PM_{2.5}$ mass (43.5%) for Stack C as shown Figure 6-2 since the H_2O in equilibrium with H_2SO_4 under the weighing room conditions will be measured by gravimetry, but not measured in chemical speciation. The poor correlation between $PM_{2.5}$ mass measured by filter and DustTrak or OPC in Figure 5-2 is probably due to the different RH in the filter weighing room, the stack, and inside the instruments. The submicron size distribution of particles in Stack C also supports that these particles are likely H_2SO_4 mist.

Wet stacks present other difficulties in extracting large droplets through the buttonhook nozzle. An in-stack dilution system is being tested by U.S. EPA to more completely capture these droplets for dilution with drier air that would better evaporate the droplet in the dilution chamber (Baldwin et al., 2010; Neulicht et al., 2009).

Total carbon (TC) constitutes 12.9 ± 2.3%, 6.9 ± 0.6%, and 1.4 ± 1.8% of $PM_{2.5}$ for Stacks A, B, and C, respectively. Although carbon accounted for a minor fraction of $PM_{2.5}$, it was a major fraction of non-sulfate $PM_{2.5}$. Figure 6-3 shows the carbon fraction abundances. For Stack A, most carbon is in the lower temperature OC1 (140°C, 100% helium [He] atmosphere), OC2 (280°C, 100% He atmosphere), and EC1 (580°C, 98% He/2% O_2 atmosphere) fractions; for Stack B, most of the carbon is in OC2 and EC1 fractions. Carbon is a minor part (<1.4%) of $PM_{2.5}$ mass for Stack C, and most of the carbon is in OC4 (580°C, 100% He atmosphere), OP (580°C, at 98% He/2% O_2 atmosphere), and EC1 fractions. This differs from emission profiles from boilers, process heaters, and steam generators measured from petroleum industries, where carbon was found to be the largest contributor to $PM_{2.5}$.

Figure 6-4 shows $PM_{2.5}$ source profiles several oil refinery stacks for comparison. The gas-fired boiler and the process heater were fired with refinery process gas, and were not equipped with NO_x, SO_2 or PM air pollution controls. The FCCU was equipped with a CO heater fired by refinery process gas and an electrostatic precipitator (ESP). The boiler source profile distributed most evenly among different species, with sulfate being the most abundant (20%), followed by EC (10%), ammonium (9%), sulfur (6%), and OC (5%). The FCCU source profile was dominated by sulfate (91%), followed by silicon (6%) and aluminum (3.6%) with TC being <1%. The process heater source profile was dominated by OC (35%) and EC (27%), with sulfate being only ~4%. The different source profiles observed in different facilities and different combustion devices are due to different fuel gas used in the combustion and the industrial processes upstream of the stacks.

Table 6-2. Average $PM_{2.5}$ source profile abundances for the three stacks. Data are reported as average ± uncertainty, where the uncertainty is the larger of standard deviation and uncertainty of average of multiple runs[a].

Chemical Species	$PM_{2.5}$ Source Profile		
	A	B	C
Cl^-	1.601±0.995	0.157±0.207	0.000±0.017
NO_2^-	0.000±0.019	0.032±0.085	0.001±0.011
NO_3^-	0.069±0.039	0.234±0.142	0.005±0.012
$PO_4^{\equiv}$	0.008±0.020	0.411±0.749	0.069±0.060
$SO_4^=$	39.167±4.867	67.893±2.453	49.650±3.557
NH_4^+	15.148±2.007	24.893±1.103	0.926±1.016
Na^+	0.051±0.017	0.040±0.028	0.035±0.027
Mg^{++}	0.022±0.008	0.042±0.007	0.029±0.010
K^+	0.046±0.013	0.033±0.022	0.076±0.049
Ca^{++}	0.115±0.046	0.108±0.059	0.087±0.062
OC1	2.144±2.280	0.100±0.212	0.080±0.092
OC2	2.804±1.022	3.625±0.614	0.000±0.017
OC3	0.284±0.361	0.659±0.325	0.127±0.218
OC4	0.526±0.188	0.554±0.206	0.198±0.204
OPT	0.000±0.079	1.066±0.390	1.077±1.105
OPR	0.000±0.024	0.116±0.306	0.690±0.897
OCT	5.642±2.844	5.332±0.813	1.251±1.707
OCR	5.750±2.835	4.741±0.980	0.950±1.468
EC1	6.513±1.097	2.004±0.598	0.926±1.178
EC2	0.672±0.250	0.359±0.197	0.182±0.078
EC3	0.003±0.007	0.000±0.024	0.015±0.010
ECT	7.406±1.091	2.021±0.395	0.172±0.107
ECR	7.158±1.052	2.146±0.433	0.416±0.321
TC	12.908±2.305	6.887±0.590	1.348±1.775
Na	0.900±0.228	1.597±0.277	0.653±0.112
Mg	0.137±0.047	0.173±0.088	0.101±0.016
Al	1.008±0.116	0.285±0.040	0.266±0.178
Si	4.656±1.791	0.389±0.044	1.029±0.789
P	0.000±0.002	0.000±0.006	0.000±0.001
S	13.209±1.937	19.921±0.904	8.718±1.578
Cl	1.220±0.751	0.249±0.201	0.000±0.001
K	0.165±0.022	0.058±0.020	0.114±0.083
Ca	0.182±0.036	0.139±0.029	0.121±0.056
Sc	0.002±0.004	0.001±0.012	0.001±0.002
Ti	0.465±0.073	0.103±0.023	0.068±0.051
V	0.150±0.021	0.042±0.012	0.292±0.215
Cr	0.002±0.001	0.020±0.043	0.000±0.001
Mn	0.088±0.014	0.036±0.015	0.005±0.003

Table 6-2 (continued)

Chemical Species	$PM_{2.5}$ Source Profile		
	A	B	C
Fe	2.862±0.383	1.633±0.544	0.259±0.158
Co	0.000±0.000	0.000±0.000	0.000±0.000
Ni	0.078±0.027	0.250±0.224	0.038±0.027
Cu	0.030±0.031	0.079±0.108	0.004±0.006
Zn	0.026±0.020	0.063±0.076	0.015±0.008
Ga	0.001±0.002	0.004±0.006	0.000±0.001
As	0.000±0.000	0.000±0.000	0.004±0.004
Se	0.001±0.002	0.000±0.004	0.010±0.001
Br	0.007±0.003	0.006±0.004	0.000±0.001
Rb	0.000±0.001	0.000±0.002	0.001±0.001
Sr	0.012±0.002	0.006±0.004	0.002±0.001
Y	0.004±0.001	0.003±0.003	0.001±0.001
Zr	0.017±0.004	0.007±0.007	0.006±0.004
Nb	0.000±0.002	0.002±0.005	0.000±0.001
Mo	0.011±0.003	0.005±0.005	0.044±0.032
Pd	0.000±0.003	0.000±0.009	0.000±0.002
Ag	0.001±0.003	0.000±0.008	0.000±0.002
Cd	0.001±0.003	0.003±0.010	0.000±0.002
In	0.000±0.002	0.002±0.006	0.000±0.001
Sn	0.001±0.003	0.002±0.008	0.000±0.001
Sb	0.001±0.005	0.000±0.015	0.000±0.003
Cs	0.000±0.001	0.000±0.002	0.000±0.000
Ba	0.000±0.000	0.000±0.001	0.000±0.000
La	0.000±0.001	0.001±0.002	0.000±0.000
Ce	0.000±0.001	0.000±0.003	0.000±0.000
Sm	0.001±0.001	0.002±0.004	0.000±0.001
Eu	0.000±0.004	0.000±0.013	0.000±0.002
Tb	0.000±0.001	0.000±0.004	0.000±0.001
Hf	0.001±0.009	0.000±0.029	0.001±0.005
Ta	0.000±0.008	0.007±0.024	0.000±0.004
W	0.006±0.011	0.007±0.035	0.003±0.006
Ir	0.001±0.002	0.003±0.007	0.000±0.001
Au	0.002±0.005	0.004±0.016	0.000±0.003
Hg	0.000±0.002	0.000±0.005	0.000±0.001
Tl	0.000±0.002	0.000±0.005	0.000±0.001
Pb	0.005±0.004	0.012±0.009	0.004±0.004
U	0.002±0.003	0.007±0.008	0.000±0.002
Sum of Species[b]	78.382±4.253	103.862±3.691	54.353±3.738

[a] Average of 6 tests for Stacks A and C, and 7 tests for Stack B.

[b] Including TC, Na^{+}, Mg^{++}, K, Cl, Ca, $PO_4^{\equiv}$, and $SO_4^{=}$
Excluding OC and EC fractions, OC, EC, Na, Mg, P, S, $CO_3^{=}$, K^{+}, Cl^{-}, and Ca^{++}

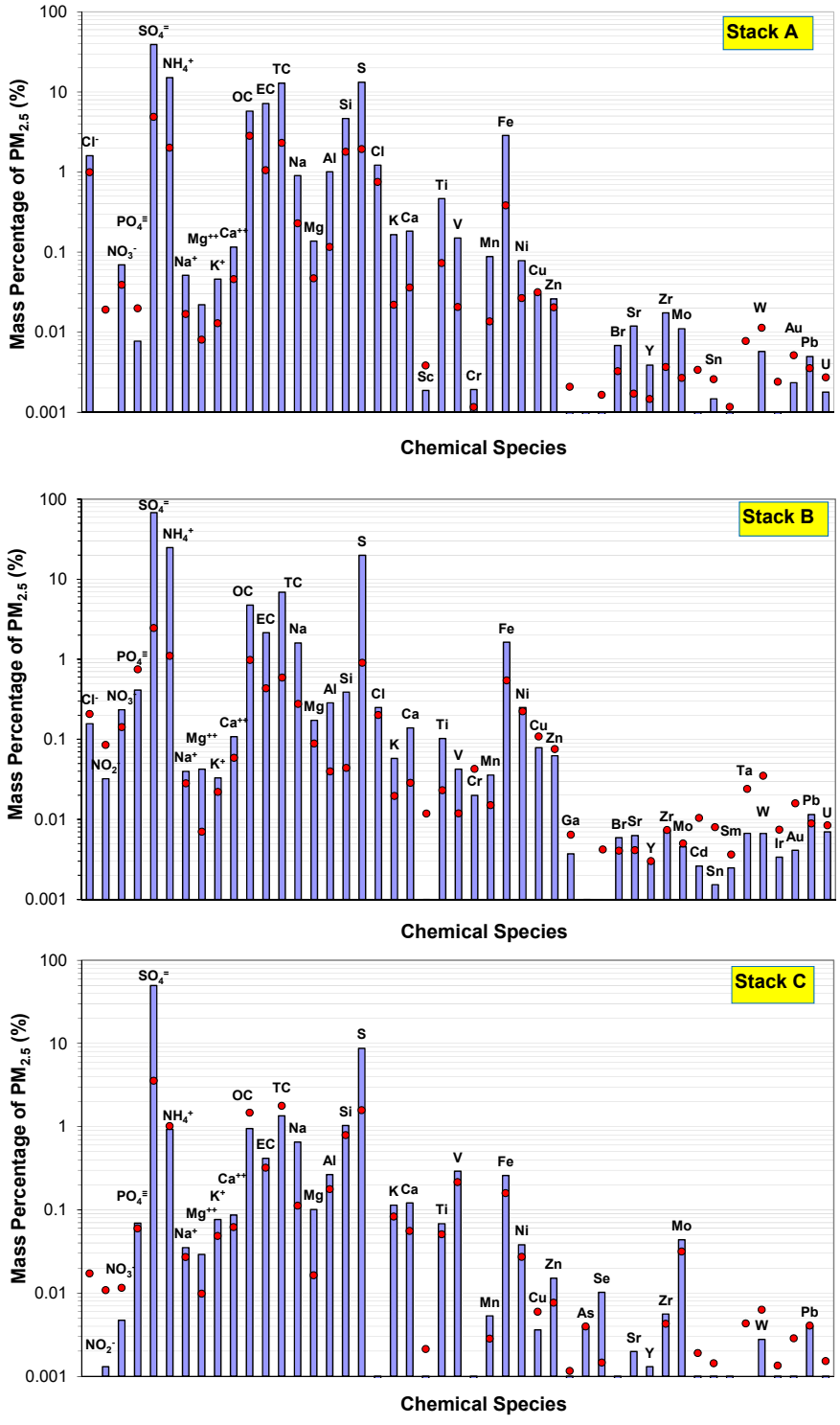

Figure 6-1. Average $PM_{2.5}$ source profiles from the three stacks. (The height of each bar indicates the average fractional abundance for the indicated chemical [normalized to $PM_{2.5}$ mass concentration from the Teflon®-membrane filter], while the dot shows the standard error of the average of multiple runs.)

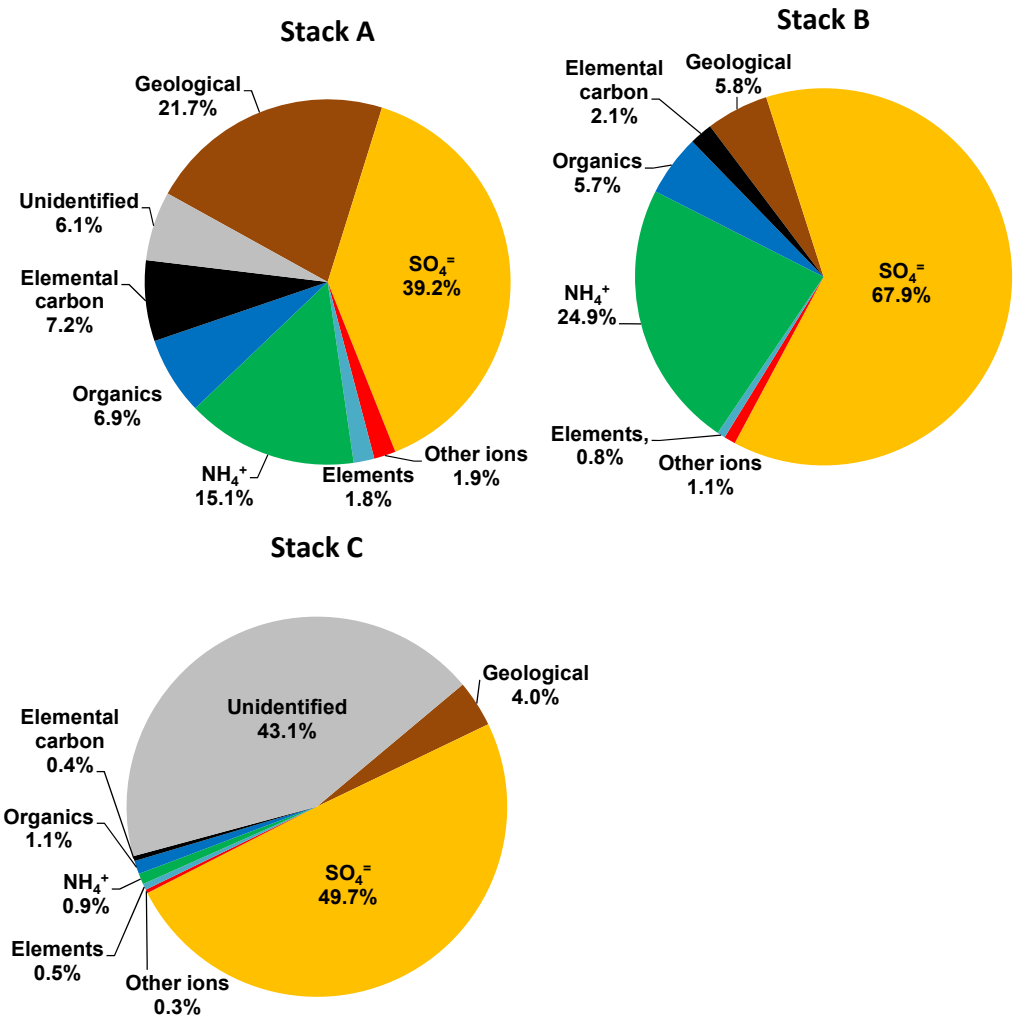

Figure 6-2. $PM_{2.5}$ source profiles for the three stacks. Geological material includes Al_2O_3, SiO_2, CaO, and Fe_2O_3; other soluble ions include Cl^-, NO_2^-, NO_3^-, $PO_4^{\equiv}$, Na^+, Mg^{++}, K^+, and Ca^{++}, and elements include all elements measured by XRF in Table 6-2 from P to U, excluding S, Ca, and Fe.

Trace element abundances are low (typically < 0.1%) with elevated abundances for S (9-20%), mostly in the form of $SO_4^{=}$. Stacks A and B has higher abundance of Fe (2.8 ± 0.4% and 1.6 ± 0.5%, respectively) than Stack C (0.3 ± 0.2%). Abundances of Cs, Ba, rare earth elements, and Pb by ICP/MS are listed in Table 6-4. All these elements are <0.01% of $PM_{2.5}$. Abundances in samples from Stack A are 2.5-5 times of those found in samples from Stack B, and 4.5-7.5 times of those from Stack C for most rare earth elements. Abundances of the stable lead isotopes measured by the ICP/MS are plotted in Figure 6-5, along with their natural abundances. On average, the stack samples are 5.5% less abundant for ^{204}Pb, 6.0% more abundant for ^{206}Pb, 6.1% less abundant for 207Pb, and 0.05% less abundant for ^{208}Pb compared to the natural abundance. Figure 6-6 plots Pb isotope ratios. Note that while Stacks A and B have larger overlaps in Pb isotope ratios, Stack C has higher ^{208}Pb /^{207}Pb and lower ^{204}Pb /^{207}Pb ratios than Stacks A and B.

Table 6-5 lists abundances for 113 non-polar organic compounds normalized to $PM_{2.5}$ or OC. The sum of non-polar compounds accounts for 0.029±0.016%, 0.038±0.009%, and 0.002±0.001% of $PM_{2.5}$ in Stacks A, B, and C, respectively, and 0.521±0.176%, 0.839±0.293%,

and 0.952±1.350% of OC, respectively. n-alkanes are the most abundant category, accounting for 0.019±0.012%, 0.028±0.007%, and 0.002±0.001% of $PM_{2.5}$, and 0.34±0.14%, 0.62±0.22%, and 0.73±0.98% of OC for Stacks A, B, and C, respectively. Other non-polar compounds including PAHs have very low abundances. The top ten most abundant compounds in each stack and their abundances normalized to OC are listed in Table 6-6. n-tricosane (n-C23), n-tetracosane (n-C24), n-pentacosane (n-C25), and n-hexacosane (n-C26) are among the top 10 abundant compounds in all three stacks. 1-octadecene is abundant in Stacks A and B, but is below MDL in Stack C. Figure 6-7 illustrates source profile for the most abundant (>0.0001% of OC) non-polar compounds from the three stacks. The abundance patterns are similar for Stacks A and B. They have common abundant species, but Stack B has higher abundance for most compounds. On the other hand, the abundance pattern in Stack C is more different from those in Stacks B and C. The most abundant n-alkanes in Stack C are lighter (peaks at n-c22) than that in Stacks A and B (peaks at n-c24). While Stacks A and B have PAHs, iso/anteiso-alkanes, hopanes, steranes, methyl-alkane, and 1-octadecene at detectable levels, all these compounds are below the detection limit in Stack C.

Table 6-7 lists abundances for carbohydrates, organic acids and WSOC classes. Most species are below MDLs.

Table 6-3. $PM_{2.5}$ mass on Teflon® filters before and after the XRF measurement.

Stack	Run ID	$PM_{2.5}$ mass before XRF (mg)	$PM_{2.5}$ mass after XRF (mg)	Ratio After/ Before XRF	Average Ratio
A	A-1	2.570	2.330	0.91	0.93±0.02
	A-2	1.082	0.977	0.90	
	A-3	1.463	1.376	0.94	
	A-4	1.366	1.288	0.94	
	A-5	1.613	1.505	0.93	
	A-6	1.409	1.312	0.93	
B	B-1	0.648	0.629	0.97	0.99±0.01
	B-2	0.472	0.472	1.00	
	B-3	0.526	0.527	1.00	
	B-4	0.670	0.664	0.99	
	B-5	0.522	0.514	0.98	
	B-6	0.253	0.254	1.00	
	B-7	0.414	0.413	1.00	
C	C-1	1.896	0.883	0.47	0.23±0.14
	C-2	2.958	0.861	0.29	
	C-3	2.347	0.590	0.25	
	C-4	2.312	0.419	0.18	
	C-5	3.892	0.527	0.14	
	C-6	3.628	0.303	0.08	

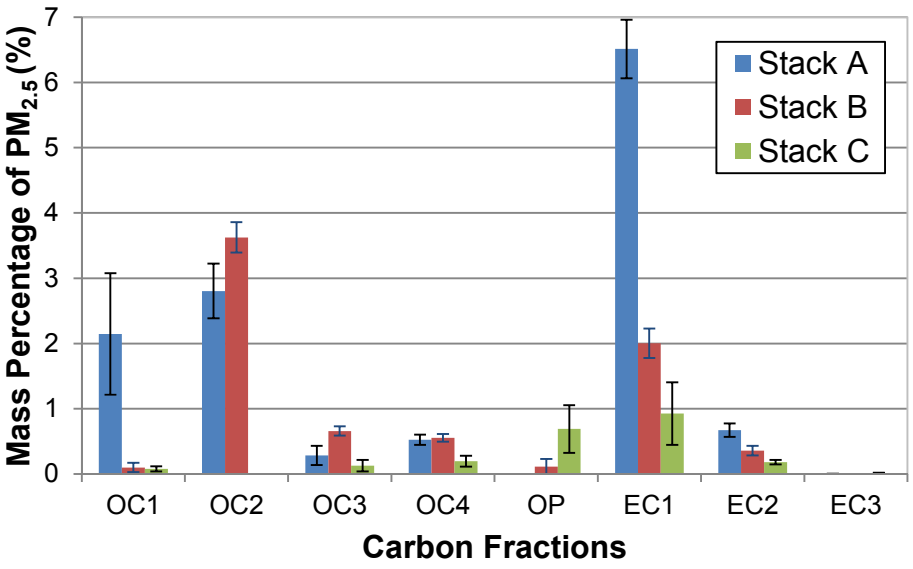

Figure 6-3. Abundance of carbon fractions (percentage of $PM_{2.5}$). OC1 to OC4 are organic carbon fractions evolved in a 100% helium (He) atmosphere at 140, 280, 480, and 580 °C, respectively. EC1 to EC3 are elemental carbon fractions evolved in a 98% He/2% O_2 atmosphere at 580, 740, and 840 °C, respectively. OP is pyrolyzed carbon by reflectance (OPR) or transmittance (OPT). The thermal analysis followed the IMPROVE_A thermal/optical reflectance analysis (TOR) protocol (Chow et al., 2007a).

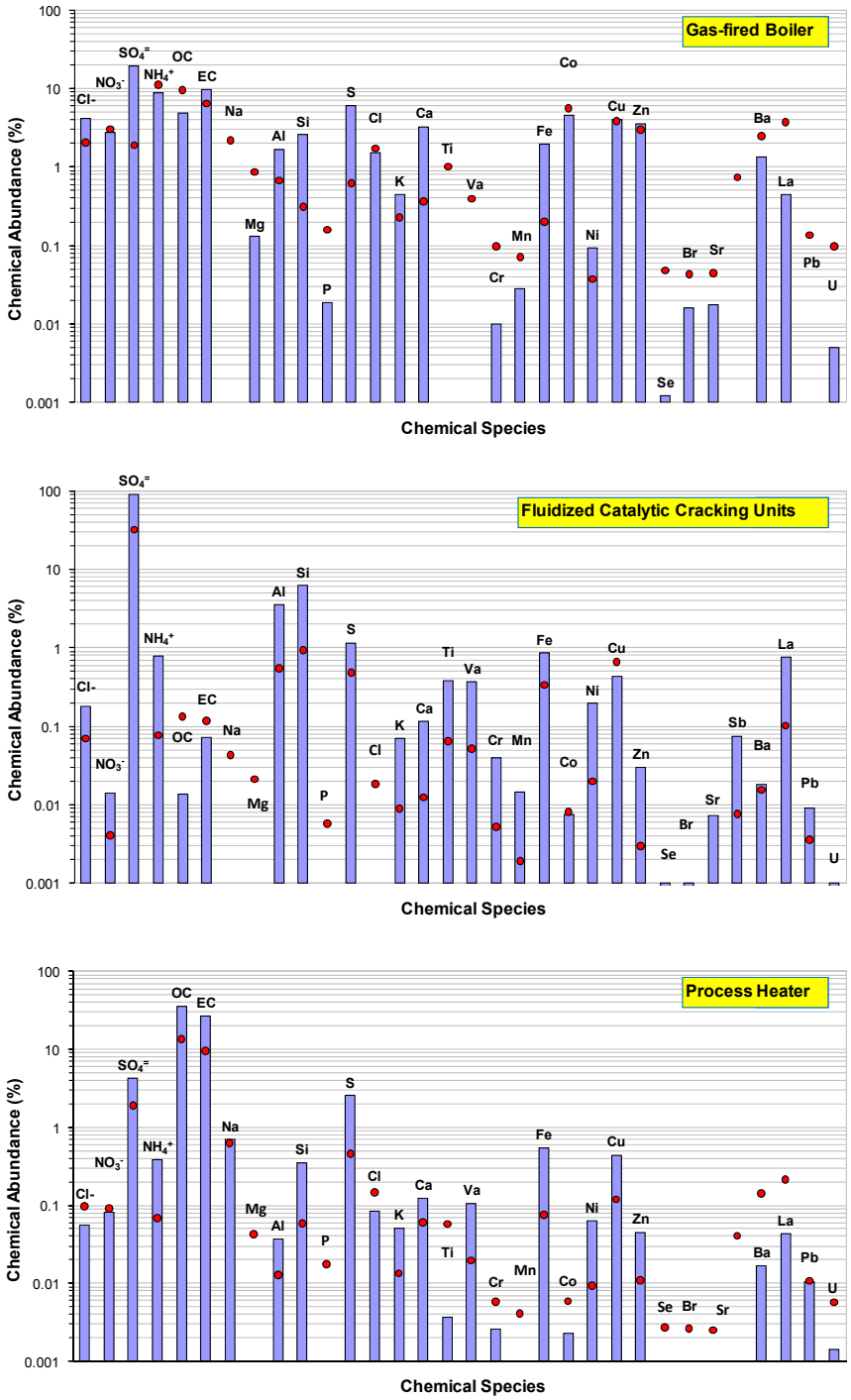

Figure 6-4. Composite $PM_{2.5}$ source profiles from a gas-fired boiler, a fluidized catalytic cracking unit, and a process heater n two oil refinery facilities (Chang and England, 2004b; Chang and England, 2004a; England et al., 2001a; England et al., 2001b; England et al., 2001c).

Table 6-4. Summary of the source profiles of Cs, Ba, rare earth elements, and Pb in $PM_{2.5}$ collected from the three stacks and measured by ICP/MS. Data are reported as average ± uncertainty, where the uncertainty is the larger of standard deviation and uncertainty of average of multiple runs[a].

Element	Stack A	Stack B	Stack C
Cs	0.00E+00 ± 5.62E-06	0.00E+00 ± 1.56E-05	1.61E-05 ± 2.52E-05
Ba	7.83E-03 ± 1.59E-03	2.79E-03 ± 7.29E-04	1.33E-03 ± 8.04E-04
La	2.83E-03 ± 5.70E-04	6.84E-04 ± 1.68E-04	3.76E-04 ± 2.69E-04
Ce	5.80E-03 ± 1.17E-03	1.44E-03 ± 3.81E-04	9.33E-04 ± 6.95E-04
Pr	6.47E-04 ± 1.36E-04	1.59E-04 ± 4.48E-05	1.02E-04 ± 7.44E-05
Nd	2.43E-03 ± 5.13E-04	6.00E-04 ± 1.57E-04	3.81E-04 ± 2.77E-04
Sm	4.35E-04 ± 1.05E-04	1.11E-04 ± 5.59E-05	6.82E-05 ± 4.86E-05
Eu	8.12E-05 ± 2.89E-05	3.27E-06 ± 2.03E-05	1.07E-05 ± 1.08E-05
Gd	3.24E-04 ± 2.45E-04	0.00E+00 ± 1.56E-05	3.14E-05 ± 4.63E-05
Tb	4.55E-05 ± 2.87E-05	1.20E-05 ± 2.22E-05	9.10E-06 ± 6.56E-06
Dy	2.31E-04 ± 2.19E-04	5.39E-05 ± 5.32E-05	4.79E-05 ± 3.59E-05
Ho	4.27E-05 ± 3.75E-05	1.20E-05 ± 2.71E-05	9.38E-06 ± 6.90E-06
Er	1.21E-04 ± 1.51E-04	2.59E-05 ± 4.02E-05	2.49E-05 ± 1.91E-05
Tm	1.58E-05 ± 2.70E-05	0.00E+00 ± 1.56E-05	3.15E-06 ± 4.69E-06
Yb	9.67E-05 ± 9.02E-05	5.50E-06 ± 3.08E-05	1.51E-05 ± 1.35E-05
Lu	1.25E-05 ± 1.17E-05	0.00E+00 ± 1.56E-05	2.13E-06 ± 4.26E-06
Pb	3.93E-03 ± 1.01E-03	7.11E-03 ± 1.17E-02	4.64E-03 ± 3.43E-03

[a] Average of 6 tests for Stacks A and C, and 7 tests for Stack B.

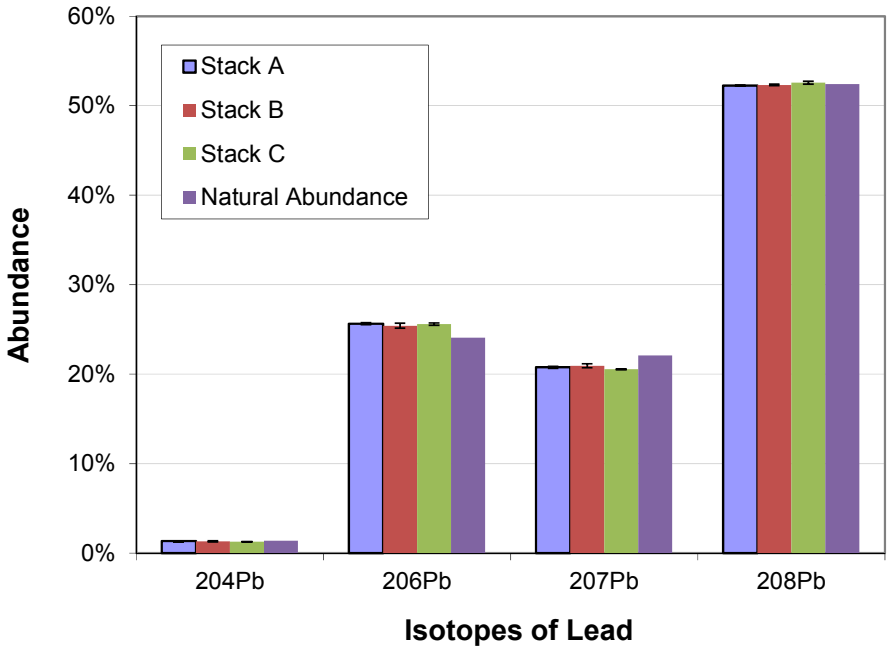

Figure 6-5. Abundance of stable lead isotopes in the stack samples vs. natural abundance.

a)

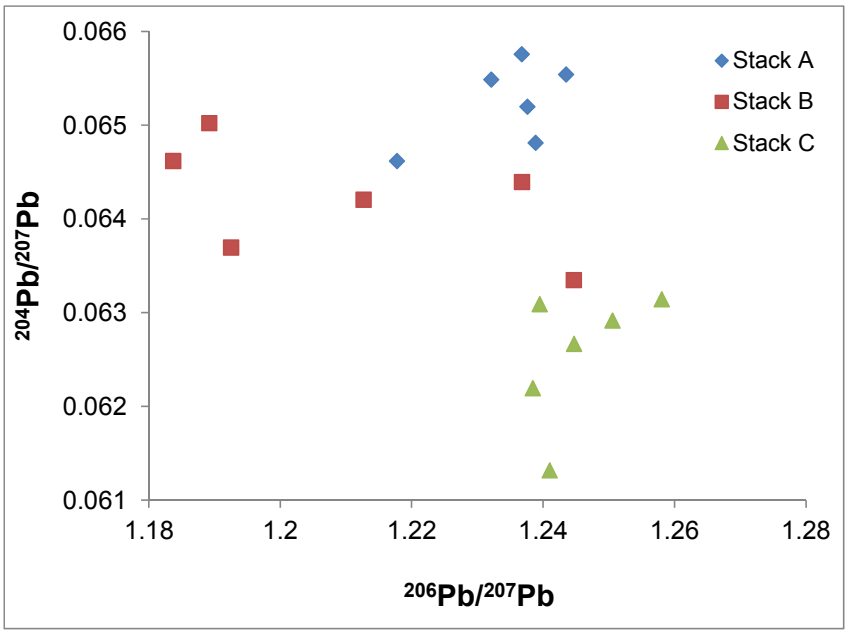

b)

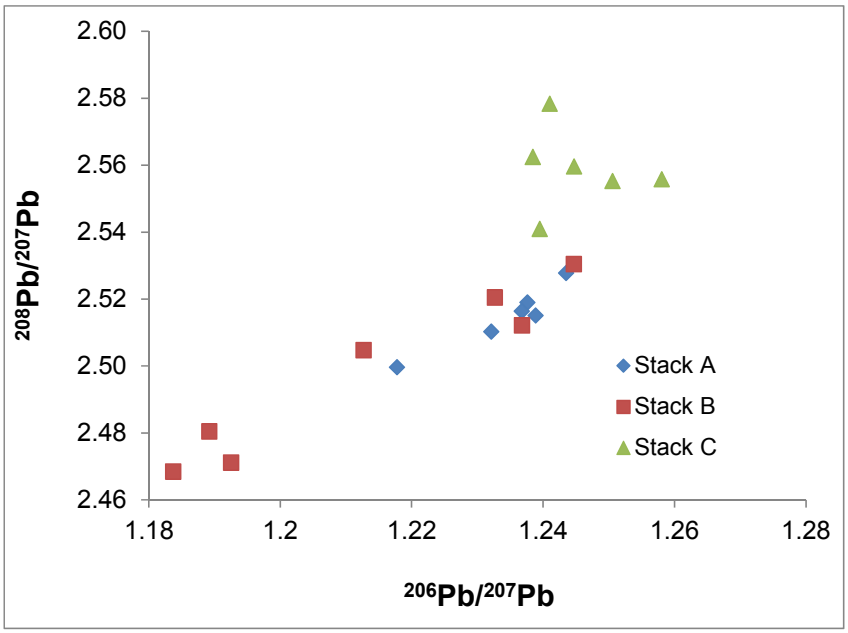

Figure 6-6. Lead isotope ratios of a) $^{204}Pb/^{207}Pb$ vs $^{206}Pb/^{207}Pb$ and b) $^{208}Pb/^{207}Pb$ vs $^{206}Pb/^{207}Pb$.

Table 6-5. Source profile (% of $PM_{2.5}$ and OC mass) of non-polar organic compounds from $PM_{2.5}$ filter samples analyzed by thermal desorption-gas chromatography/mass spectrometry (TD-GC/MS). Data are reported as average ± uncertainty, where the uncertainty is the larger of standard deviation and uncertainty of average of multiple runs[b].

Compounds	MW	Profile Normalized to $PM_{2.5}$ (%)			Profile Normalized to OC (%)		
		A	B	C	A	B	C
PAHs							
acenaphthylene	152	0.00000±0.00030	0.00001±0.00094	0.00000±0.00017	0.00007±0.00698	0.00022±0.02300	0.00000±0.20051
acenaphthene	154	0.00000±0.00016	0.00000±0.00051	0.00000±0.00009	0.00012±0.00379	0.00000±0.01248	0.00000±0.10882
fluorene	166	0.00001±0.00011	0.00009±0.00035	0.00000±0.00006	0.00024±0.00262	0.00219±0.00866	0.00014±0.07541
phenanthrene	178	0.00014±0.00007	0.00006±0.00017	0.00000±0.00003	0.00355±0.00279	0.00143±0.00415	0.00027±0.03599
anthracene	178	0.00005±0.00002	0.00005±0.00007	0.00000±0.00001	0.00101±0.00067	0.00118±0.00169	0.00000±0.01457
fluoranthene	202	0.00003±0.00003	0.00007±0.00010	0.00000±0.00002	0.00069±0.00075	0.00164±0.00249	0.00000±0.02142
pyrene	202	0.00010±0.00005	0.00016±0.00016	0.00000±0.00003	0.00227±0.00142	0.00389±0.00401	0.00000±0.03427
benzo[a]anthracene	228	0.00012±0.00010	0.00004±0.00031	0.00000±0.00006	0.00233±0.00227	0.00081±0.00747	0.00000±0.06512
chrysene	228	0.00018±0.00013	0.00004±0.00016	0.00000±0.00003	0.00372±0.00286	0.00098±0.00394	0.00000±0.03427
benzo[b]fluoranthene	252	0.00005±0.00011	0.00001±0.00033	0.00000±0.00006	0.00056±0.00245	0.00015±0.00806	0.00000±0.07026
benzo[j+k]fluoranthene	252	0.00006±0.00011	0.00001±0.00011	0.00000±0.00002	0.00075±0.00133	0.00019±0.00275	0.00000±0.02399
benzo[a]fluoranthene	252	0.00000±0.00005	0.00000±0.00017	0.00000±0.00003	0.00000±0.00122	0.00000±0.00403	0.00000±0.03513
benzo[e]pyrene	252	0.00001±0.00011	0.00000±0.00035	0.00000±0.00006	0.00007±0.00262	0.00006±0.00865	0.00000±0.07540
benzo[a]pyrene	252	0.00005±0.00013	0.00002±0.00036	0.00000±0.00007	0.00066±0.00269	0.00064±0.00885	0.00000±0.07712
perylene	252	0.00056±0.00138	0.00000±0.00039	0.00000±0.00007	0.00676±0.01656	0.00000±0.00953	0.00000±0.08312
indeno[1,2,3-cd]pyrene	276	0.00004±0.00006	0.00000±0.00017	0.00000±0.00003	0.00040±0.00125	0.00000±0.00413	0.00000±0.03599
dibenzo[a,h]anthracene	278	0.00000±0.00012	0.00000±0.00038	0.00000±0.00007	0.00000±0.00280	0.00000±0.00924	0.00000±0.08055
benzo[ghi]perylene	276	0.00001±0.00008	0.00000±0.00025	0.00000±0.00005	0.00006±0.00185	0.00000±0.00609	0.00000±0.05313
coronene	300	0.00000±0.00009	0.00000±0.00029	0.00000±0.00005	0.00000±0.00218	0.00000±0.00718	0.00000±0.06255
dibenzo[a,e]pyrene	302	0.00000±0.00004	0.00000±0.00011	0.00000±0.00002	0.00000±0.00084	0.00000±0.00275	0.00000±0.02399
9-fluorenone	180	0.00018±0.00013	0.00024±0.00040	0.00001±0.00007	0.00451±0.00383	0.00603±0.00972	0.00205±0.08398
dibenzothiophene	184	0.00028±0.00052	0.00054±0.00164	0.00000±0.00030	0.00653±0.01216	0.01186±0.04011	0.00000±0.34901
1 methyl phenanthrene	192	0.00012±0.00006	0.00049±0.00056	0.00003±0.00005	0.00280±0.00213	0.01160±0.01573	0.01406±0.06967
2 methyl phenanthrene	192	0.00004±0.00003	0.00003±0.00006	0.00000±0.00001	0.00094±0.00089	0.00083±0.00150	0.00000±0.01285
3,6 dimethyl phenanthrene	206	0.00010±0.00022	0.00000±0.00035	0.00000±0.00006	0.00123±0.00262	0.00000±0.00855	0.00000±0.07455
methylfluoranthene	216	0.00000±0.00004	0.00000±0.00011	0.00000±0.00002	0.00000±0.00084	0.00000±0.00275	0.00000±0.02399
retene	219	0.00010±0.00016	0.00004±0.00049	0.00020±0.00032	0.00120±0.00361	0.00078±0.01189	0.06780±0.11070
benzo(ghi)fluoranthene	226	0.00015±0.00024	0.00003±0.00076	0.00000±0.00014	0.00363±0.00559	0.00059±0.01850	0.00000±0.16130

Table 6-5. Continued

Compounds	MW	Profile Normalized to $PM_{2.5}$ (%)			Profile Normalized to OC (%)		
		A	B	C	A	B	C
PAHs							
benzo(c)phenanthrene	228	0.00001±0.00016	0.00000±0.00050	0.00000±0.00009	0.00014±0.00369	0.00000±0.01222	0.00000±0.10649
benzo(b)naphtho[1,2-d]thiophene	234	0.00003±0.00034	0.00000±0.00108	0.00000±0.00019	0.00045±0.00796	0.00005±0.02636	0.00000±0.22981
cyclopenta[cd]pyrene	226	0.00000±0.00004	0.00000±0.00011	0.00000±0.00002	0.00000±0.00084	0.00000±0.00275	0.00000±0.02399
benz[a]anthracene-7,12-dione	258	0.00024±0.00058	0.00000±0.00041	0.00000±0.00007	0.00285±0.00697	0.00000±0.01003	0.00000±0.08740
methylchrysene	242	0.00005±0.00011	0.00000±0.00017	0.00000±0.00003	0.00064±0.00131	0.00000±0.00413	0.00000±0.03599
benzo(b)chrysene	278	0.00000±0.00022	0.00000±0.00072	0.00000±0.00013	0.00000±0.00529	0.00000±0.01751	0.00000±0.15265
picene	278	0.00000±0.00013	0.00000±0.00042	0.00000±0.00008	0.00000±0.00310	0.00000±0.01022	0.00000±0.08911
anthanthrene	276	0.00000±0.00023	0.00000±0.00071	0.00000±0.00013	0.00000±0.00523	0.00000±0.01724	0.00000±0.15029
Alkane/Alkene/Phthalate							
***n*-alkane**							
n-pentadecane (*n*-C15)	*212*	0.00006±0.00011	0.00022±0.00035	0.00001±0.00006	0.00133±0.00257	0.00528±0.00853	0.00646±0.07657
n-hexadecane (*n*-C16)	*226*	0.00012±0.00011	0.00172±0.00117	0.00002±0.00006	0.00266±0.00286	0.03540±0.02137	0.01164±0.08322
n-heptadecane (*n*-C17)	*240*	0.00044±0.00038	0.00106±0.00159	0.00003±0.00006	0.00999±0.01042	0.02675±0.04423	0.01531±0.07958
n-octadecane (*n*-C18)	*254*	0.00073±0.00062	0.00166±0.00186	0.00004±0.00005	0.01539±0.01612	0.03904±0.05304	0.02081±0.08420
n-nonadecane (*n*-C19)	*268*	0.00077±0.00110	0.00159±0.00095	0.00007±0.00010	0.01833±0.03043	0.03605±0.02558	0.01861±0.06325
n-icosane (*n*-C20)	*282*	0.00048±0.00071	0.00034±0.00024	0.00010±0.00004	0.00625±0.00634	0.00764±0.00601	0.06787±0.26088
n-heneicosane (*n*-C21)	*296*	0.00189±0.00157	0.00081±0.00069	0.00019±0.00008	0.02879±0.01158	0.01929±0.01982	0.11081±0.38069
n-docosane (*n*-C22)	*310*	0.00046±0.00037	0.00147±0.00130	0.00023±0.00012	0.01024±0.01112	0.03639±0.03726	0.12393±0.38643
n-tricosane (*n*-C23)	*324*	0.00084±0.00044	0.00236±0.00090	0.00016±0.00008	0.01769±0.01034	0.05166±0.02098	0.09268±0.30982
n-tetracosane (*n*-C24)	*338*	0.00501±0.00519	0.00566±0.00192	0.00013±0.00006	0.09627±0.09415	0.11862±0.03638	0.07623±0.27388
n-pentacosane (*n*-C25)	*352*	0.00358±0.00532	0.00317±0.00127	0.00010±0.00005	0.05250±0.05949	0.06681±0.02340	0.06775±0.26612
n-hexacosane (*n*-C26)	*366*	0.00198±0.00235	0.00249±0.00105	0.00007±0.00004	0.03200±0.03126	0.05280±0.02149	0.04050±0.16157
n-heptacosane (*n*-C27)	*380*	0.00074±0.00071	0.00201±0.00091	0.00005±0.00004	0.01271±0.00847	0.04314±0.01940	0.02524±0.09457
n-octacosane (*n*-C28)	*394*	0.00013±0.00009	0.00147±0.00054	0.00003±0.00005	0.00208±0.00218	0.03185±0.01186	0.01260±0.07506
n-nonacosane (*n*-C29)	*408*	0.00015±0.00011	0.00099±0.00037	0.00002±0.00006	0.00290±0.00245	0.02148±0.00854	0.00895±0.07603
n-triacontane (*n*-C30)	*422*	0.00011±0.00012	0.00051±0.00039	0.00001±0.00007	0.00263±0.00287	0.01083±0.00953	0.00475±0.08392
n-hentriacotane (*n*-C31)	*436*	0.00010±0.00010	0.00021±0.00031	0.00000±0.00006	0.00163±0.00233	0.00469±0.00769	0.00082±0.06684
n-dotriacontane (*n*-C32)	*450*	0.00004±0.00012	0.00006±0.00036	0.00000±0.00007	0.00075±0.00268	0.00140±0.00885	0.00016±0.07712
n-tritriactotane (*n*-C33)	*464*	0.00012±0.00009	0.00005±0.00023	0.00000±0.00004	0.00197±0.00170	0.00110±0.00560	0.00021±0.04884
n-tetratriactoane (*n*-C34)	*478*	0.00004±0.00009	0.00003±0.00027	0.00000±0.00005	0.00064±0.00200	0.00074±0.00659	0.00000±0.05741
n-pentatriacontane (*n*-C35)	*492*	0.00008±0.00009	0.00003±0.00029	0.00001±0.00005	0.00117±0.00215	0.00062±0.00708	0.00082±0.06170

Table 6-5. Continued

Compounds	MW	Profile Normalized to $PM_{2.5}$ (%)			Profile Normalized to OC (%)		
		A	B	C	A	B	C
n-hexatriacontane (*n*-C36)	*506*	0.00002±0.00011	0.00001±0.00035	0.00000±0.00006	0.00051±0.00257	0.00020±0.00845	0.00029±0.07369
n-heptatriacontane (*n*-C37)	*521*	0.00006±0.00011	0.00002±0.00035	0.00004±0.00009	0.00080±0.00260	0.00042±0.00855	0.00415±0.07456
n-octatriacontane (*n*-C38)	*535*	0.00047±0.00038	0.00019±0.00051	0.00000±0.00006	0.00870±0.00945	0.00468±0.01239	0.00000±0.07369
n-nonatriacontane (*n*-C39)	*549*	0.00078±0.00061	0.00028±0.00074	0.00019±0.00047	0.01353±0.01258	0.00672±0.01778	0.02139±0.07063
n-tetracontane (*n*-C40)	*563*	0.00015±0.00038	0.00000±0.00034	0.00000±0.00006	0.00154±0.00377	0.00000±0.00826	0.00000±0.07198
iso/anteiso-alkane							
iso-nonacosane (iso-C29)	408	0.00004±0.00021	0.00004±0.00067	0.00000±0.00012	0.00066±0.00498	0.00086±0.01639	0.00018±0.14292
anteiso-nonacosane (anteiso-C29)	408	0.00004±0.00021	0.00005±0.00067	0.00000±0.00012	0.00070±0.00498	0.00100±0.01639	0.00037±0.14292
iso-triacontane (iso-C30)	422	0.00003±0.00014	0.00004±0.00045	0.00000±0.00008	0.00045±0.00336	0.00074±0.01106	0.00004±0.09642
anteiso-triacontane (anteiso-C30)	422	0.00002±0.00014	0.00005±0.00045	0.00000±0.00008	0.00041±0.00336	0.00116±0.01106	0.00008±0.09642
iso-hentriacotane (iso-C31)	436	0.00003±0.00027	0.00002±0.00084	0.00000±0.00015	0.00043±0.00624	0.00050±0.02056	0.00000±0.17924
anteiso-hentriacotane (anteiso-C31)	436	0.00001±0.00027	0.00002±0.00084	0.00000±0.00015	0.00026±0.00624	0.00038±0.02056	0.00000±0.17924
iso-dotriacontane (iso-C32)	450	0.00007±0.00025	0.00002±0.00079	0.00000±0.00014	0.00116±0.00586	0.00050±0.01931	0.00000±0.16835
anteiso-dotriacontane (anteiso-C32)	450	0.00003±0.00025	0.00003±0.00079	0.00000±0.00014	0.00054±0.00586	0.00058±0.01931	0.00000±0.16835
iso-tritriactotane (iso-C33)	464	0.00001±0.00020	0.00001±0.00063	0.00000±0.00011	0.00022±0.00465	0.00020±0.01533	0.00000±0.13369
anteiso-tritriactotane (anteiso-C33)	464	0.00002±0.00020	0.00001±0.00063	0.00000±0.00011	0.00033±0.00465	0.00024±0.01533	0.00000±0.13369
hopane							
22,29,30-trisnorneophopane (Ts)	370	0.00012±0.00011	0.00008±0.00035	0.00000±0.00006	0.00209±0.00258	0.00172±0.00851	0.00000±0.07418
22,29,30-trisnorphopane (Tm)	370	0.00007±0.00011	0.00008±0.00035	0.00000±0.00006	0.00151±0.00258	0.00164±0.00851	0.00000±0.07418
αβ-norhopane (C29αβ-hopane)	398	0.00017±0.00016	0.00013±0.00036	0.00000±0.00007	0.00313±0.00268	0.00284±0.00883	0.00000±0.07689
22,29,30-norhopane (29Ts)	398	0.00007±0.00012	0.00011±0.00036	0.00000±0.00007	0.00122±0.00268	0.00257±0.00883	0.00000±0.07689
αα- + βα-norhopane (C29αα- + βα -hopane)	398	0.00052±0.00055	0.00009±0.00052	0.00000±0.00009	0.00837±0.00623	0.00187±0.01270	0.00000±0.11066
αβ-hopane (C30αβ -hopane)	412	0.00012±0.00011	0.00009±0.00034	0.00000±0.00006	0.00210±0.00255	0.00193±0.00838	0.00000±0.07307
αα-hopane (30αα-hopane)	412	0.00005±0.00013	0.00001±0.00041	0.00000±0.00007	0.00079±0.00300	0.00014±0.00989	0.00000±0.08620
βα-hopane (C30βα -hopane)	412	0.00004±0.00013	0.00002±0.00041	0.00000±0.00007	0.00069±0.00300	0.00029±0.00989	0.00000±0.08620
αβS-homohopane (C31αβS-hopane)	426	0.00013±0.00012	0.00003±0.00037	0.00000±0.00007	0.00242±0.00277	0.00059±0.00912	0.00000±0.07955
αβR-homohopane (C31αβR-hopane)	426	0.00006±0.00014	0.00003±0.00044	0.00000±0.00008	0.00137±0.00322	0.00057±0.01062	0.00000±0.09257
αβS-bishomohopane (C32αβS-hopane)	440	0.00003±0.00004	0.00000±0.00010	0.00000±0.00002	0.00051±0.00074	0.00000±0.00243	0.00000±0.02120
αβR-bishomohopane (C32αβR-hopane)	440	0.00004±0.00004	0.00000±0.00012	0.00000±0.00002	0.00057±0.00086	0.00000±0.00284	0.00000±0.02476
22S-trishomohopane (C33)	454	0.00002±0.00003	0.00000±0.00010	0.00000±0.00002	0.00030±0.00074	0.00000±0.00243	0.00000±0.02120
22R-trishomohopane (C33)	454	0.00003±0.00004	0.00000±0.00012	0.00000±0.00002	0.00032±0.00086	0.00000±0.00284	0.00000±0.02476
22S-tretrahomohopane (C34)	468	0.00002±0.00003	0.00000±0.00010	0.00000±0.00002	0.00027±0.00074	0.00000±0.00243	0.00000±0.02120

Table 6-5. Continued

Compounds	MW	Profile Normalized to $PM_{2.5}$ (%)			Profile Normalized to OC (%)		
		A	B	C	A	B	C
22R-tetrashomohopane (C34)	468	0.00002±0.00004	0.00000±0.00012	0.00000±0.00002	0.00035±0.00086	0.00000±0.00284	0.00000±0.02476
22S-pentashomohopane(C35)	482	0.00002±0.00003	0.00000±0.00010	0.00000±0.00002	0.00032±0.00074	0.00000±0.00243	0.00000±0.02120
22R-pentashomohopane(C35)	482	0.00002±0.00004	0.00000±0.00012	0.00000±0.00002	0.00034±0.00086	0.00000±0.00284	0.00000±0.02476
sterane							
ααα 20S-Cholestane	372	0.00001±0.00008	0.00003±0.00024	0.00000±0.00004	0.00029±0.00176	0.00072±0.00581	0.00000±0.05067
αββ 20R-Cholestane	372	0.00007±0.00011	0.00002±0.00010	0.00000±0.00002	0.00099±0.00103	0.00035±0.00247	0.00000±0.02152
αββ 20s-Cholestane	372	0.00006±0.00008	0.00002±0.00012	0.00000±0.00002	0.00083±0.00087	0.00031±0.00286	0.00000±0.02490
ααα 20R-Cholestane	372	0.00001±0.00004	0.00002±0.00012	0.00000±0.00002	0.00022±0.00087	0.00050±0.00286	0.00000±0.02490
ααα 20S 24S-Methylcholestane	386	0.00004±0.00006	0.00002±0.00014	0.00000±0.00002	0.00056±0.00100	0.00051±0.00331	0.00000±0.02883
αββ 20R 24S-Methylcholestane	386	0.00001±0.00004	0.00001±0.00014	0.00000±0.00002	0.00019±0.00100	0.00021±0.00331	0.00000±0.02883
αββ 20S 24S-Methylcholestane	386	0.00002±0.00004	0.00001±0.00014	0.00000±0.00002	0.00038±0.00100	0.00027±0.00331	0.00000±0.02883
ααα 20R 24R-Methylcholestane	386	0.00007±0.00013	0.00001±0.00016	0.00000±0.00003	0.00177±0.00374	0.00017±0.00387	0.00000±0.03373
ααα 20S 24R/S-Ethylcholestane	386	0.00031±0.00077	0.00004±0.00013	0.00000±0.00002	0.00856±0.02097	0.00081±0.00321	0.00000±0.02799
αββ 20R 24R-Ethylcholestane	400	0.00001±0.00003	0.00000±0.00011	0.00000±0.00002	0.00010±0.00079	0.00002±0.00259	0.00000±0.02260
αββ 20S 24R-Ethylcholestane	400	0.00004±0.00005	0.00000±0.00011	0.00000±0.00002	0.00068±0.00079	0.00006±0.00259	0.00000±0.02260
ααα 20R 24R-Ethylcholestane	400	0.00000±0.00009	0.00000±0.00028	0.00000±0.00005	0.00000±0.00208	0.00000±0.00685	0.00000±0.05974
methyl-alkane							
2-methylnonadecane	282	0.00068±0.00056	0.00068±0.00057	0.00002±0.00010	0.01158±0.00873	0.01502±0.01390	0.01591±0.13531
3-methylnonadecane	282	0.00040±0.00039	0.00077±0.00037	0.00002±0.00007	0.00782±0.00686	0.01694±0.00931	0.01419±0.09823
branched-alkane							
pristane	268	0.00047±0.00023	0.00072±0.00048	0.00007±0.00006	0.01121±0.00856	0.01515±0.00934	0.05226±0.22089
phytane	282	0.00061±0.00035	0.00064±0.00041	0.00006±0.00007	0.01389±0.01089	0.01383±0.01039	0.04468±0.19876
squalane	422	0.00004±0.00020	0.00004±0.00061	0.00000±0.00011	0.00074±0.00453	0.00091±0.01492	0.00086±0.13016
cycloalkane							
octylcyclohexane	196	0.00000±0.00033	0.00000±0.00103	0.00000±0.00019	0.00000±0.00760	0.00000±0.02504	0.00000±0.21834
decylcyclohexane	224	0.00000±0.00028	0.00002±0.00088	0.00000±0.00016	0.00016±0.00647	0.00041±0.02132	0.00006±0.18590
tridecylcyclohexane	266	0.00003±0.00021	0.00008±0.00066	0.00000±0.00012	0.00086±0.00490	0.00159±0.01613	0.00024±0.14064
n-heptadecylcyclohexane	322	0.00009±0.00017	0.00013±0.00052	0.00001±0.00009	0.00159±0.00385	0.00283±0.01270	0.00484±0.11190
nonadecylcyclohexane	350	0.00005±0.00015	0.00007±0.00048	0.00000±0.00009	0.00082±0.00355	0.00150±0.01171	0.00200±0.10239
alkene							
1-octadecene	252	0.00154±0.00141	0.00347±0.00183	0.00000±0.00029	0.03474±0.03882	0.07752±0.04847	0.00035±0.33762

Table 6-5. Continued							
Compounds	**MW**	**Profile Normalized to $PM_{2.5}$ (%)**			**Profile Normalized to OC (%)**		
		A	**B**	**C**	**A**	**B**	**C**
Sum of categories							
PAHs		0.00270±0.00286	0.00192±0.00301	0.00024±0.00054	0.04819±0.03305	0.04512±0.07339	0.08432±0.64222
n-alkane		0.01938±0.01180	0.02843±0.00696	0.00152±0.00107	0.34300±0.13974	0.62360±0.21575	0.73198±0.97500
iso/anteiso-alkane		0.00030±0.00070	0.00029±0.00219	0.00000±0.00039	0.00517±0.01618	0.00617±0.05333	0.00067±0.46490
hopane		0.00157±0.00133	0.00067±0.00128	0.00000±0.00023	0.02667±0.01514	0.01416±0.03130	0.00000±0.27281
sterane		0.00067±0.00083	0.00019±0.00054	0.00000±0.00010	0.01458±0.02356	0.00393±0.01322	0.00000±0.11522
methyl-alkane		0.00109±0.00092	0.00145±0.00068	0.00004±0.00012	0.01940±0.01514	0.03196±0.01673	0.03011±0.16720
branched-alkane		0.00113±0.00040	0.00141±0.00085	0.00013±0.00015	0.02585±0.01728	0.02989±0.02032	0.09781±0.32441
cycloalkane		0.00017±0.00053	0.00030±0.00166	0.00001±0.00030	0.00343±0.01229	0.00633±0.04050	0.00713±0.35357
alkene		0.00154±0.00141	0.00347±0.00183	0.00000±0.00029	0.03474±0.03882	0.07752±0.04847	0.00035±0.33762
Sum of all non-polar species		0.02855±0.01562	0.03813±0.00885	0.00195±0.00125	0.52103±0.17634	0.83869±0.29326	0.95237±1.35012

[a] See Tables A-1 and A-2 of Appendix A for analytical MDL for each measurement.

[b] Average of 6 tests for Stacks A and C, and 7 tests for Stack B.

Table 6-6. Ten most abundant non-polar compounds normalized to organic carbon (% OC) for each stack.

	Stack A		**Stack B**		**Stack C**	
Rank	**Compound**	**% of OC**	**Compound**	**% of OC**	**Compound**	**% of OC**
1	*n*-tetracosane (*n*-C24)	0.09627±0.09415	*n*-tetracosane (*n*-C24)	0.11862±0.03638	*n*-docosane (*n*-C22)	0.12393±0.38643
2	*n*-pentacosane (*n*-C25)	0.05250±0.05949	1-octadecene	0.07752±0.04847	*n*-heneicosane (*n*-C21)	0.11081±0.38069
3	1-octadecene	0.03474±0.03882	*n*-pentacosane (*n*-C25)	0.06681±0.02340	*n*-tricosane (*n*-C23)	0.09268±0.30982
4	*n*-hexacosane (*n*-C26)	0.03200±0.03126	*n*-hexacosane (*n*-C26)	0.05280±0.02149	*n*-tetracosane (*n*-C24)	0.07623±0.27388
5	*n*-heneicosane (*n*-C21)	0.02879±0.01158	*n*-tricosane (*n*-C23)	0.05166±0.02098	*n*-icosane (*n*-C20)	0.06787±0.26088
6	*n*-nonadecane (*n*-C19)	0.01833±0.03043	*n*-heptacosane (*n*-C27)	0.04314±0.01940	retene	0.06780±0.11070
7	*n*-tricosane (*n*-C23)	0.01769±0.01034	*n*-octadecane (*n*-C18)	0.03904±0.05304	*n*-pentacosane (*n*-C25)	0.06775±0.26612
8	*n*-octadecane (*n*-C18)	0.01539±0.01612	*n*-docosane (*n*-C22)	0.03639±0.03726	pristane	0.05226±0.22089
9	phytane	0.01389±0.01089	*n*-nonadecane (*n*-C19)	0.03605±0.02558	phytane	0.04468±0.19876
10	*n*-nonatriacontane (*n*-C39)	0.01353±0.01258	*n*-hexadecane (*n*-C16)	0.03540±0.02137	*n*-hexacosane (*n*-C26)	0.04050±0.16157

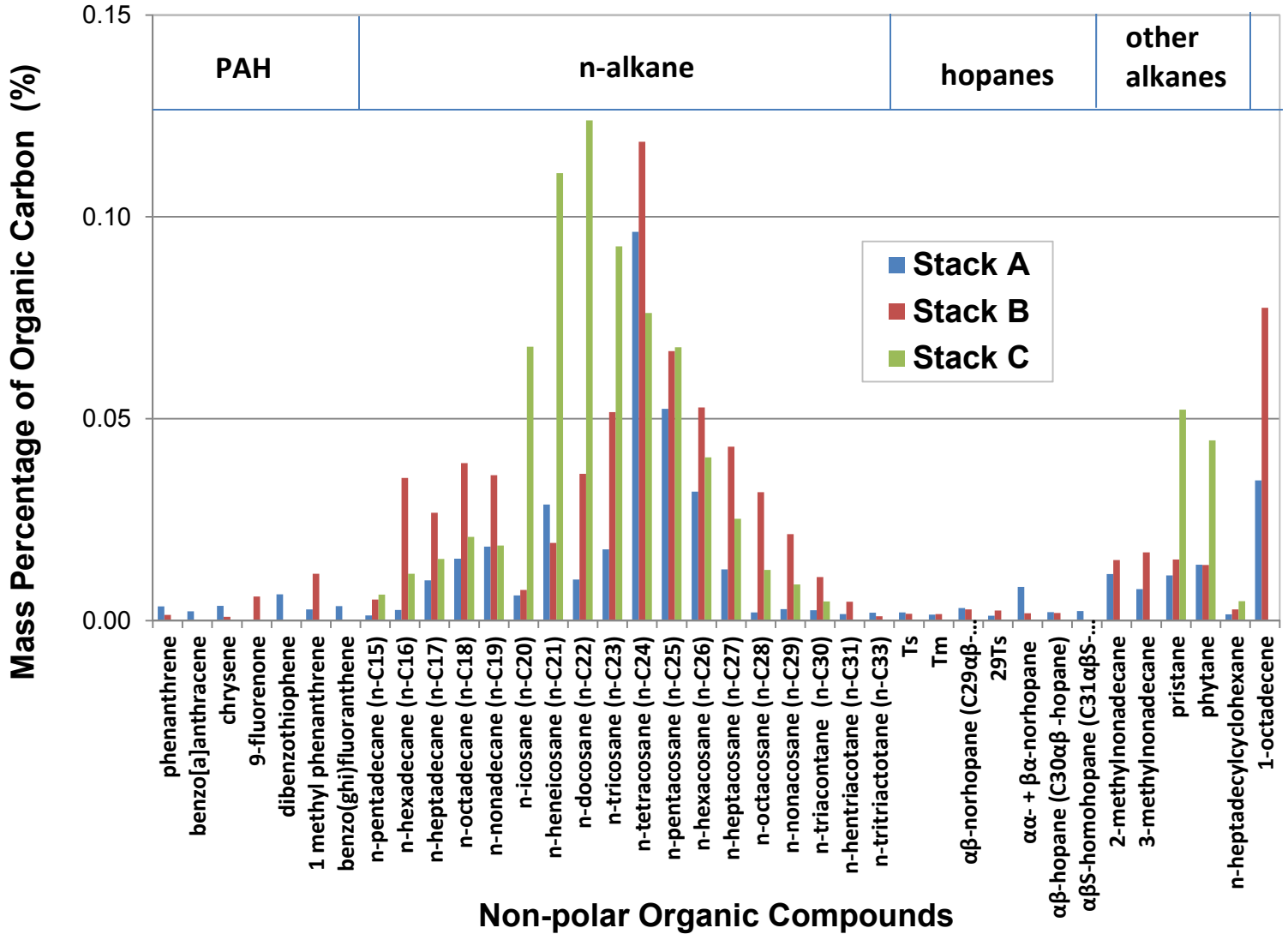

Figure 6-7. Source profile of non-polar organic compounds normalized to organic carbon (OC). Only species with abundance $>10^{-4}$ % are plotted.

Table 6-7. Source profile (% of $PM_{2.5}$ and OC mass) of $PM_{2.5}$ carbohydrate, organic acids and water soluble organic carbon (WSOC). Data are reported as average ± uncertainty, where the uncertainty is the larger of standard deviation and uncertainty of average of multiple runs[a].

Compound	MW	Profile Normalized to $PM_{2.5}$ (%)			Profile Normalized to OC (%)		
		A	B	C	A	B	C
Carbohydrates							
Glycerol (C3H8O3)	92	0.0040±0.0023	0.0023±0.0037	0.0063±0.0018	0.0690±0.0301	0.0427±0.0861	7.2103±33.7235
Inositol (C6H12O6)	180	0.0000±0.0011	0.0000±0.0035	0.0000±0.0006	0.0000±0.0259	0.0000±0.0855	0.0000±0.7451
Erythritol (C4H10O4)	122	0.0000±0.0017	0.0000±0.0053	0.0000±0.0009	0.0000±0.0389	0.0000±0.1282	0.0000±1.1177
Xylitol (C5H12O5)	152	0.0253±0.0162	0.0000±0.0035	0.0000±0.0006	0.3647±0.2313	0.0000±0.0855	0.0000±0.7451
Levoglucosan (C6H10O5)/Arabitol (C5H12O5)	162	0.0132±0.0132	0.0000±0.0070	0.0000±0.0013	0.1317±0.1317	0.0000±0.1709	0.0000±1.4902
Sorbitol (C6H14O6)	182	0.0000±0.0028	0.0000±0.0088	0.0514±0.0048	0.0000±0.0648	0.0000±0.2137	33.8312±135.3510
Mannosan (C6H10O5)	162	0.0000±0.0017	0.0000±0.0053	0.0000±0.0009	0.0000±0.0389	0.0000±0.1282	0.0000±1.1177
Trehalose (C12H22O11)	342	0.0000±0.0023	0.0000±0.0070	0.0000±0.0013	0.0000±0.0518	0.0000±0.1709	0.0000±1.4902
Mannitol (C6H14O6)	182	0.0000±0.0017	0.0000±0.0053	0.0000±0.0009	0.0000±0.0389	0.0000±0.1282	0.0000±1.1177
Arabinose (C5H10O5)	150	0.0000±0.0017	0.0000±0.0053	0.0000±0.0009	0.0000±0.0389	0.0000±0.1282	0.0000±1.1177
Glucose (C6H12O6)/Xylose (C5H10O5)	180	0.0075±0.0075	0.0000±0.0035	0.0000±0.0006	0.2042±0.2042	0.0000±0.0855	0.0000±0.7451
Galactose (C6H12O6)	180	0.0000±0.0023	0.0000±0.0070	0.0000±0.0013	0.0000±0.0518	0.0000±0.1709	0.0000±1.4902
Maltitol (C12H24O11)/Fructose (C6H12O6)	344	0.0000±0.0028	0.0000±0.0088	0.0000±0.0016	0.0000±0.0648	0.0000±0.2137	0.0000±1.8628
Organic Acids							
Lactic acid (C3H6O3)	90	0.0465±0.0281	0.0248±0.0107	0.0104±0.0050	0.7849±0.3401	0.5312±0.1995	12.4351±65.8653
Acetic acid (C2H4O2)	60	0.0049±0.0049	0.0627±0.0323	0.0048±0.0036	0.0860±0.0860	1.3841±0.4544	0.6503±2.2395
Formic acid (CH2O)	46	0.0000±0.0034	0.0000±0.0105	0.0000±0.0019	0.0000±0.0778	0.0000±0.2564	0.0000±2.2353
Methanesulfonic acid (CH4SO3)	96	0.2023±0.0367	0.3403±0.2129	0.0000±0.0013	4.3300±0.8239	7.9184±3.6892	0.0000±1.4902
Glutaric acid (C5H8O4)	132	0.0000±0.0028	0.0000±0.0088	0.0000±0.0016	0.0000±0.0648	0.0000±0.2137	0.0000±1.8628
Succinic acid (C4H6O4)	118	0.0000±0.0022	0.0000±0.0070	0.0000±0.0013	0.0000±0.0519	0.0000±0.1709	0.0000±1.4902
Malonic acid (C3H4O4)	104	0.0000±0.0034	0.0000±0.0105	0.0000±0.0019	0.0000±0.0778	0.0000±0.2564	0.0000±2.2353
Maleic acid (C4H4O4)	116	0.0000±0.0028	0.0000±0.0088	0.0000±0.0016	0.0000±0.0648	0.0000±0.2137	0.0000±1.8628
Oxalic acid (C2H2O4)	90	0.0132±0.0037	0.0243±0.0107	0.0026±0.0026	0.2678±0.0716	0.5000±0.1964	0.2877±1.4945
WSOC							
Neutral compounds		0.0607±0.0293	0.2868±0.1813	0.0410±0.0152	1.1801±0.6169	6.6587±2.7521	28.8075±120.3012
Mono-/di- carboxylic acids		0.0295±0.0468	0.1117±0.1531	0.0304±0.0278	0.6937±1.0853	2.4579±3.5724	14.6806±58.1752
Polycarboxylic acids (including HULIS)		0.0239±0.0703	0.0497±0.2210	0.0013±0.0396	0.5025±1.6237	0.9129±5.3463	0.1461±46.5698
Sum of speciated WSOC		0.1140±0.0902	0.4483±0.3467	0.0727±0.0508	2.3764±2.0511	10.0296±7.0993	43.6360±178.0838
Total WSOC		0.0212±0.2433	0.8224±0.8384	0.2114±0.1531	0.2552±5.6108	16.8181±19.2403	204.5345±1073.1974

[a] Average of 6 tests for Stacks A and C, and 7 tests for Stack B.

7 Summary of Major Findings

A dilution sampling and measurement system was used to quantify emission rates and source profiles from three stacks in two facilities. Stack velocity was measured by a type-S pitot tube. Gases (CO, CO_2, and NO), $PM_{2.5}$, PM_{10}, and mass distributions for particles in the size range of ~0.23-25 μm were measured in real time. NH_3, H_2S, SO_2, $PM_{2.5}$ mass, filter light transmission (b_{abs}), elements, Pb isotopes, ions, carbon fractions, water-soluble organic carbon (WSOC), carbohydrates, organic acids, and speciated organic compounds were taken on gas- and particle- absorbing filters. Emission rates and chemical source profiles were derived from these measurements.

Mass distributions of particles from Stacks A and B were bimodal, with ~50% mass in PM_1, ~30% mass in $PM_{1\text{-}2.5}$, and ~20% mass in $PM_{2.5\text{-}10}$. Particles from Stack C were unimodal and much smaller, with 96% mass in PM_1 and ~99% mass in $PM_{2.5}$.

Stack B had the highest CO concentrations (843 ppm or 915 mg/m^3), while Stack C had the highest CO_2 (1.31×10^5 ppm or 2.36×10^5 mg/m^3), NO (134 ppm or 164 mg/m^3), and PM concentrations (38 mg/m^3 for PM_{10}). In all three stacks, CO_2 had the largest ER (177-270 tonnes/hr) among the gases measured, followed by CO, SO_2, NO, and NH_3. The ER for H_2S was low (5–38 g/hr). Stack A had the highest ER for CO (1.6 tonnes/hr), NO (0.3 tonnes/hr), SO_2 (>1.0 tonnes/hr), H_2S (38 g/hr), and PM_{10} (68.6 kg/hr).

Stack B had the lowest PM ER (11 kg/hr for PM_{10}), ~15-25% of the other two stacks. Stack C has 1-2 orders of magnitude lower NH_3 ER, only 1.1% and 0.2% of the Stacks A and B, respectively. It also has significantly lower SO_2 ER, only <19% and 28% of the Stacks A and B.

For Stack A, the NO_x and TSP ERs from dilution sampling were respectively 52% and 17% of those from compliance tests in 2007. The PM_{10} ER by in-stack filter method (modified U.S. EPA Method 201A) and dilution sampling method differed by <15%. The $PM_{2.5}$ ER from this study was 2.7 times higher than the in-stack survey, while the TSP was only 66% of the in-stack survey. For Stack B, NO_x ER by dilution sampling was 45% higher than compliance tests, SO_2 ERs were similar by the two methods, and the TSP ER by dilution sampling was only ~3% of the TSP or 21% of the filterable PM of compliance tests in 2007. For Stack C, the TSP ER from dilution sampling was 16% lower than one compliance test in 2010.

Soluble $SO_4^=$ was the $PM_{2.5}$ component with the highest concentrations and ERs among all $PM_{2.5}$ constituents for all three stacks, accounting for ~>40% of the $PM_{2.5}$ emissions. Ce is the rare earth element that has the highest ERs for all three stacks. Non-polar compound ERs are low for all three stacks, with Stack A being the highest, while C being the lowest. n-Alkanes have the highest ERs among all non-polar organic compounds. Most PAHs, all hopanes, and all steranes are below MDL in Stack C. Most carbohydrates and organic acids are below the MDLs. WSOCs are also below or only slightly above the MDLs.

With respect to source profiles, Stack B had the highest abundance of NH_3 and SO_2 (1025±241% and 9205±1762% of $PM_{2.5}$, respectively), while Stack C had the lowest abundance of NH_3 and SO_2 (0.43±0.05% and 472±62% of $PM_{2.5}$, respectively). Soluble $SO_4^=$ was the most abundant species contributing 39.2 ± 2.0%, 67.9 ± 0.9%, and 49.7 ± 1.5% to $PM_{2.5}$ mass for Stacks A, B, and C, respectively. NH_4^+ was the main identified cation for Stacks A and B, where it accounted for 15.1± 0.8% and 24.9 ± 0.4% of $PM_{2.5}$. NH_4^+ only accounted 0.9± 0.4% of $PM_{2.5}$ in Stack C, indicating that most of the $SO_4^=$ was present as H_2SO_4 rather than neutralized $(NH_4)_2SO_4$. There were 6.1% and 43.1% unidentified compositions from Stacks A and C,

respectively. Stack C $PM_{2.5}$ mass lost ~77% after exposing to the vacuum in XRF, indication a substantial amount of water associated with volatile H_2SO_4.

Carbon accounted for a minor fraction of $PM_{2.5}$ but an important fraction of non-sulfate $PM_{2.5}$, with the total carbon (TC) being 12.9 ± 0.9%, 6.9 ± 0.2%, and <1.4% of $PM_{2.5}$ for the three stacks, respectively. Trace element abundances were low (typically < 0.1%) with elevated abundances for S (9–20%), mostly in the form of $SO_4^=$. Stacks A and B had higher abundances of Fe (2.8 ± 0.2% and 1.6 ± 0.2%, respectively) than Stack C (0.3 ± 0.1%). Rare earth elements were all <0.01% of $PM_{2.5}$. Abundances in samples from Stack A were 2.5–5 times of those found in samples from Stack B, and 4.5–7.5 times of those from Stack C for most rare earth elements. On average, the stack samples were 5.5% less abundant for ^{204}Pb, 6.0% more abundant for ^{206}Pb, 6.1% less abundant for ^{207}Pb, and 0.05% less abundant for ^{208}Pb compared to the naturally-occurring abundances. Stack C showed higher ^{208}Pb /^{207}Pb and lower ^{204}Pb /^{207}Pb ratios than Stacks A and B.

Organic compound abundances were low. n-Alkanes were the most abundant category among quantified non-polar organic compounds, accounting for 0.019±0.012%, 0.028±0.007%, and 0.002±0.001% of $PM_{2.5}$, and 0.34±0.14%, 0.62±0.22%, and 0.73±0.98% of OC for Stacks A, B, and C, respectively. Other non-polar compounds including PAHs had low abundances.

8 References

Alberta Environment (1995). Alberta stack sampling code 1995. Report Number ISBN# 0773214062; prepared by Alberta Environment, Edmondton, AB, Canada, http://www.qp.alberta.ca/570.cfm.

ASTM International (2010). Standard Guideline for Determining PM2.5 and PM10 Mass in Stack Gases: D2203-WK8124_Guideline.

Bachmann, J.D. (2007). Will the circle be unbroken: A history of the US national ambient air quality standards-2007 Critical Review. *J. Air Waste Manage. Assoc.*, **57**(6):652-697. http://pubs.awma.org/gsearch/journal/2007/6/10.3155-1047-3289.57.6.652.pdf.

Baldwin, T.A.; Lundgren, D.A.; Bivins, D.G.; Watson, J.G.; Chow, J.C.; Wang, X.; Gronstal, S. (2010). Extraction and dilution methods for PM2.5 sampling in wet and dry stacks. In *Proceedings, Leapfrogging Opportunities for Air Quality Improvement*, Chow, J. C., Watson, J. G., Cao, J. J., Eds.; Air & Waste Management Association: Pittsburgh, PA, 454.

Budd, A.L.; Baldwin, T.A.; Chow, J.C.; Watson, J.G.; Sodeman, D.A. (2007). Lab work to evaluate $PM_{2.5}$ collection with a dilution monitoring device for data gathering for emission factor development. Report Number 68-D-08-079; prepared by Baldwin Environmental, Inc. and Desert Research Institute, Reno, NV, for U.S. Environmental Protection Agency, Eastern Research Group, Research Triangle Park, NC.

Chang, M.C.; England, G.C. (2004a). Development of fine particulate emission factors and speciation profiles for oil and gas-fired combustion systems. Other report: Pilot-scale dilution sampler design and validation tests (laboratory study). prepared by GE Energy and Environmental Research Corp., Irvine, CA, for USDOE National Energy Technology Laboratory, Gas Research Institute, and American Petroleum Institute, Pittsburgh PA, Des Plaines IL, and Washington DC.

Chang, M.C.; England, G.C. (2004b). Development of fine particulate emission factors and speciation profiles for oil and gas-fired combustion systems, Update: Critical review of source sampling and analysis methodologies for characterizing organic aerosol and fine particulate source emission profiles. prepared by GE Energy and Environmental Research Corp., Irvine, CA, for USDOE National Energy Technology Laboratory, Gas Research Institute, and American Petroleum Institute, Pittsburgh PA, Des Plaines IL, and Washington DC.

Chang, M.-C.O.; Chow, J.C.; Watson, J.G. (2004a). Characterization of particulate emissions from casting processes using a dilution sampling system. A preliminary study to optimize the dilution sampling system in a foundry process. prepared by Desert Research Institute, Reno, NV, for Technikon LLC, McClellan, CA.

Chang, M.-C.O.; Chow, J.C.; Watson, J.G.; Hopke, P.K.; Yi, S.M.; England, G.C. (2004b). Measurement of ultrafine particle size distributions from coal-, oil-, and gas-fired stationary combustion sources. *J. Air Waste Manage. Assoc.*, **54**(12):1494-1505. http://pubs.awma.org/gsearch/journal/2004/12/chang.PDF.

Chang, M.-C.O.; Chow, J.C.; Watson, J.G.; Glowacki, C.; Sheya, S.A.; Prabhu, A. (2005). Characterization of fine particulate emissions from casting processes. *Aerosol Sci. Technol.*, **39**(10):947-959. http://www.tandfonline.com/doi/pdf/10.1080/02786820600623711.

Chow, J.C.; Watson, J.G. (1999). Ion chromatography in elemental analysis of airborne particles. In *Elemental Analysis of Airborne Particles, Vol. 1*, Landsberger, S., Creatchman, M., Eds.; Gordon and Breach Science: Amsterdam, 97-137.

Chow, J.C.; Watson, J.G. (2008). New directions: Beyond compliance air quality measurements. *Atmos. Environ.*, **42**(21):5166-5168. doi:10.1016/j.atmosenv.2008.05.004.

Chow, J.C.; Watson, J.G. (2012). Chemical analyses of particle filter deposits. In *Aerosols Handbook : Measurement, Dosimetry, and Health Effects*, 2; Ruzer, L., Harley, N. H., Eds.; CRC Press/Taylor & Francis: New York, NY, 179-204.

Chow, J.C.; Watson, J.G.; Cao, J.J. (2010a). Highlights from "Leapfrogging Opportunities for Air Quality Improvement". *EM*, **16**(October):38-43.

Chow, J.C.; Watson, J.G.; Green, M.C.; Frank, N.H. (2010b). Filter light attenuation as a surrogate for elemental carbon. *J. Air Waste Manage. Assoc.*, **60**(11):1365-1375. http://www.tandfonline.com/doi/pdf/10.3155/1047-3289.60.11.1365.

Chow, J.C.; Watson, J.G.; Crow, D.; Lowenthal, D.H.; Merrifield, T.M. (2001). Comparison of IMPROVE and NIOSH carbon measurements. *Aerosol Sci. Technol.*, **34**(1):23-34. http://www.tandfonline.com/doi/pdf/10.1080/02786820600623711.

Chow, J.C.; Watson, J.G.; Chen, L.-W.A.; Rice, J.; Frank, N.H. (2010c). Quantification of PM2.5 organic carbon sampling artifacts in US networks. *Atmos. Chem. Phys.*, **10**(12):5223-5239. http://www.atmos-chem-phys.net/10/5223/2010/acp-10-5223-2010.pdf.

Chow, J.C.; Watson, J.G.; Pritchett, L.C.; Pierson, W.R.; Frazier, C.A.; Purcell, R.G. (1993). The DRI Thermal/Optical Reflectance carbon analysis system: Description, evaluation and applications in U.S. air quality studies. *Atmos. Environ.*, **27A**(8):1185-1201.

Chow, J.C.; Watson, J.G.; Chen, L.-W.A.; Arnott, W.P.; Moosmüller, H.; Fung, K.K. (2004a). Equivalence of elemental carbon by Thermal/Optical Reflectance and Transmittance with different temperature protocols. *Environ. Sci. Technol.*, **38**(16):4414-4422.

Chow, J.C.; Watson, J.G.; Chen, L.-W.A.; Chang, M.C.O.; Robinson, N.F.; Trimble, D.; Kohl, S.D. (2007a). The IMPROVE_A temperature protocol for thermal/optical carbon analysis: Maintaining consistency with a long-term database. *J. Air Waste Manage. Assoc.*, **57**(9):1014-1023.

Chow, J.C.; Yu, J.Z.; Watson, J.G.; Ho, S.S.H.; Bohannan, T.L.; Hays, M.D.; Fung, K.K. (2007b). The application of thermal methods for determining chemical composition of carbonaceous aerosols: A Review. *Journal of Environmental Science and Health-Part A*, **42**(11):1521-1541.

Chow, J.C.; Watson, J.G.; Kuhns, H.D.; Etyemezian, V.; Lowenthal, D.H.; Crow, D.J.; Kohl, S.D.; Engelbrecht, J.P.; Green, M.C. (2004b). Source profiles for industrial, mobile, and area sources in the Big Bend Regional Aerosol Visibility and Observational (BRAVO) Study. *Chemosphere*, **54**(2):185-208.

Chow, J.C.; Watson, J.G.; Chen, L.-W.A.; Paredes-Miranda, G.; Chang, M.-C.O.; Trimble, D.L.; Fung, K.K.; Zhang, H.; Yu, J.Z. (2005). Refining temperature measures in thermal/optical carbon analysis. *Atmos. Chem. Phys.*, **5**(4):2961-2972. 1680-7324/acp/2005-5-2961. http://www.atmos-chem-phys.net/5/2961/2005/acp-5-2961-2005.pdf.

Chow, J.C.; Watson, J.G.; Feldman, H.J.; Nolan, J.; Wallerstein, B.R.; Hidy, G.M.; Lioy, P.J.; McKee, H.C.; Mobley, J.D.; Bauges, K.; Bachmann, J.D. (2007c). 2007 Critical review discussion - Will the circle be unbroken: A history of the U.S. National Ambient Air Quality Standards. *J. Air Waste Manage. Assoc.*, **57**(10):1151-1163. http://pubs.awma.org/gsearch/journal/2007/10/10.3155-1047-3289.57.10.1151.pdf.

Clearstone Engineering Ltd. (2006). An inventory of GHGs, CACs and H2S emissions by the Canadian bitumen industry: 1990 to 2003- Volume 2, CAC and H2S emissions. prepared by Clearstone Engineering, Ltd., Calgary, AB, Canada, Calgara, AB, Canada.

Clearstone Engineering Ltd.; Golder Associates, I. (2003). A priority ranking of air emissions in the oilsands region. prepared by Clearstone Engineering, Ltd., Calgary, AB, Canada.

Cooper, J.A.; Miller, E.A.; Redline, D.C.; Spidell, R.L.; Caldwell, L.M.; Sarver, R.H.; Tansyy, B.L. (1989). PM_{10} source apportionment of Utah Valley winter episodes before, during, and after closure of the West Orem steel plant. prepared by NEA, Inc., Beaverton, OR, for Kimball, Parr, Crockett and Waddops, Salt Lake City, UT.

Corio, L.A.; Sherwell, J. (2000). In-stack condensible particulate matter measurements and issues. *J. Air Waste Manage. Assoc.*, **50**(2):207-218.

England, G.C.; Toby, B.; Zielinska, B. (1998a). Critical review of source sampling and analysis methodologies for characterizing organic aerosol and fine particulate source emission profiles. Report Number 344; prepared by American Petroleum Institute, Washington, D.C..

England, G.C.; Zielinska, B.; Loos, K.; Crane, I.; Ritter, K. (2000). Characterizing $PM_{2.5}$ emission profiles for stationary sources: Comparison of traditional and dilution sampling techniques. *Fuel Processing Technology*, **65**:177-188.

England, G.C.; Wien, S.; Zimperman, R.; Zielinska, B.; McDonald, J. (2001a). Gas fired boiler test report site A: Characterization of fine particulate emission factors and speciation profiles from stationary petroleum industry combustion sources. Report Number 4703; prepared by American Petroleum Institute, Washington, DC, http://api-ep.api.org/filelibrary/ACF4B.pdf.

England, G.C.; Wien, S.; Zimperman, R.; Zielinska, B.; McDonald, J. (2001b). Gas fired heater test report site B: Characterization of fine particulate emission factors and speciation profiles from stationary petroleum industry combustion sources. Report Number 4704; prepared by American Petroleum Institute, Washington, DC, http://api-ep.api.org/filelibrary/ACF4B.pdf.

England, G.C.; Wien, S.; Zimperman, R.; Zielinska, B.; McDonald, J. (2001c). Gas fired steam heater test report site C: Characterization of fine particulate emission factors and speciation profiles from stationary petroleum

industry combustion sources. Report Number 4712; prepared by American Petroleum Institute, Washington, DC, http://api-ep.api.org/filelibrary/ACF4B.pdf.

England, G.C.; Wein, S.; Zielinska, B.; Loos, K.; Crane, I.; Ritter, K. (1998b). Characterization of organic aerosol and $PM_{2.5}$ source emission profiles for petroleum industry combustion sources. 14 June 98 A.D.bSan Diego, CA.

England, G.C.; Watson, J.G.; Chow, J.C.; Zielinska, B.; Chang, M.-C.O.; Loos, K.R.; Hidy, G.M. (2007a). Dilution-based emissions sampling from stationary sources: Part 1. Compact sampler, methodology and performance. *J. Air Waste Manage. Assoc.*, **57**(1):65-78. http://pubs.awma.org/gsearch/journal/2007/1/england.pdf.

England, G.C.; Watson, J.G.; Chow, J.C.; Zielinska, B.; Chang, M.-C.O.; Loos, K.R.; Hidy, G.M. (2007b). Dilution-based emissions sampling from stationary sources: Part 2. Gas-fired combustors compared with other fuel-fired systems. *J. Air Waste Manage. Assoc.*, **57**(1):79-93. http://pubs.awma.org/gsearch/journal/2007/1/england2.pdf.

Harris, D.B. (1986). Source sampling systems used to develop source signatures. In *Transactions, Receptor Methods for Source Apportionment: Real World Issues and Applications*, Pace, T. G., Ed.; Air Pollution Control Association: Pittsburgh, PA, 46-55.

Heinsohn, R.J.; Davis, J.W.; Knapp, K.T. (1980). Dilution source sampling systems. *Environ. Sci. Technol.*, **14**(10):1205-1209.

Hildemann, L.M.; Cass, G.R.; Markowski, G.R. (1989). A dilution stack sampler for collection of organic aerosol emissions: Design, characterization and field tests. *Aerosol Sci. Technol.*, **10**(10-11):193-204.

Ho, S.S.H.; Yu, J.Z. (2004). In-injection port thermal desorption and subsequent gas chromatography-mass spectrometric analysis of polycyclic aromatic hydrocarbons and *n*-alkanes in atmospheric aerosol samples. *J. Chromatogr. A*, **1059**(1-2):121-129.

Hueglin, C.; Scherrer, L.; Burtscher, H. (1997). An accurate continuously adjustable dilution system (1:10 to $1:10^4$) for submicron aerosols. *J. Aerosol Sci.*, **28**(6):1049-1055.

Huynh, C.K.; Vu Duc, T.; Schwab, C.; Rollier, H. (1984). In-stack dilution techniques for the sampling of polycyclic organic compounds. Applications to effluents of a domestic waste incineration plant. *Atmos. Environ.*, **18**(2):255-259.

Jimenez, S.; Ballester, J. (2005). A comparative study of different methods for the sampling of high temperature combustion aerosols. *Aerosol Sci. Technol.*, **39**(9):811-821.

Kulkarni, P.; Baron, P.A.; Willeke, K. (2011). *Aerosol Measurement Principles, Techniques and Applications, Third Edition*. John Wiley & Sons, Inc.: Hoboken, NJ, USA.

Lee, S.W.; Pomalis, R.; Kan, B. (2000). A new methodology for source characterization of oil combustion particulate matter. *Fuel Processing Technology*, **65**:189-202.

Lee, S.W.; He, I.; Young, B. (2004). Important aspects in source PM2.5 emissions measurement and characterization from stationary combustion systems. *Fuel Proc. Technol.*, **85**:687-699.

Lighty, J.S.; Veranth, J.M.; Sarofim, A.F. (2000). Critical review: Combustion aerosols: Factors governing their size and composition and implications to human health. *J. Air Waste Manage. Assoc.*, **50**(9):1565-1618.

Lipsky, E.M.; Robinson, A.L. (2005). Design and evaluation of a portable dilution sampling system for measuring fine particle emissions from combustion systems. *Aerosol Sci. Technol.*, **39**(6):542-553.

Lipsky, E.M.; Stanier, C.O.; Pandis, S.N.; Robinson, A.L. (2002). Effects of sampling conditions on the size distribution of fine particulate matter emitted from a pilot-scale pulverized-coal combustor. *Energy & Fuels*, **16**(2):302-310.

Lipsky, E.M.; Pekney, N.J.; Walbert, G.F.; O'Dowd, W.J.; Freeman, M.C.; Robinson, A. (2004). Effects of dilution sampling on fine particle emissions from pulverized coal combustion. *Aerosol Sci. Technol.*, **38**(6):574-587.

Maguhn, J.; Karg, E.; Kettrup, A.; Zimmermann, R. (2003). On-line analysis of the size distribution of fine and ultrafine aerosol particles in flue and stack gas of a municipal waste incineration plant: Effects of dynamic process control measures and emission reduction devices. *Environ. Sci. Technol.*, **37**(20):4761-4770.

McDonald, J.D.; Zielinska, B.; Fujita, E.M.; Sagebiel, J.C.; Chow, J.C.; Watson, J.G. (2000). Fine particle and gaseous emission rates from residential wood combustion. *Environ. Sci. Technol.*, **34**(11):2080-2091.

Myers, R.E.; Logan, T. (2002). Progress on Developing a Federal Reference PM Fine Source Test Method. In *11th International Emission Inventory Conference - "Emission Inventories - Partnering for the Future"*, 15 April 2002U.S. EPA: Atlanta, GA.

Neulicht, R.; Watson, J.G.; Chow, J.C.; Baldwin, T.A. (2009). Quality assurance project plan for pre-field laboratory quality assurance evaluation of $PM_{2.5}$ dilution monitoring device. prepared by Research Triangle Institute, Research Triangle Park, NC, for U.S. Environmental Protection Agency, Research Triangle Park, NC.

Olmez, I.; Sheffield, A.E.; Gordon, G.E.; Houck, J.E.; Pritchett, L.C.; Cooper, J.A.; Dzubay, T.G.; Bennett, R.L. (1988). Compositions of particles from selected sources in Philadelphia for receptor model applications. *J. Air Poll. Control Assoc.*, **38**(11):1392-1402.

Richards, J.; Holder, T.; Goshaw, D. (2005). Optimized Method 202 Sampling Train to Minimize the Biases Associated with Method 202 Measurement of Condensable Particulate Matter Emissions. In *Proceedings, Specialty Conference on Hazardous Waste Combustion*, Air & Waste Management Association: Pittsburgh, PA, 1-9.

Richardson, C.B.; Hightower, R.L.; Pigg, A.L. (1986). Optical measurement of the evaporation of sulfuric acid droplets. *Appl. Optics*, **25**(7):1226-1229.

Seames, W.S.; Fernandez, A.; Wendt, J.O. (2002). A study of fine particulate emissions from combustion of treated pulverized municipal sewage sludge. *Environ. Sci. Technol.*, **36**(12):2772-2776. PM:12099478.

Seinfeld, J.H.; Pandis, S.N. (1997). *Atmospheric Chemistry and Physics*. John Willey & Sons, Inc: New York.

Sheya, S.A.; Glowacki, C.; Chang, M.-C.O.; Chow, J.C.; Watson, J.G. (2008). Hot filter/impinger and dilution sampling for fine particulate matter characterization from ferrous metal casting processes. *J. Air Waste Manage. Assoc.*, **58**(4):553-561. http://pubs.awma.org/gsearch/journal/2008/4/10.3155-1047-3289.58.4.553.pdf.

Sousa, J.A.; Houck, J.E.; Cooper, J.A.; Daisey, J.M. (1987). The mutagenic activity of particulate organic matter collected with a dilution sampler at coal-fired power plants. *J. Air Poll. Control Assoc.*, **37**(12):1439-1444.

Tsukada, M.; Nishikawa, N.; Horikawa, A.; Wada, M.; Liu, Y.; Kamiya, H. (2008). Emission potential of condensable suspended particulate matter from flue gas of solid waste combustion. *Powder Technology*, **180**(1-2):140-144.

U.S.EPA (1997). Revised requirements for designation of reference and equivalent methods for $PM_{2.5}$ and ambient air surveillence for particulate matter - final rule. *Federal Register*, **62**(138):38763-38854. http://www.epa.gov/ttn/amtic/files/cfr/recent/pm-mon.pdf.

U.S.EPA. (2000a). Method 5 - Determination of Particulate Matter Emissions from Stationary Sources (40 CFR 60. Appendix A to Part 60).

U.S.EPA (2000b). Method 17. In-Stack Particulate-Determination of particulate matter emissions from stationary sources. prepared by U.S. EPA, Research Triangle Park, NC, http://www.epa.gov/ttn/emc/promgate.html.

U.S.EPA (2000c). Method 6. Determination of sulfur dioxide emissions from stationary sources. prepared by U.S. EPA, Research Triangle Park, NC, http://www.epa.gov/ttn/emc/promgate/m-06.pdf.

U.S.EPA (2000d). Method 7. Determination of nitrogen oxide emissions from stationary sources. prepared by U.S. EPA, Research Triangle Park, NC, http://www.epa.gov/ttn/emc/promgate/m-06.pdf.

U.S.EPA (2004). Conditional test method (CTM) 039: Measurement of PM2.5 and PM10 emissions by dilution sampling (constant sampling rate procedures. prepared by U.S. Environmental Protection Agency, Research Triangle Park, NC, http://www.epa.gov/ttn/emc/ctm/ctm-039.pdf.

U.S.EPA (2010a). Method 201A - Determination of PM10 and PM2.5 Emissions From Stationary Sources (Constant Sampling Rate Procedure): 55 FR 14246 04/17/90 (Appendix M of 40 CFR 51). prepared by U.S. Environmental Protection Agency, Office of Air Quality Planning and Standards, Technical Support Division, Research Triangle Park, NC, http://www.epa.gov/ttn/emc/promgate/m-201a.pdf.

U.S.EPA (2010b). Method 202 - Dry Impinger Method for Determining Condensible Particulate Emissions from Stationary Sources: (Appendix M of 40 CFR 51). prepared by U.S. Environmental Protection Agency, Office of Air Quality Planning and Standards, Technical Support Division, Research Triangle Park, NC, http://www.epa.gov/ttn/emc/promgate/m-202.pdf.

U.S.EPA. (2011). Method 2 - Determination of Stack Gas Velocity and Volumetric Flow Rate (Type S Pitot Tube)(40 CFR 60. Appendix A to Part 60).

Wang, X.L.; Watson, J.G.; Chow, J.C.; Kohl, S.D.; Chen, L.-W.A.; Sodeman, D.A.; Legge, A.H.; Percy, K.E. (2012). Measurement of real-world stack emissions with a dilution sampling system. In *Alberta Oil Sands: Energy, Industry, and the Environment*, Percy, K. E., Ed.; Elsevier Press: Amsterdam, The Netherlands, 171-192.

Watson, J.G. (2002). Visibility: Science and regulation. *J. Air Waste Manage. Assoc.*, **52**(6):628-713.

Watson, J.G.; Chow, J.C. (2001). Source characterization of major emission sources in the Imperial and Mexicali valleys along the U.S./Mexico border. *Sci. Total Environ.*, **276**(1-3):33-47.

Watson, J.G.; Chow, J.C. (2013). Source apportionment. In *Encyclopedia of Environmetrics*, El-Shaarwi, A. H., Piegorsch, W. W., Eds.; John Wiley & Sons, Ltd.: Chichester, UK.

Watson, J.G.; Chow, J.C.; Houck, J.E. (2001a). $PM_{2.5}$ chemical source profiles for vehicle exhaust, vegetative burning, geological material, and coal burning in northwestern Colorado during 1995. *Chemosphere*, **43**(8):1141-1151.

Watson, J.G.; Turpin, B.J.; Chow, J.C. (2001b). The measurement process: Precision, accuracy, and validity. In *Air Sampling Instruments for Evaluation of Atmospheric Contaminants, Ninth Edition*, 9th; Cohen, B. S., McCammon, C. S. J., Eds.; American Conference of Governmental Industrial Hygienists: Cincinnati, OH, 201-216.

Watson, J.G.; Chen, L.-W.A.; Chow, J.C.; Lowenthal, D.H.; Doraiswamy, P. (2008). Source apportionment: Findings from the U.S. Supersite Program. *J. Air Waste Manage. Assoc.*, **58**(2):265-288. http://pubs.awma.org/gsearch/journal/2008/2/10.3155-1047-3289.58.2.265.pdf.

Watson, J.G.; Chow, J.C.; Lowenthal, D.H.; Chen, L.-W.A.; Wang, X.L. (2012a). Reformulation of $PM_{2.5}$ mass reconstruction assumptions for the San Joaquin Valley. prepared by Desert Research Institute, Reno, NV, for San Joaquin Valley Unified Air Pollution Control District, Fresno, CA.

Watson, J.G.; Chow, J.C.; Moosmüller, H.; Green, M.C.; Frank, N.H.; Pitchford, M.L. (1998). Guidance for using continuous monitors in $PM_{2.5}$ monitoring networks. Report Number EPA-454/R-98-012; prepared by U.S. Environmental Protection Agency, Research Triangle Park, NC, http://www.epa.gov/ttn/amtic/pmpolgud.html.

Watson, J.G.; Chow, J.C.; Lowenthal, D.H.; Robinson, N.F.; Cahill, C.F.; Blumenthal, D.L. (2002). Simulating changes in source profiles from coal-fired power stations: Use in chemical mass balance of $PM_{2.5}$ in the Mt. Zirkel Wilderness. *Energy & Fuels*, **16**(2):311-324.

Watson, J.G.; Chow, J.C.; Wang, X.L.; Kohl, S.D.; Chen, L.-W.A.; Etyemezian, V. (2012b). Overview of real-world emission characterization methods. In *Alberta Oil Sands: Energy, Industry, and the Environment*, Percy, K. E., Ed.; Elsevier Press: Amsterdam, The Netherlands, 145-170.

Yi, H.H.; Hao, J.M.; Duan, L.; Li, X.H.; Guo, X.M. (2006). Characteristics of inhalable particulate matter concentration and size distribution from power plants in China. *J. Air Waste Manage. Assoc.*, **56**(9):1243-1251.

Zielinska, B.; McDonald, J.D.; Hayes, T.; Chow, J.C.; Fujita, E.M.; Watson, J.G. (1998). Northern Front Range Air Quality Study, Volume B: Source measurements. prepared by Desert Research Institute, Reno, NV, for Colorado State University, Fort Collins, CO.

Appendix A: Analytical Minimum Detection Limits Gases and PM Constituents

Table A- 1. Summary of minimum detection limits (MDLs[a]) for mass, elements, ions (including gaseous NH_3 and SO_2), and carbon applied to this study.

Species/Compounds	Analysis Method[b]	MDL (µg/filter[c])
Mass	GRAV	1
B_{abs}	OD	0.02
Ammonia (NH_3) as NH_4^+	AC	1.5005
Sulfur Dioxide (SO_2)	IC	1.5005
H_2S as S	XRF	0.0506
Chloride (Cl^-)	IC	1.5005
Nitrite (NO_2^-)	IC	1.5005
Nitrate (NO_3^-)	IC	1.5005
Sulfate ($SO_4^=$)	IC	1.5005
Phosphate (PO_4^{3-})	IC	1.5005
Ammonium (NH_4^+)	AC	1.5005
Soluble Sodium (Na^+)	AAS	0.2362
Soluble Magnesium (Mg^{2+})	AAS	0.0945
Soluble Potassium (K^+)	AAS	0.1498
Soluble Calcium (Ca^{2+})	AAS	0.0945
Organic Carbon (OC) Fraction 1	Thermal/optical carbon	0.0516
Organic Carbon (OC) Fraction 2	Thermal/optical carbon	1.29
Organic Carbon (OC) Fraction 3	Thermal/optical carbon	3.87
Organic Carbon (OC) Fraction 4	Thermal/optical carbon	0.129
Pyrolyzed organic carbon via transmittance	Thermal/optical carbon	0.129
Pyrolyzed organic carbon via reflectance	Thermal/optical carbon	0.129
Organic Carbon (OC)	Thermal/optical carbon	5.031
Water soluble organic carbon (WSOC)	Thermal/optical carbon	9.7

Table A-1. Continued. **Species/Compounds**	**Analysis Method**[b]	**MDL (µg/filter**[c]**)**
Elemental Carbon (EC) Fraction 1	Thermal/optical carbon	0.0387
Elemental Carbon (EC) Fraction 2	Thermal/optical carbon	0.0387
Elemental Carbon (EC) Fraction 3	Thermal/optical carbon	0.0387
Elemental Carbon (EC)	Thermal/optical carbon	0.129
Carbonate Carbon (CC)	Thermal/optical carbon	0.05
Total Carbon (TC)	Thermal/optical carbon	5.418
Sodium (Na)	XRF	3.7541
Magnesium (Mg)	XRF	1.1341
Aluminum (Al)	XRF	0.4483
Silicon (Si)	XRF	0.3613
Phosphorus (P)	XRF	0.1177
Sulfur (S)	XRF	0.0506
Chlorine (Cl)	XRF	0.0487
Potassium (K)	XRF	0.0459
Calcium (Ca)	XRF	0.0727
Scandium (Sc)	XRF	0.1938
Titanium (Ti)	XRF	0.0346
Vanadium (V)	XRF	0.0082
Chromium (Cr)	XRF	0.0382
Manganese (Mn)	XRF	0.0834
Iron (Fe)	XRF	0.076
Cobalt (Co)	XRF	0.0041
Nickel (Ni)	XRF	0.0131
Copper (Cu)	XRF	0.0442
Zinc (Zn)	XRF	0.0391
Gallium (Ga)	XRF	0.1281
Arsenic (As)	XRF	0.0147
Selenium (Se)	XRF	0.029
Bromine (Br)	XRF	0.0412
Rubidium (Rb)	XRF	0.0271
Strontium (Sr)	XRF	0.0633
Yttrium (Y)	XRF	0.0376

Table A-1. Continued. **Species/Compounds**	**Analysis Method[b]**	**MDL (µg/filter[c])**
Zirconium (Zr)	XRF	0.1012
Niobium (Nb)	XRF	0.0667
Molybdenum (Mo)	XRF	0.064
Palladium (Pd)	XRF	0.1549
Silver (Ag)	XRF	0.1473
Cadmium (Cd)	XRF	0.1152
Indium (In)	XRF	0.1271
Tin (Sn)	XRF	0.1372
Antimony (Sb)	XRF	0.2063
Cesium (Cs)d	XRF	0.0585
Barium (Ba)d	XRF	0.0632
Lanthanum (La)d	XRF	0.0433
Cerium (Ce)d	XRF	0.0417
Samarium (Sm)d	XRF	0.0862
Europium (Eu)d	XRF	0.1325
Terbium (Tb)d	XRF	0.0976
Hafnium (Hf)	XRF	0.395
Tantalum (Ta)	XRF	0.2579
Wolfram (W)	XRF	0.361
Iridium (Ir)	XRF	0.1192
Gold (Au)	XRF	0.196
Mercury (Hg)	XRF	0.0971
Thallium (Tl)	XRF	0.0654
Lead (Pb)	XRF	0.0945
Thorium (Th)	XRF	0.1648
Uranium (U)	XRF	0.1648
Cesium (Cs)[d]	ICP/MS	0.005
Barium (Ba)[d]	ICP/MS	0.0005
Lanthanum (La)[d]	ICP/MS	0.0001
Cerium (Ce)[d]	ICP/MS	0.0001
Praseodymium (Pr)	ICP/MS	0.0001

Table A-1. Continued. **Species/Compounds**	**Analysis Method[b]**	**MDL (µg/filter[c])**
Neodymium (Nd)	ICP/MS	0.0001
Samarium (Sm)[d]	ICP/MS	0.0001
Europium (Eu)[d]	ICP/MS	0.0001
Gadolinium (Gd)	ICP/MS	0.0001
Terbium (Tb)[d]	ICP/MS	0.0001
Dysprosium (Dy)	ICP/MS	0.0001
Holmium (Ho)	ICP/MS	0.0001
Erbium (Er)	ICP/MS	0.0001
Thulium (Tm)	ICP/MS	0.0001
Ytterbium (Yb)	ICP/MS	0.0001
Lutetium (Lu)	ICP/MS	0.0001
Pb (Isotopes) Pb-204, Pb-206, Pb-207 and Pb-208	ICP/MS	0.0003

[a] Minimum detectable limit (MDL) is the concentration at which instrument response equals three times the standard deviation of the response to a known concentration of zero.

[b] GRAV = Gravimetry
IC = Ion chromatography with conductivity detector
AC = Automated colorimetry
AAS = Atomic absorption spectrophotometry.
Thermal/optical carbon = DRI Model 2001 thermal/optical reflectance/transmittance carbon analyzer using the IMPROVE_A protocol for OC, EC, CC, and carbon fractions; and using WSOC protocol for total WSOC
XRF = X-ray fluorescence
ICP/MS = Inductively coupled plasma – mass spectrometry

[c] Filter = 47 mm filter

[d] Quantified by both XRF and ICP/MS

Table A- 2. Summary of analytical detection limits for 125 non-polar organic compounds by thermal desorption-gas chromatography/mass spectrometry (TD-GC/MS; Chow et al., 2007b; Ho and Yu, 2004).

Compounds	Analysis[a] Method	MDL[b] ng/filter[c]	LQL[d] ng/filter
PAHs			
acenaphthylene	TD-GC/MS	10.764	10.764
acenaphthene	TD-GC/MS	5.842	5.842
fluorene	TD-GC/MS	4.048	4.048
phenanthrene	TD-GC/MS	1.932	1.932
anthracene	TD-GC/MS	0.782	1.192
fluoranthene	TD-GC/MS	1.150	1.150
pyrene	TD-GC/MS	1.840	1.840
benzo[a]anthracene	TD-GC/MS	3.496	3.496
chrysene	TD-GC/MS	1.840	1.840
benzo[b]fluoranthene	TD-GC/MS	3.772	3.772
benzo[k]fluoranthene	TD-GC/MS	1.288	1.443
benzo[a]fluoranthene	TD-GC/MS	1.886	1.886
benzo[e]pyrene	TD-GC/MS	4.048	4.048
benzo[a]pyrene	TD-GC/MS	4.140	4.140
perylene	TD-GC/MS	4.462	4.462
indeno[1,2,3-cd]pyrene	TD-GC/MS	1.932	1.932
dibenzo[a,h]anthracene	TD-GC/MS	4.324	4.324
benzo[ghi]perylene	TD-GC/MS	2.852	2.852
coronene	TD-GC/MS	3.358	3.358
dibenzo[a,e]pyrene	TD-GC/MS	1.288	1.288
1-methylnaphthalene	TD-GC/MS	2.070	2.070
2-methylnaphthalene	TD-GC/MS	0.690	0.690
2,6-dimethylnaphthalene	TD-GC/MS	4.002	4.002
9-fluorenone	TD-GC/MS	4.508	4.508
9-methylanthracene	TD-GC/MS	4.186	4.186
anthraquinone	TD-GC/MS	5.060	5.060
methylfluoranthene	TD-GC/MS	1.288	1.288
retene	TD-GC/MS	5.566	5.566
cyclopenta[cd]pyrene	TD-GC/MS	1.288	1.288
benz[a]anthracene-7,12-dione	TD-GC/MS	4.692	4.692
methylchrysene	TD-GC/MS	1.932	1.932
picene	TD-GC/MS	4.784	4.784
Alkane/Alkene/Phthalate			
***n*-alkane**			
pentadecane (*n*-C15)	TD-GC/MS	3.956	22.500
hexadecane (*n*-C16)	TD-GC/MS	4.094	32.956
heptadecane (*n*-C17)	TD-GC/MS	3.496	17.322
octadecane (*n*-C18)	TD-GC/MS	3.036	14.275
nonadecane (*n*-C19)	TD-GC/MS	2.346	11.411
icosane (*n*-C20)	TD-GC/MS	2.346	20.124
heneicosane (*n*-C21)	TD-GC/MS	3.910	16.139
docosane (*n*-C22)	TD-GC/MS	2.944	12.686
tricosane (*n*-C23)	TD-GC/MS	3.404	15.957
tetracosane (*n*-C24)	TD-GC/MS	2.530	22.520
pentacosane (*n*-C25)	TD-GC/MS	2.714	32.318
hexacosane (*n*-C26)	TD-GC/MS	2.714	27.930
heptacosane (*n*-C27)	TD-GC/MS	1.334	22.946

Table A-2 Continued.

Compounds	Analysis Method[a]	MDL[b] ng/filter[c]	LQL[d] ng/filter
Alkane/Alkene/Phthalate (continued)			
***n*-alkane (continued)**			
octacosane (*n*-C28)	TD-GC/MS	3.358	10.552
nonacosane (*n*-C29)	TD-GC/MS	3.772	5.321
triacontane (*n*-C30)	TD-GC/MS	4.416	4.416
hentriacotane (*n*-C31)	TD-GC/MS	3.588	3.588
dotriacontane (*n*-C32)	TD-GC/MS	4.140	4.140
tritriactotane (*n*-C33)	TD-GC/MS	2.622	2.622
tetratriactoane (*n*-C34)	TD-GC/MS	3.082	3.082
pentatriacontane (*n*-C35)	TD-GC/MS	3.312	3.312
hexatriacontane (*n*-C36)	TD-GC/MS	3.956	3.956
heptatriacontane (*n*-C37)	TD-GC/MS	4.002	4.002
octatriacontane (*n*-C38)	TD-GC/MS	3.956	3.956
nonatriacontane (*n*-C39)	TD-GC/MS	3.772	3.772
tetracontane (*n*-C40)	TD-GC/MS	3.864	3.864
hentetracontane (*n*-C41)	TD-GC/MS	4.048	4.048
dotetracontane (*n*-C42)	TD-GC/MS	4.140	4.140
iso/anteiso-alkane			
iso-nonacosane (iso-C29)	TD-GC/MS	3.680	3.680
anteiso-nonacosane (anteiso-C29)	TD-GC/MS	3.588	3.588
iso-triacontane (iso-C30)	TD-GC/MS	3.726	3.726
anteiso-triacontane (anteiso-C30)	TD-GC/MS	3.864	3.864
iso-hentriacotane (iso-C31)	TD-GC/MS	4.002	4.002
anteiso-hentriacotane (anteiso-C31)	TD-GC/MS	4.048	4.048
iso-dotriacontane (iso-C32)	TD-GC/MS	3.588	3.588
anteiso-dotriacontane (anteiso-C32)	TD-GC/MS	3.496	3.496
iso-tritriactotane (iso-C33)	TD-GC/MS	3.726	3.726
anteiso-tritriactotane (anteiso-C33)	TD-GC/MS	3.910	3.910
iso-tetratriactoane (iso-C34)	TD-GC/MS	3.864	3.864
anteiso-tetratriactoane (anteiso-C34)	TD-GC/MS	3.818	3.818
iso-pentatriacontane (iso-C35)	TD-GC/MS	4.048	4.048
anteiso-pentatriacontane (anteiso-C35)	TD-GC/MS	3.956	3.956
iso-hexatriacontane (iso-C36)	TD-GC/MS	4.002	4.002
anteiso-hexatriacontane (anteiso-C36)	TD-GC/MS	3.588	3.588
iso-heptatriacontane (iso-37)	TD-GC/MS	3.772	3.772
anteiso-heptatriacontane (anteiso-37)	TD-GC/MS	3.910	3.910
hopane			
22,29,30-trisnorneophopane (Ts)	TD-GC/MS	2.070	2.070
22,29,30-trisnorphopane (Tm)	TD-GC/MS	2.346	2.346
αβ-norhopane (C29αβ-hopane)	TD-GC/MS	1.472	1.472
22,29,30-norhopane (29Ts)	TD-GC/MS	2.530	2.530
αα- + βα-norhopane (C29αα- + βα -hopane)	TD-GC/MS	2.806	2.806
αβ-hopane (C30αβ -hopane)	TD-GC/MS	2.392	2.392
αα-hopane (30αα-hopane)	TD-GC/MS	2.070	2.070
βα-hopane (C30βα -hopane)	TD-GC/MS	2.208	2.208
αβS-homohopane (C31αβS-hopane)	TD-GC/MS	3.864	3.864
αβR-homohopane (C31αβR-hopane)	TD-GC/MS	3.818	3.818
αβS-bishomohopane (C32αβS-hopane)	TD-GC/MS	3.588	3.588
αβR-bishomohopane (C32αβR-hopane)	TD-GC/MS	3.726	3.726
22S-trishomohopane (C33)	TD-GC/MS	3.680	3.680
22R-trishomohopane (C33)	TD-GC/MS	4.048	4.048
22S-tretrahomohopane (C34)	TD-GC/MS	3.726	3.726
22R-tetrashomohopane (C34)	TD-GC/MS	3.772	3.772

Table A-2 Continued.

Compounds	Analysis Method[a]	MDL[b] ng/filter[c]	LQL[d] ng/filter
Alkane/Alkene/Phthalate (continued)			
22S-pentashomohopane(C35)	TD-GC/MS	3.680	3.680
22R-pentashomohopane(C35)	TD-GC/MS	3.726	3.726
sterane			
ααα 20S-Cholestane	TD-GC/MS	2.990	2.990
αββ 20R-Cholestane	TD-GC/MS	3.036	3.036
αββ 20s-Cholestane	TD-GC/MS	2.530	2.530
ααα 20R-Cholestane	TD-GC/MS	1.150	1.150
ααα 20S 24S-Methylcholestane	TD-GC/MS	2.070	2.070
αββ 20R 24S-Methylcholestane	TD-GC/MS	2.024	2.024
αββ 20S 24S-Methylcholestane	TD-GC/MS	2.346	2.346
ααα 20R 24R-Methylcholestane	TD-GC/MS	2.668	2.668
ααα 20S 24R/S-Ethylcholestane	TD-GC/MS	3.588	3.588
αββ 20R 24R-Ethylcholestane	TD-GC/MS	1.610	1.610
αββ 20S 24R-Ethylcholestane	TD-GC/MS	1.748	1.748
ααα 20R 24R-Ethylcholestane	TD-GC/MS	1.702	1.702
methyl-alkane			
2-methylnonadecane	TD-GC/MS	4.048	4.048
3-methylnonadecane	TD-GC/MS	4.324	4.324
branched-alkane			
pristane	TD-GC/MS	4.554	35.768
phytane	TD-GC/MS	4.554	47.343
squalane	TD-GC/MS	4.600	4.600
cycloalkane			
octylcyclohexane	TD-GC/MS	4.324	4.860
decylcyclohexane	TD-GC/MS	3.220	3.220
tridecylcyclohexane	TD-GC/MS	6.072	6.072
n-heptadecylcyclohexane	TD-GC/MS	3.864	3.864
nonadecylcyclohexane	TD-GC/MS	3.220	3.220
alkene	TD-GC/MS		
1-octadecene	TD-GC/MS	3.680	3.680
phthalate	TD-GC/MS		
dimethylphthalate	TD-GC/MS	2.622	5.453
diethyl phthalate	TD-GC/MS	4.002	5.871
di-n-butyl phthalate	TD-GC/MS	2.116	3.788
butyl benzyl phthalate	TD-GC/MS	3.956	3.956
bis(2-ethylhexyl)phthalate	TD-GC/MS	3.450	3.450
di-n-octyl phthalate	TD-GC/MS	3.910	3.910

[a] TD-GC/MS = thermal desorption-gas chromatography/mass spectrometry

[b] MDL (minimum detectable limit) is the concentration at which instrument response equals three times the standard deviation of the response to a known concentration of zero.

[c] Filter assumed to be a 47 mm filter with 11.9 square centimeter deposit area

[d] LQL (lower quantifiable limit) is the large of three times the standard deviation of the concentrations measured on field blanks or MDL.

Table A-3. Summary of minimum detection limits (MDLs[a]) for carbohydrates, organic acids, and total water soluble organic carbon (WSOC).

Species	**Analysis Method**	**MDL (ug/filter[b])**
Carbohydrates		
Glycerol (C3H8O3)	IC-PAD[c]	0.04
Inositol (C6H12O6)	IC-PAD	0.04
Erythritol (C4H10O4)	IC-PAD	0.06
Xylitol (C5H12O5)	IC-PAD	0.04
Levoglucosan (C6H10O5)	IC-PAD	0.08
Sorbitol (C6H14O6)	IC-PAD	0.1
Mannosan (C6H10O5)	IC-PAD	0.06
Trehalose (C12H22O11)	IC-PAD	0.08
Mannitol (C6H14O6)	IC-PAD	0.06
Arabinose (C5H10O5)	IC-PAD	0.06
Glucose (C6H12O6)	IC-PAD	0.04
Galactose (C6H12O6)	IC-PAD	0.08
Maltitol (C12H24O11)	IC-PAD	0.1
Organic Acids		
Lactic acid (C3H6O3)	IC-ECD[d]	0.06
Acetic acid (C2H4O2)	IC-ECD	0.12
Formic acid (CH2O)	IC-ECD	0.12
Methanesulfonic acid (CH4SO3)	IC-ECD	0.08
Glutaric acid (C5H8O4)	IC-ECD	0.1
Succinic acid (C4H6O4)	IC-ECD	0.08
Malonic acid (C3H4O4)	IC-ECD	0.12
Maleic acid (C4H4O4)	IC-ECD	0.1
Oxalic acid (C2H2O4)	IC-ECD	0.08
WSOC	**TOC**	**2.44**

[a] Minimum detectable limit (MDL) is the concentration at which instrument response equals three times the standard deviation of the response to a known concentration of zero.

[b] Filter assumed to be a 47 mm filter with 11.9 square centimeter deposit area

[c] IC-PAD = Ion chromatography with pulsed ampereometric detector

[d] IC-ECD = Ion chromatography with electrical conductivity detector

Appendix B: Real-time Stack Temperature, Velocity, and Pollutant Concentrations

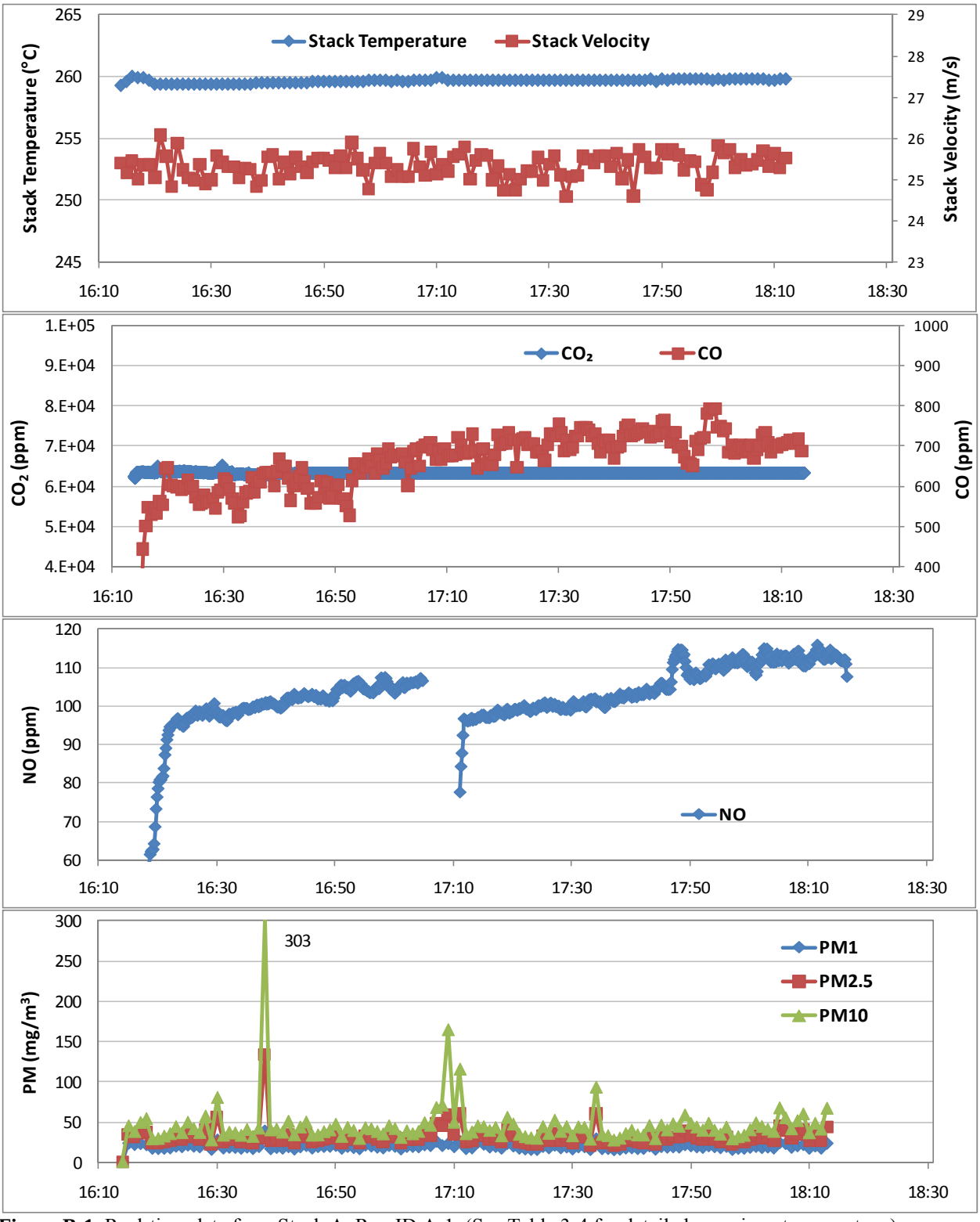

Figure B-1. Real-time data from Stack A, Run ID A-1. (See Table 3-4 for detailed experiment parameters.)

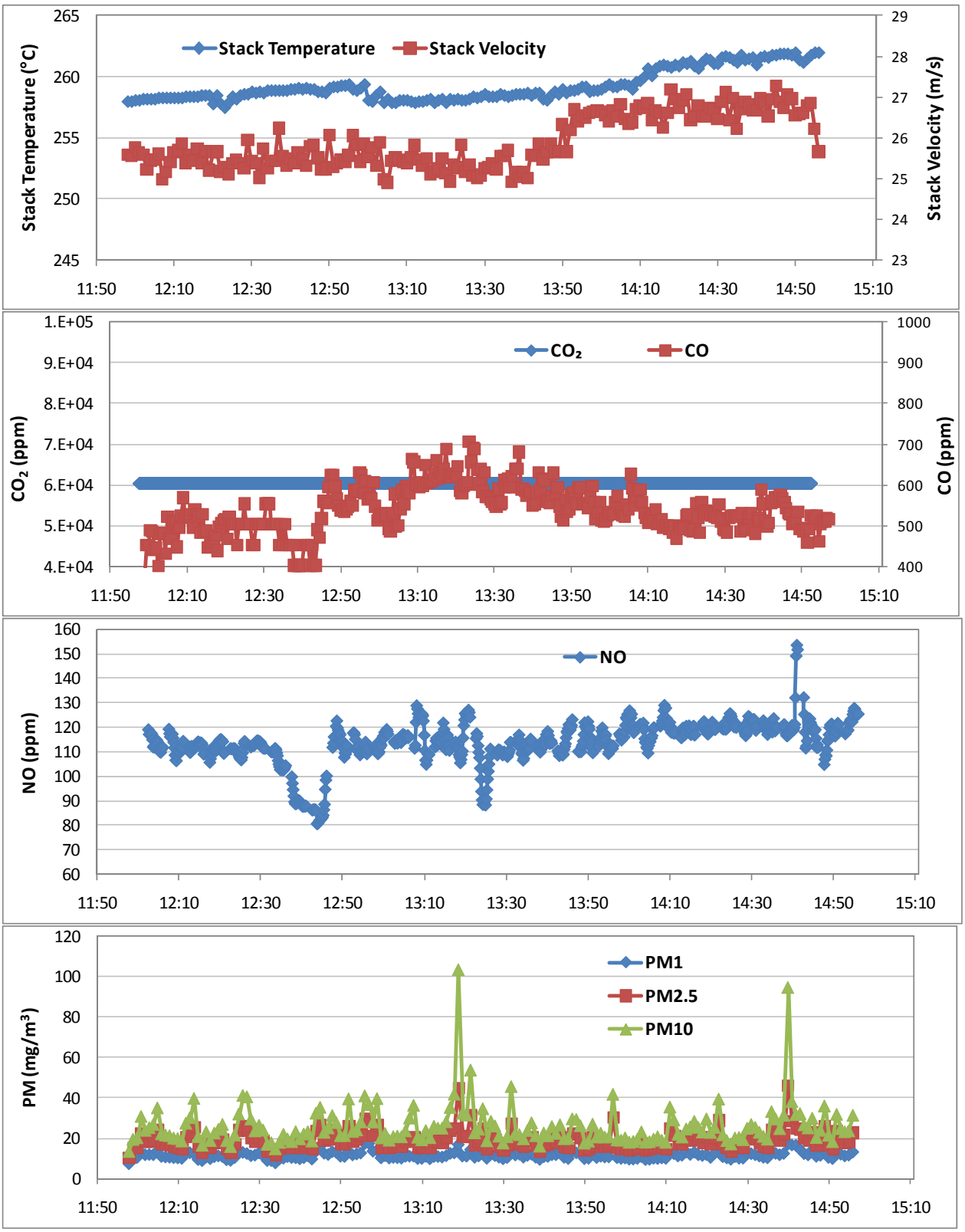

Figure B-2. Real-time data from Stack A, Run ID A-2. (See Table 3-4 for detailed experiment parameters.)

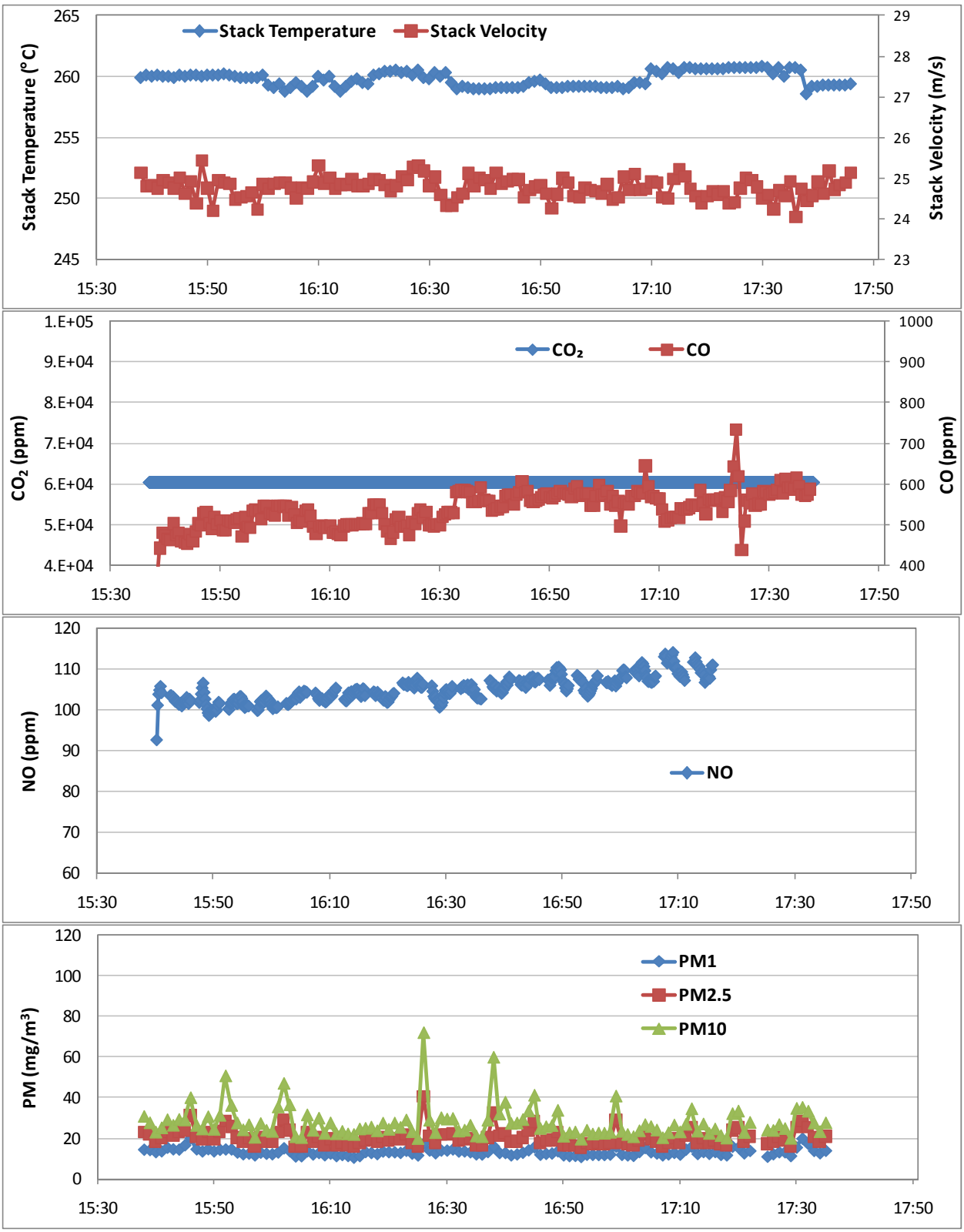

Figure B-3. Real-time data from Stack A, Run ID A-3. (See Table 3-4 for detailed experiment parameters.)

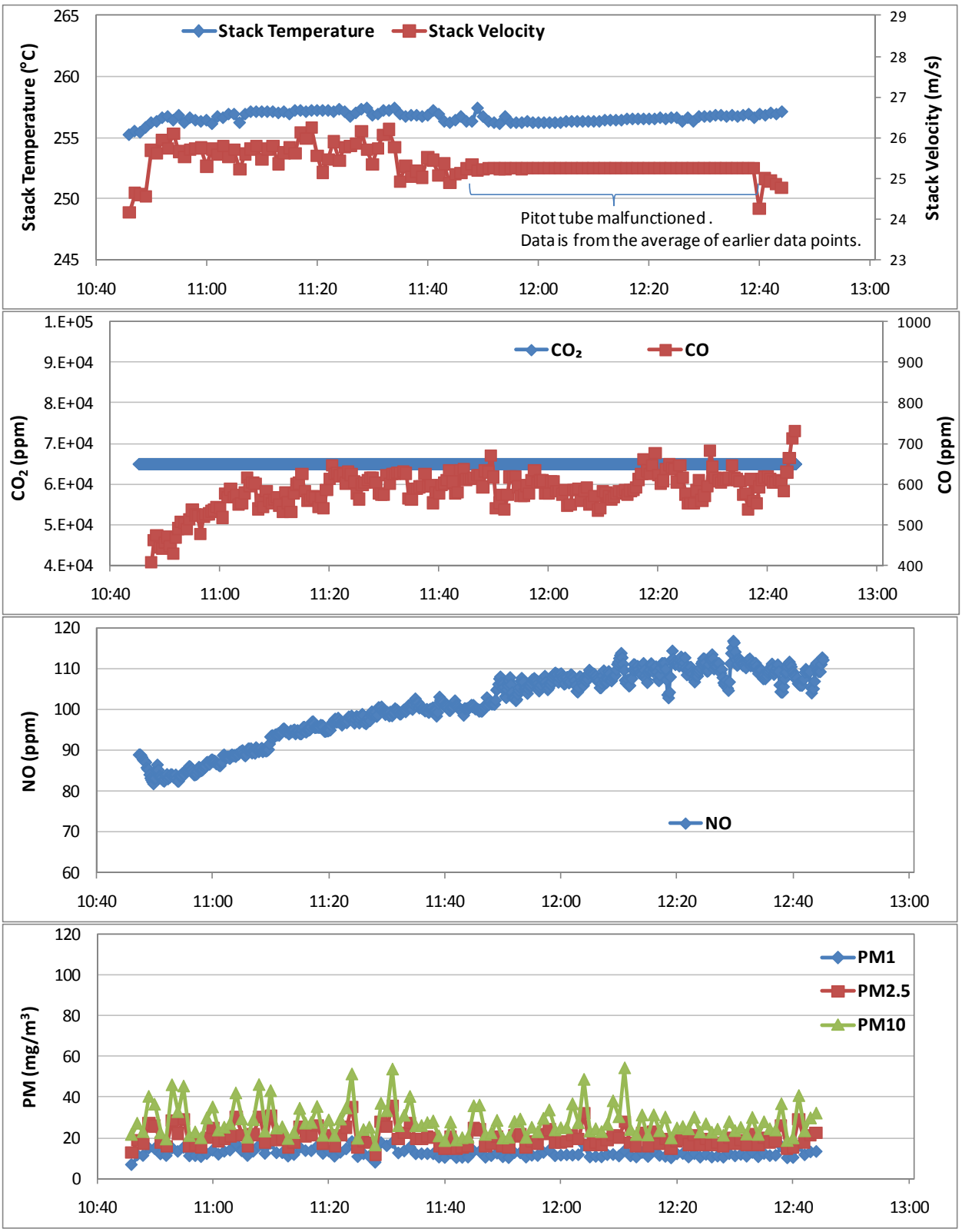

Figure B-4. Real-time data from Stack A, Run ID A-4. (See Table 3-4 for detailed experiment parameters.)

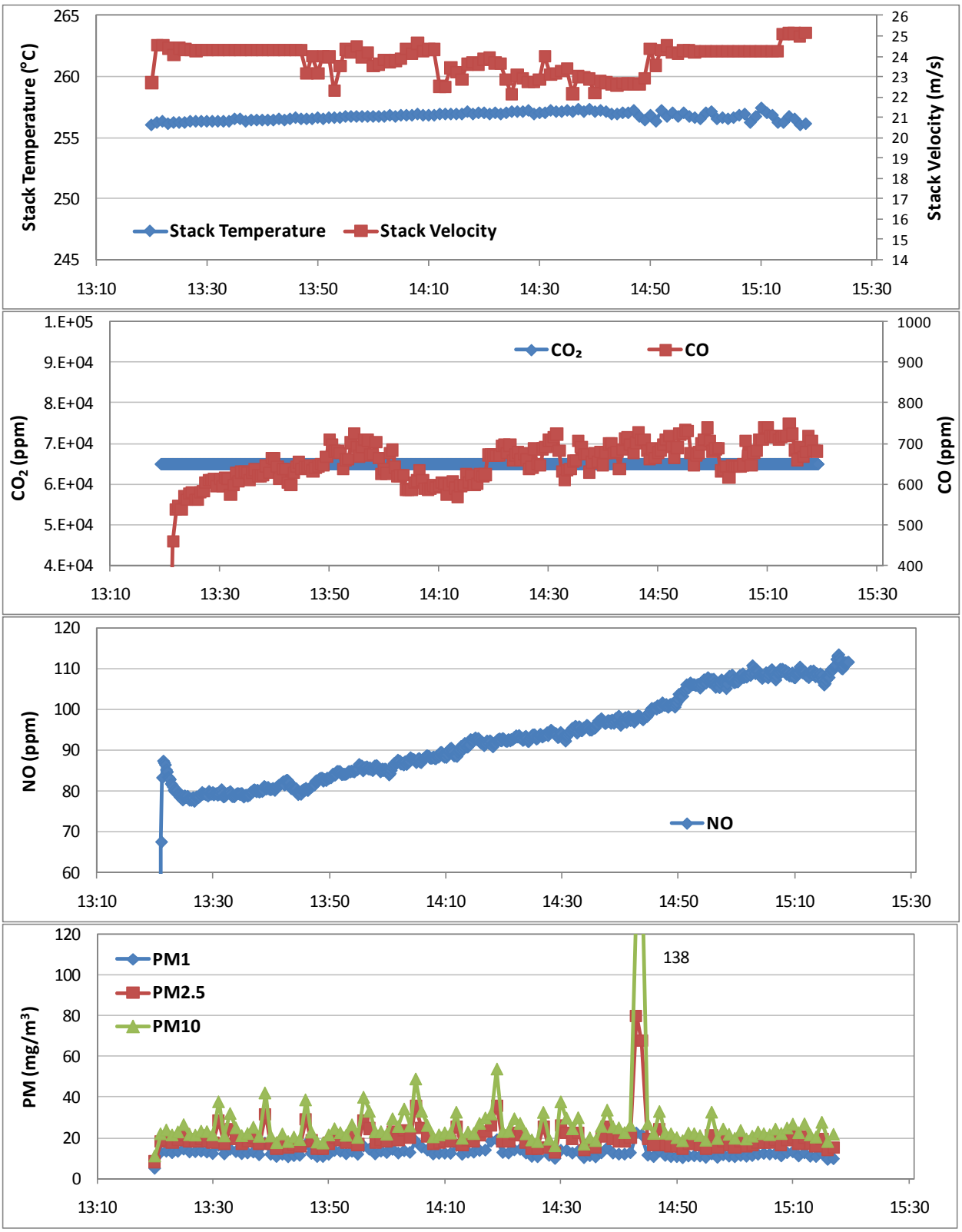

Figure B-5. Real-time data from Stack A, Run ID A-5. (See Table 3-4 for detailed experiment parameters.).

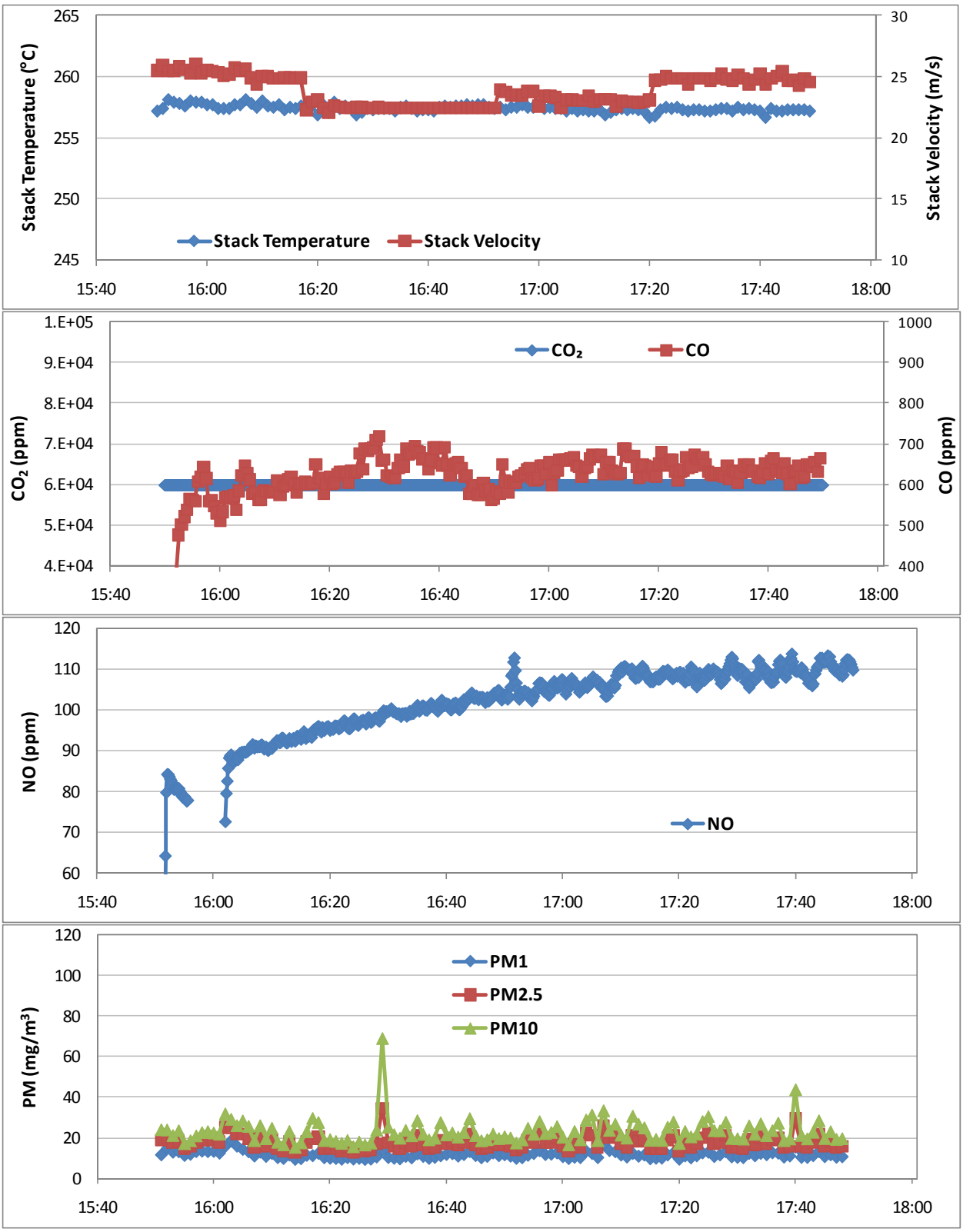

Figure B-6. Real-time data from Stack A, Run ID A-6. (See Table 3-4 for detailed experiment parameters.)

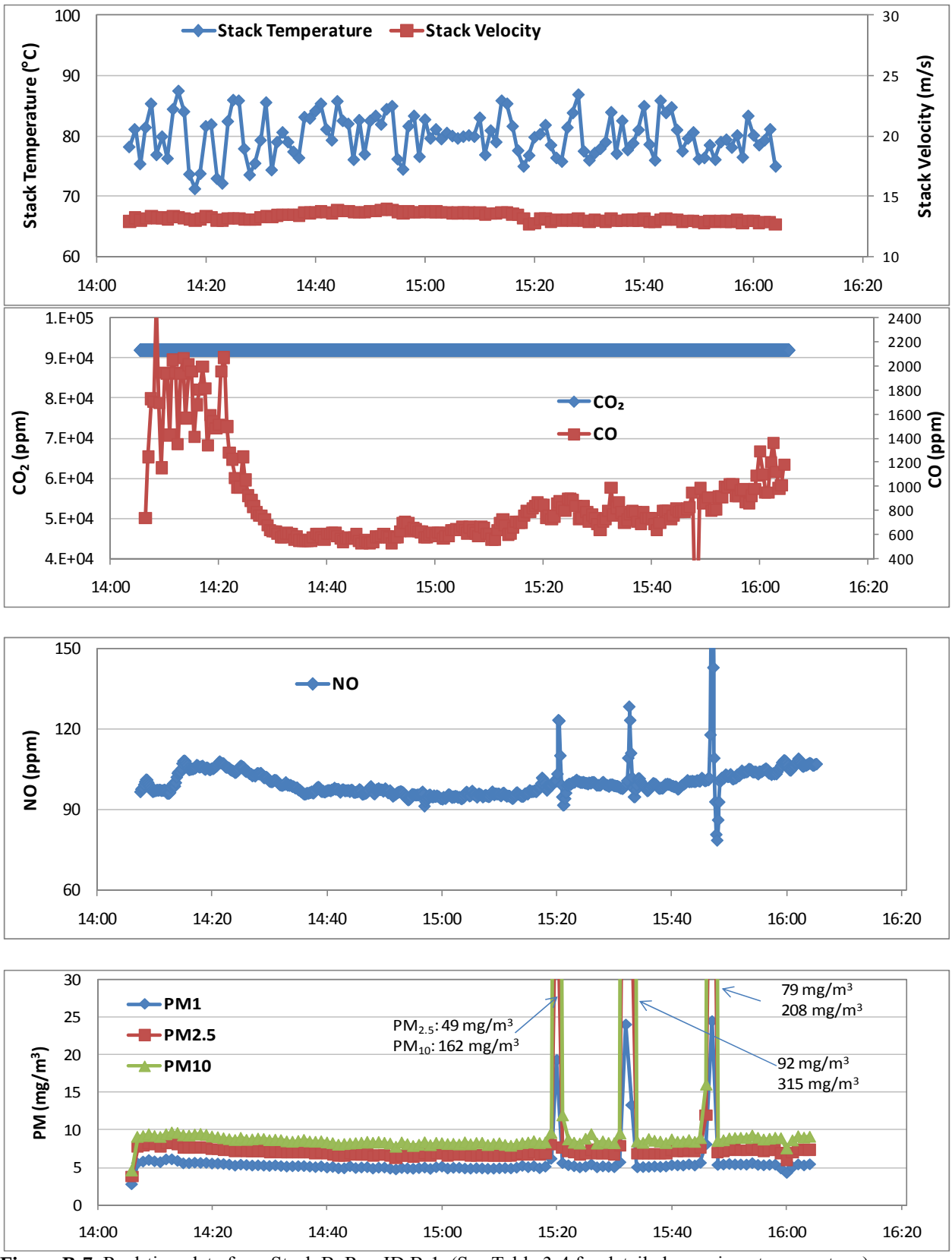

Figure B-7. Real-time data from Stack B, Run ID B-1. (See Table 3-4 for detailed experiment parameters.)

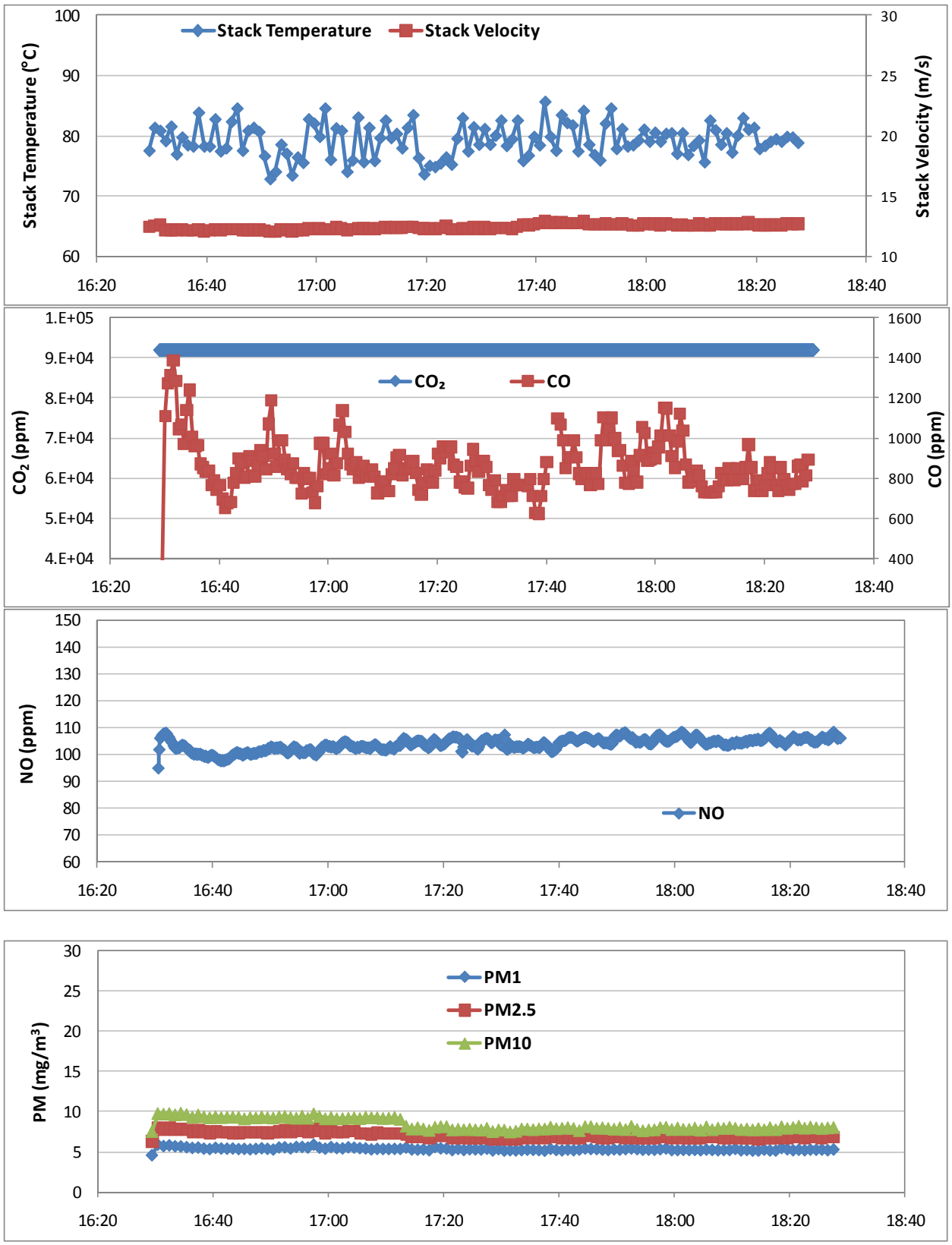

Figure B-8. Real-time data from Stack B, Run ID B-2. (See Table 3-4 for detailed experiment parameters.).

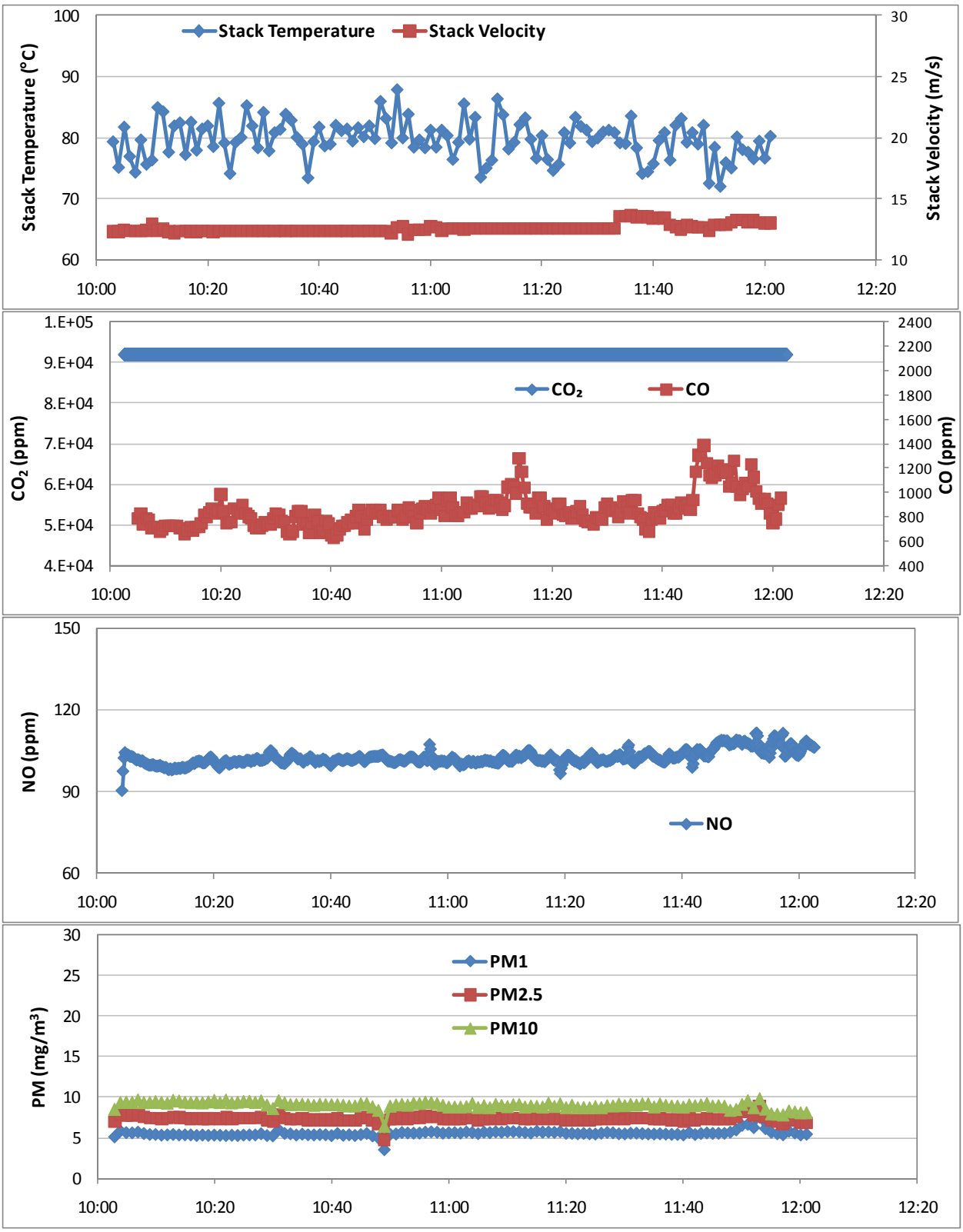

Figure B-9. Real-time data from Stack B, Run ID B-3. (See Table 3-4 for detailed experiment parameters.)

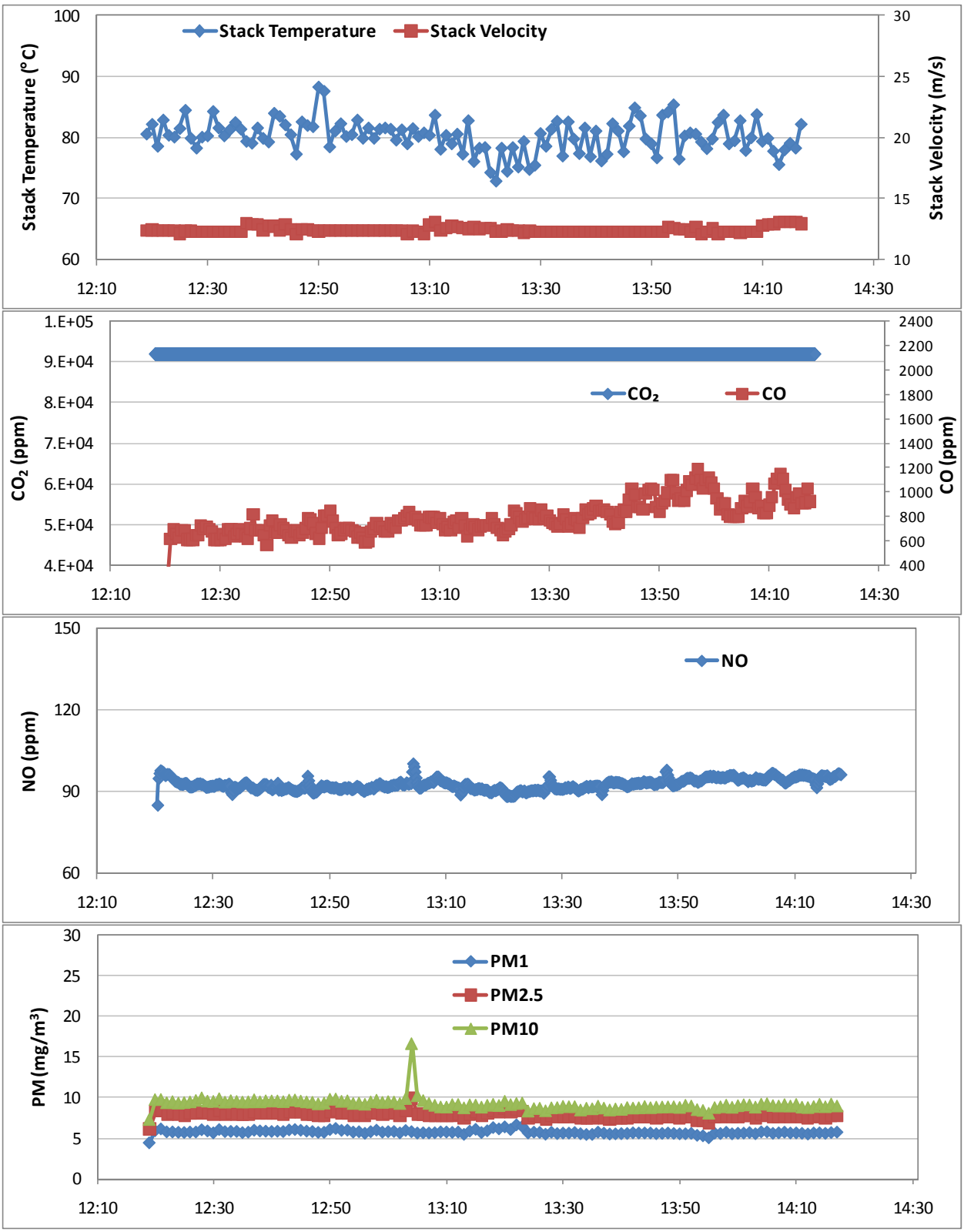

Figure B-10. Real-time data from Stack B, Run ID B-4. (See Table 3-4 for detailed experiment parameters.)

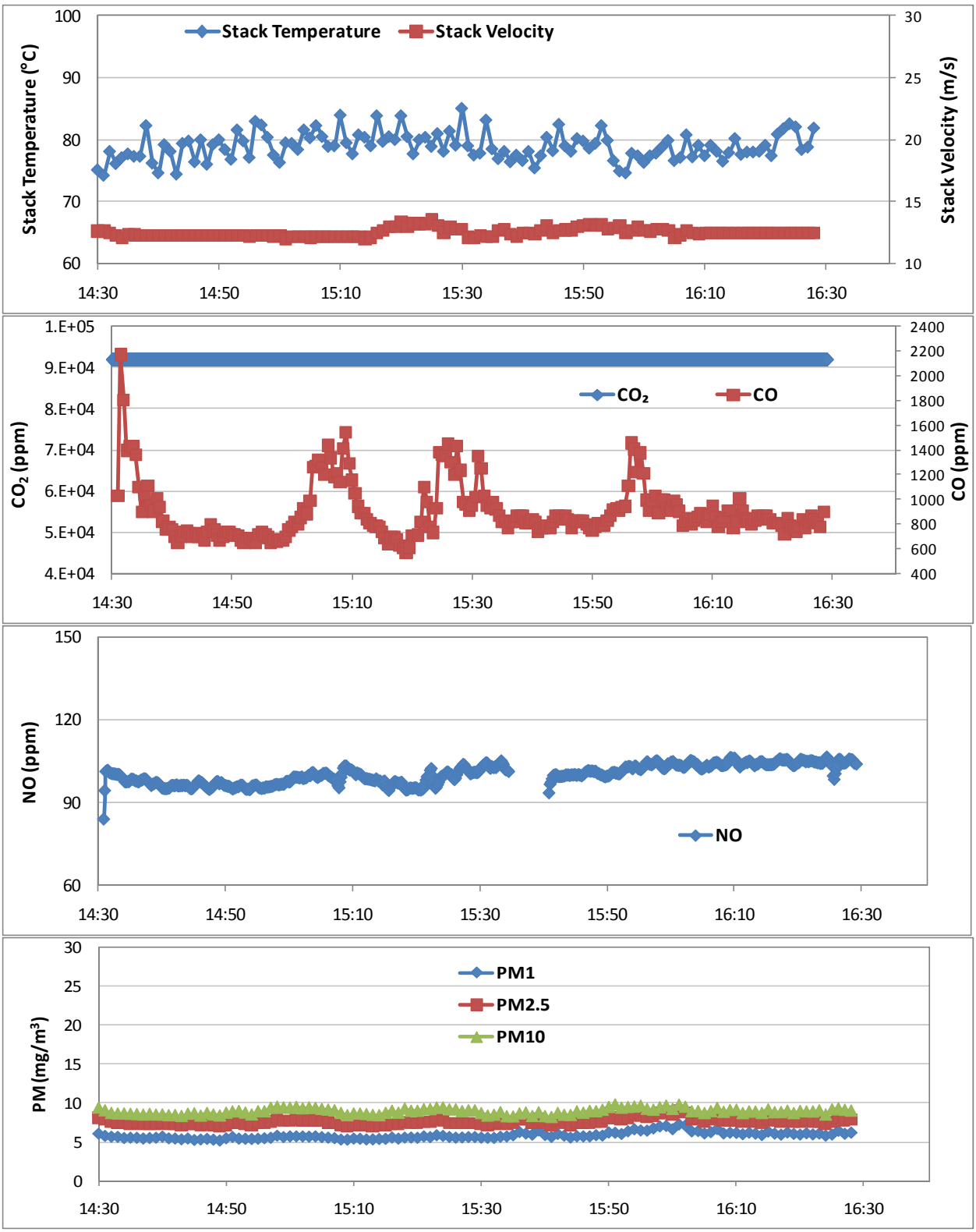

Figure B-11. Real-time data from Stack B, Run ID B-5. (See Table 3-4 for detailed experiment parameters.)

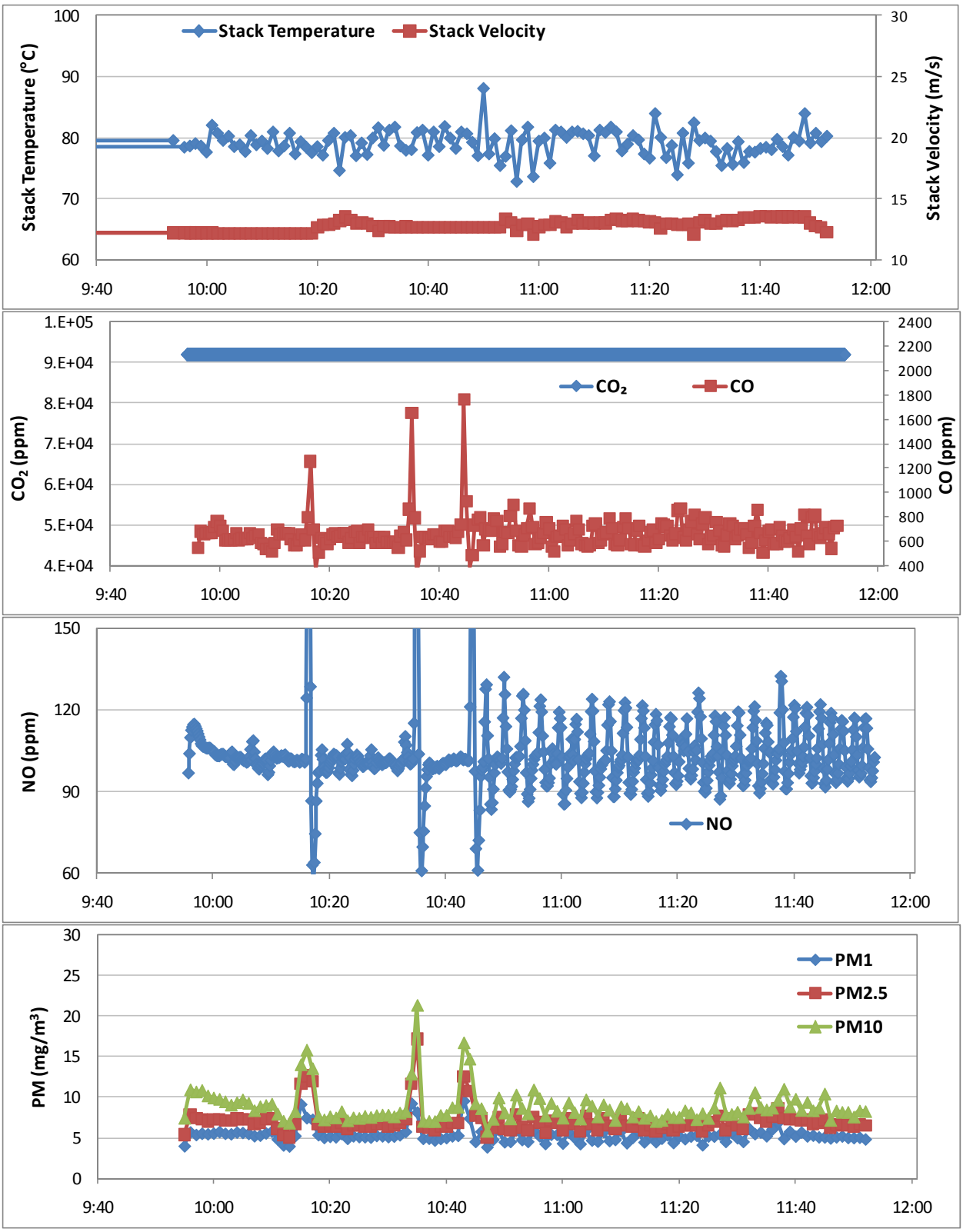

Figure B-12. Real-time data from Stack B, Run ID B-6. (See Table 3-4 for detailed experiment parameters.)

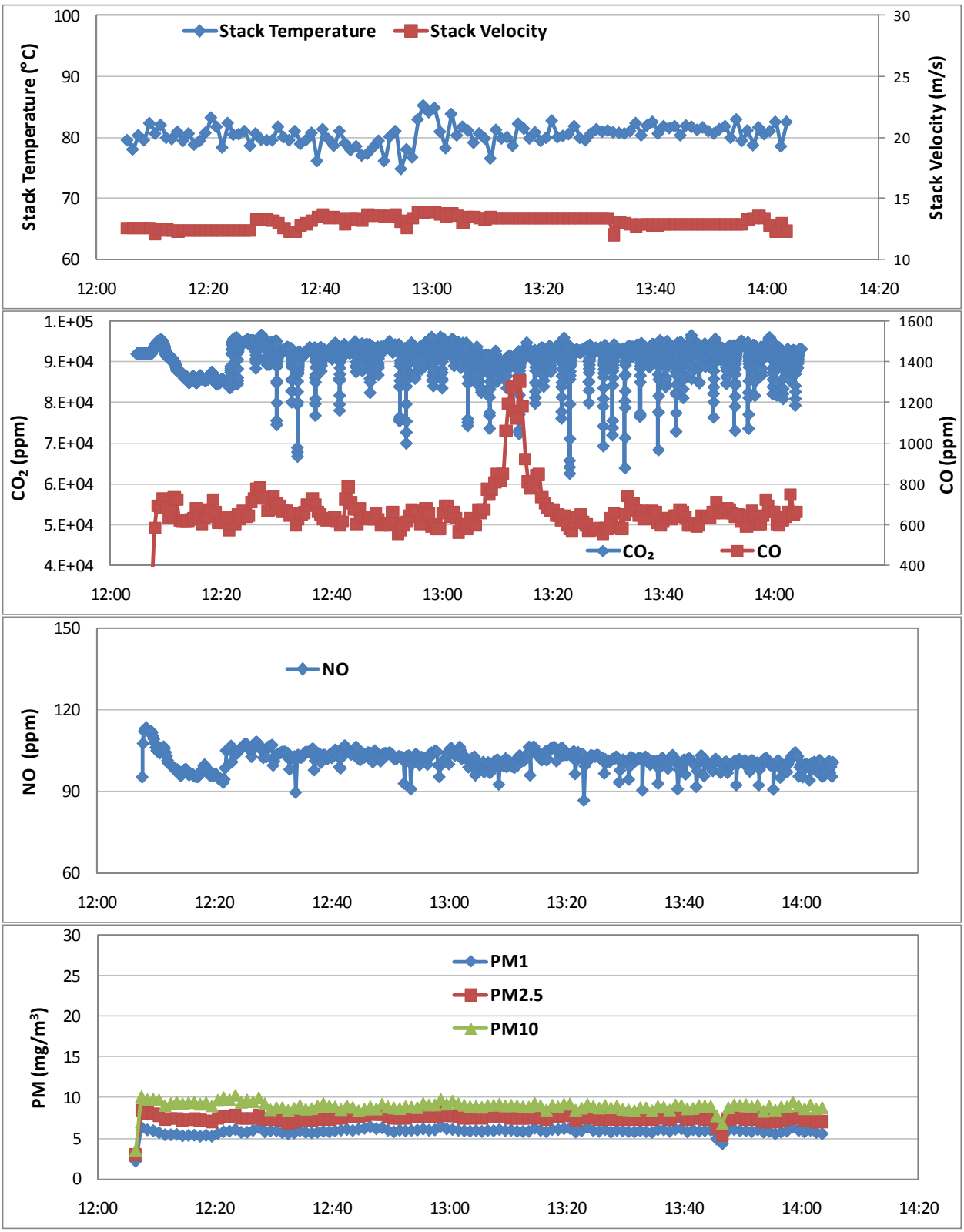

Figure B-13. Real-time data from Stack B, Run ID B-7. (See Table 3-4 for detailed experiment parameters.)

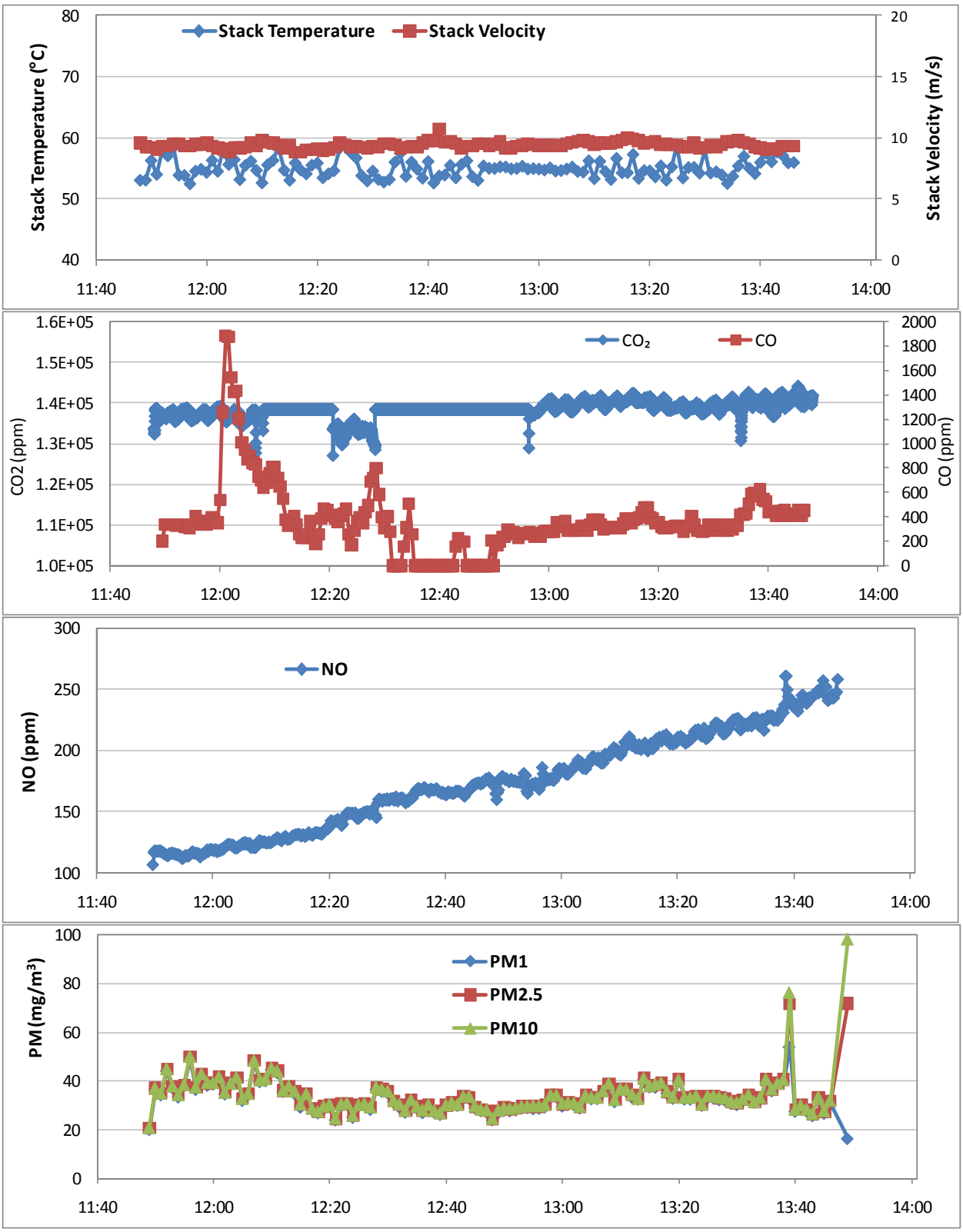

Figure B-14. Real-time data from Stack C, Run ID C-1. (See Table 3-4 for detailed experiment parameters.)

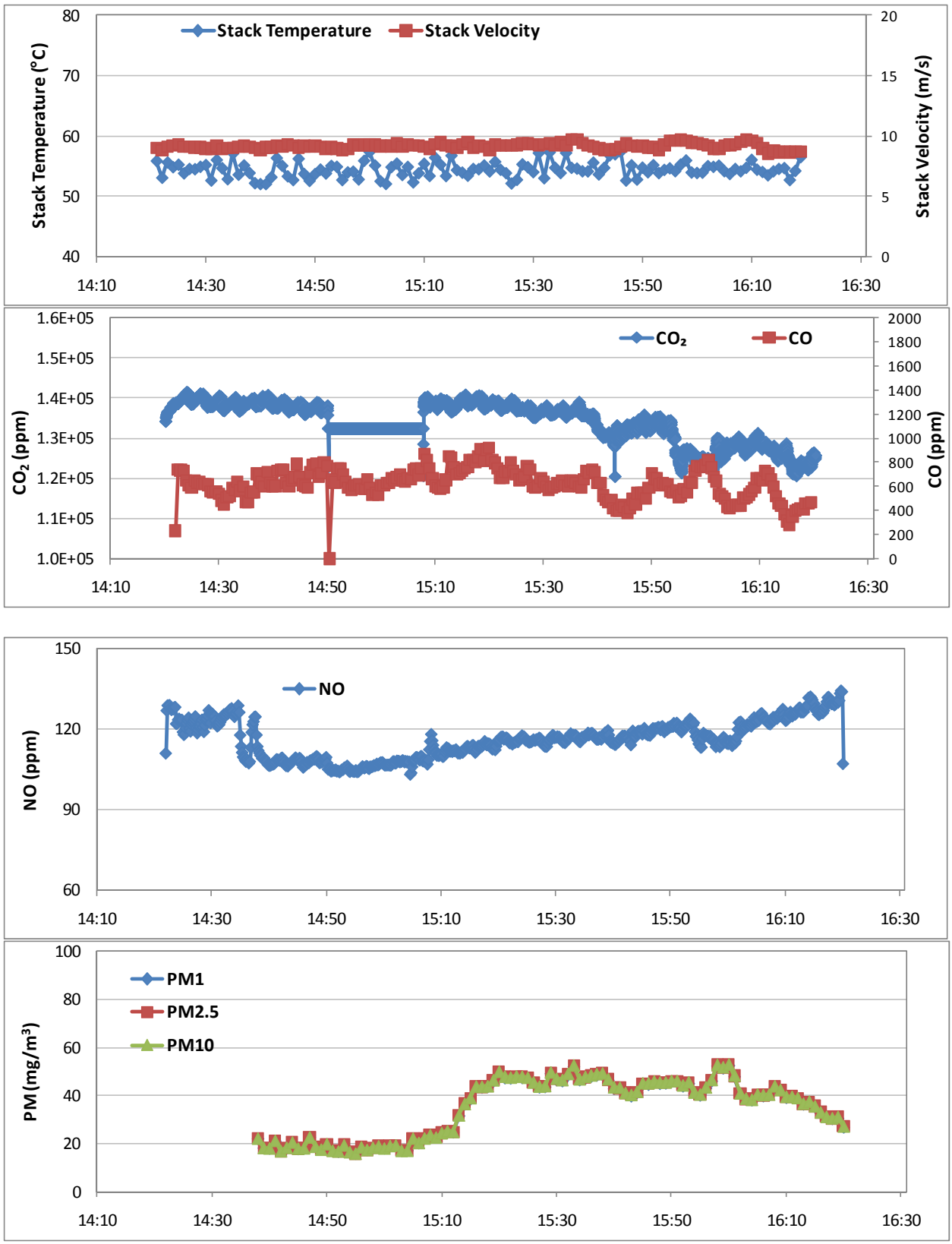

Figure B-15. Real-time data from Stack C, Run ID C-2. (See Table 3-4 for detailed experiment parameters.)

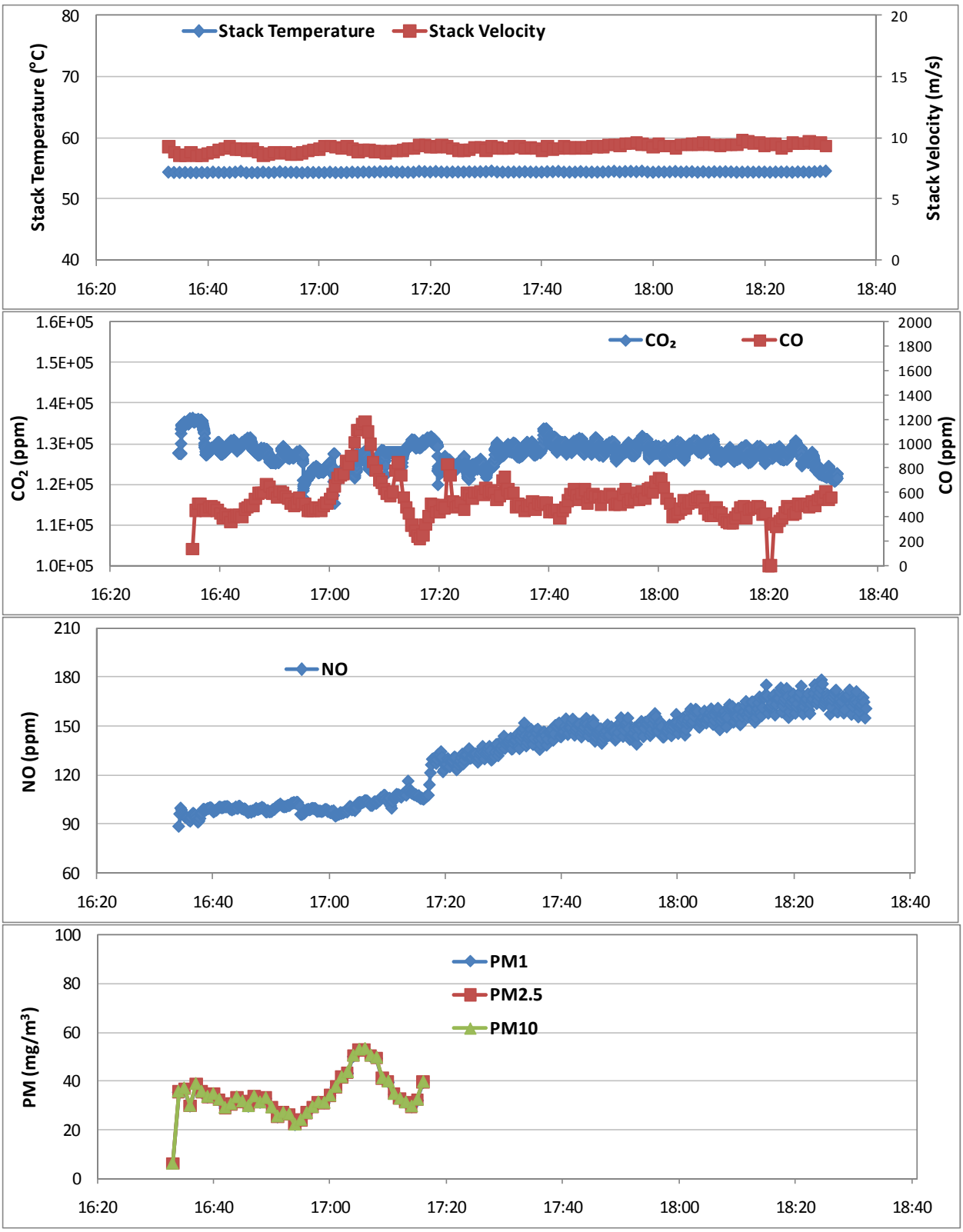

Figure B-16. Real-time data from Stack C, Run ID C-3. (See Table 3-4 for detailed experiment parameters.)

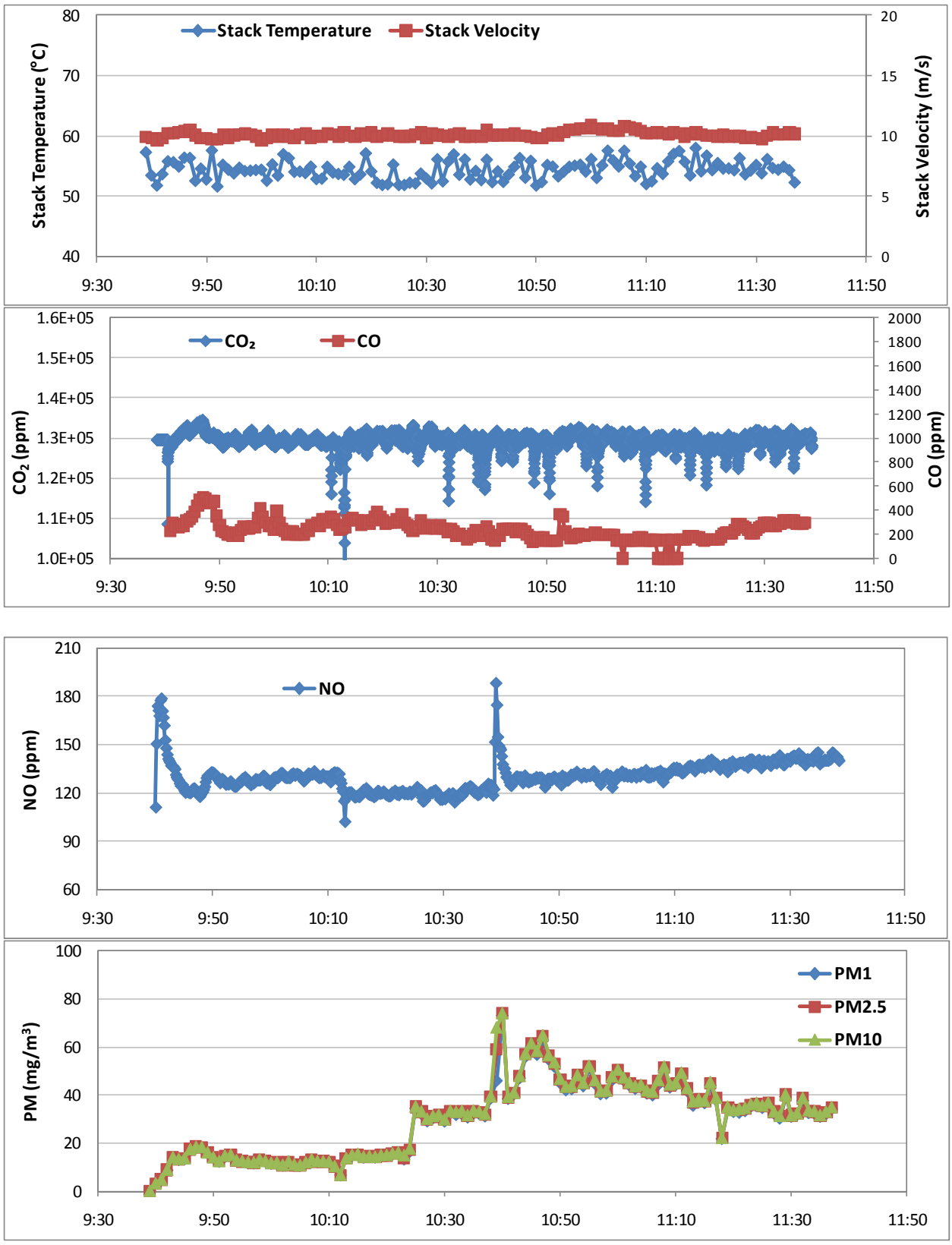

Figure B-17. Real-time data from Stack C, Run ID C-4. (See Table 3-4 for detailed experiment parameters.)

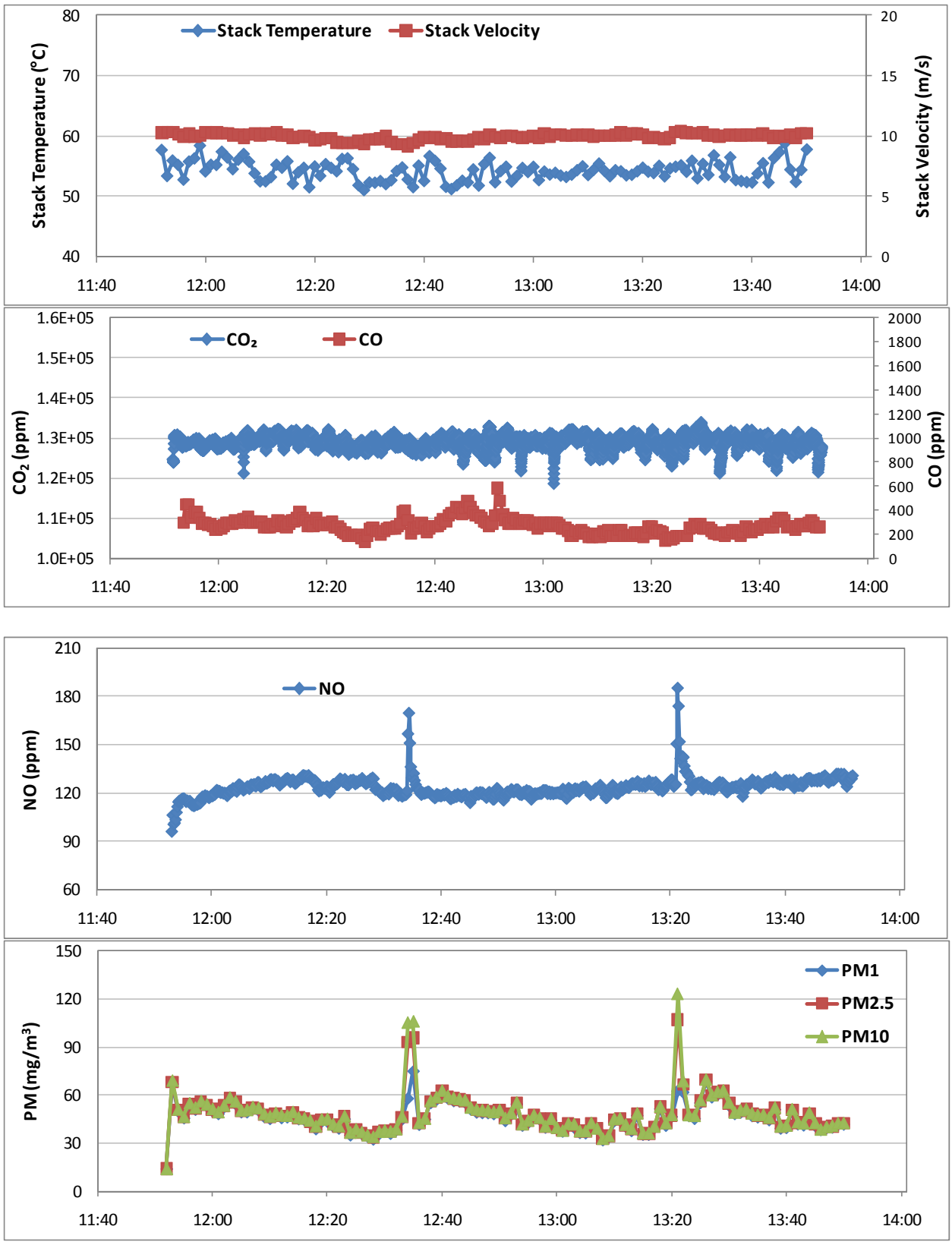

Figure B-18. Real-time data from Stack C, Run ID C-5. (See Table 3-4 for detailed experiment parameters.)

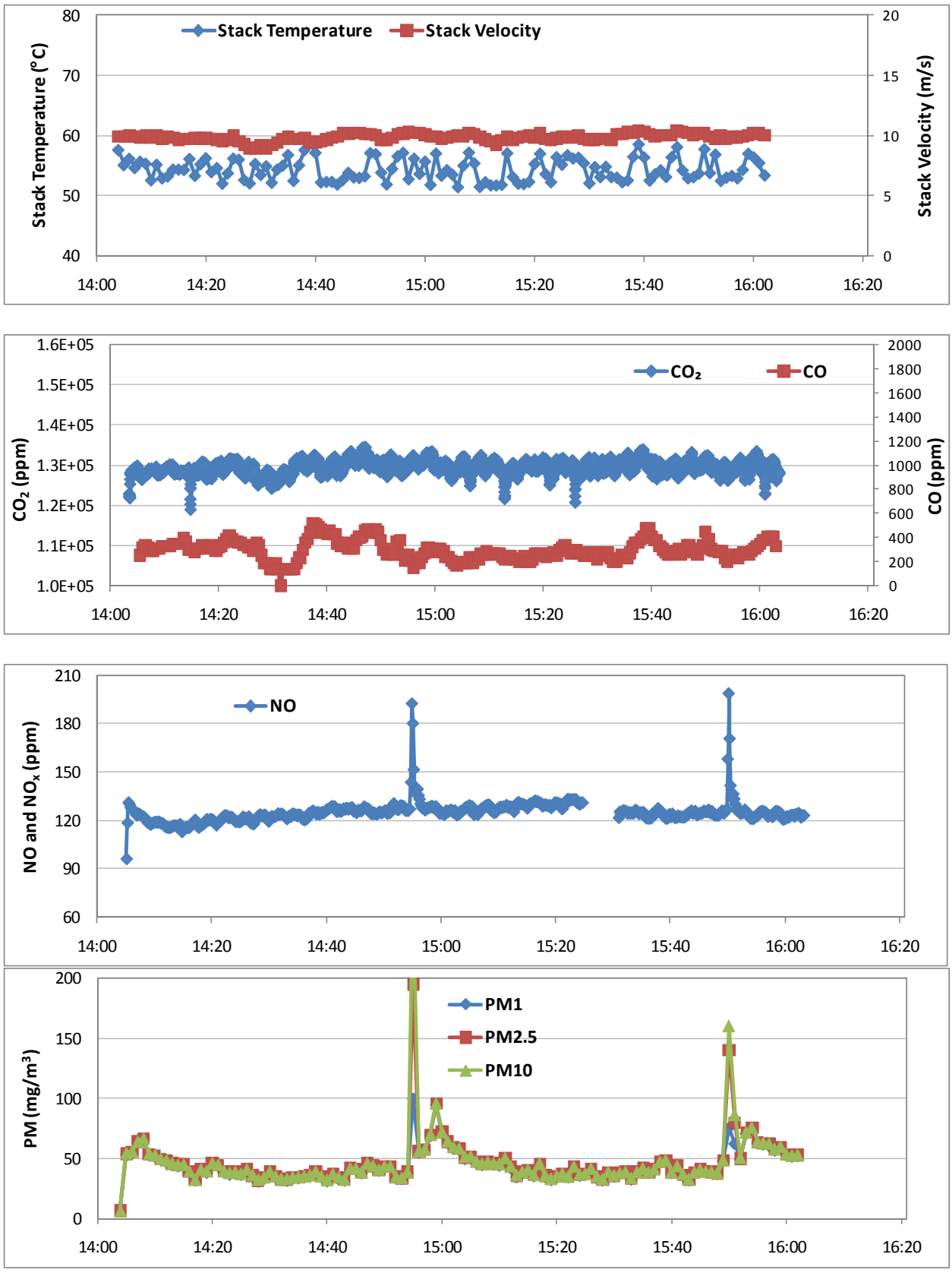

Figure B-19. Real-time data from Stack C, Run ID C-6. (See Table 3-4 for detailed experiment parameters.)